Journal of Materials Research and Technology 31 (2024) 213–243

Contents lists available at ScienceDirect

Journal of Materials Research and Technology

journal homepage: www.elsevier.com/locate/jmrt

# Current trends in additive manufacturing of selective laser melting for biomedical implant applications

A.N. Aufa [a], Mohamad Zaki Hassan [a,*], Zarini Ismail [b], Faizir Ramlie [a], Khairur Rijal Jamaludin [a], Mohd Yusof Md Daud [a], James Ren [c]

[a] Faculty of Artificial Intelligent, Universiti Teknologi Malaysia, Jalan Sultan Yahya Petra, 54100, Kuala Lumpur, Malaysia
[b] Faculty of Medicine and Health Sciences, Universiti Sains Islam Malaysia, Bandar Baru Nilai, 71800, Nilai, Negeri Sembilan, Malaysia
[c] School of Engineering, Liverpool John Moores University, James Parson Building, Byrom Street, Liverpool, L3 3AF, United Kingdom

ARTICLE INFO

Handling editor, L Murr

*Keywords:*
Selective laser melting
Biomaterials
Metals
Osseointegration
Corrosion
Surface modification

ABSTRACT

Additive manufacturing (AM) has obtained great attentions in the productions of customizable implants with complex shapes and good mechanical properties. AM fabricated implants of Ti alloy (Ti), stainless steel (SS), cobalt chromium (CoCr), iron (Fe) have been revolutionized in the productions of medical instruments, such as in artificial organs, including heart stents, drug delivery, scaffolds and orthopedic implants. However, high Young's modulus, superior mechanical characteristic, lack of surface integration, high corrosions, failed bone remodeling, and antibacterial performance are still incomparable to be used in anatomical structure. This review studied the issue of metallic implants designed by powder bed fusion of selective laser melting (SLM) techniques on the surface morphology, stress shielding effects, osseointegration, and antibacterial capabilities owing to implant failure. The rate of degradation and corrosion resistance of the metallic SLM implant, which would have an impact on cell proliferation and bone remodeling between the surrounding tissue, were discussed. The current review article also highlighted the various SLM parameters, like mechanical, chemical, and biological modifications, that might enhance the implant. Finally, applications, challenges, opportunities, and future developments of metallic implants using SLM techniques were addressed.

## 1. Introduction

The emerging technology known as additive manufacturing (AM) has the ability to produce significant results in the field of biomedical. This AM principle is a layer-by-layer manufacturing by utilizing pre-tooled (three-dimensional printing) 3D model computer-aided design (CAD) programming in a protective setting [1]. AM has the advantage of rapidly and accurately producing customized implants, complex parts at a reasonable cost with less waste being generated [2,3]. This AM technology has various potential applications in electronics, automotive, aeronautical, medicine and dentals. Among these, biomedical field has attracted the AM applications attributed to the freedom of fabrications and development of patients specific implants, such as prosthetics, stents, scaffolds, and drug delivery systems [4–6]. The widely use of AM in medical field attributed to their customizations and personalization of fabricating medical implants based on the fractured and infected sites. Based on the report by American Professional Association, the AM medical implants are estimated to rise by up to $9.7 billion by the year of 2027 with 35% growth yearly specifically in dental application [7]. The use of AM implants revenue in medical industries are increasing to about 11% from the AM printed components whether on devices or implants such as orthopedic and dental [8]. The metallic biomaterial mechanical properties should include high strength with low modulus so it can function for a longer period to withstand high load of contract and relax of skeletal muscle [9]. The stress shielding effects or implant resorption occurs when there is a mismatch of mechanical properties of the metallic implant and native body. This effects lead to the implant failure and failed bone remodeling. Thus, the development of metallic materials by using AM technique is viable for the customizations of biomedical implants with porous structure and mechanical characteristics that match to the anatomical structure.

The surface of the implant plays a crucial role in cell adhesion or osteointegration which involves the microstructure, macrostructure as well as the nanostructure characteristics. The cell remodeling were fastens with a rougher AM surface as compared to the smoother surface. This alloy for the osteogenic cell attachment on the surface. Metallic

* Corresponding author.
*E-mail address:* mzaki.kl@utm.my (M.Z. Hassan).

https://doi.org/10.1016/j.jmrt.2024.06.041
Received 1 May 2024; Received in revised form 5 June 2024; Accepted 7 June 2024
Available online 12 June 2024
2238-7854/© 2024 The Authors. Published by Elsevier B.V. This is an open access article under the CC BY-NC-ND license (http://creativecommons.org/licenses/by-nc-nd/4.0/).

alloy are commonly used in the field of biomedical part from composite and polymers, due to their higher biocompatibility and bioinert. The biocompatible implant materials include cobalt(Co), titanium (Yi), magnesium (Mg) and stainless steel (SS). These implant able to react with anatomical microenvironment without causing toxicity. The main properties of the implant should consist of: (a) porous and lattice structure, (b) bio activeness and biocompatibility, (c) good mechanical properties, (d) high corrosion resistance, (e) wear resistance, and (f) good osseointegration. These properties are mainly for the successful cell attachment and among these characteristic, pore is more prominent for the design of the metallic materials to allow the exchange of oxygen and minerals between the cells in the interconnected pores [5]. Apart from that, the mechanical characteristic should be matched to the neighboring tissue where the implant is placed so that it can withstand the stress shielding effects. Current metallic implants concerns are linked to the lack of corrosion resistance and low osseointegration which may compromise the function of the biomedical implants. The implants degradations may cause revision of surgeries, pain and failed implants.

For implants in the field of AM, there are seven techniques consist of binder jetting (BJ), directed energy deposition (DED), material extrusion (ME), material jetting (MJ), powder bed fusion (PBF), sheet lamination as well as vat photopolymerization (VPP). These AM techniques have been well recognized and identified in the ISO/ASTM 52900 Standard [10]. Nevertheless, not all these AM techniques can be utilized in medical devices and fabrication. As shown in Table 1, the benefit and drawbacks of these AM processes are summarized for the biomaterials fabrication. Furthermore, selecting the proper AM process for the fabrication of metallic materials is crucial for the development of biomaterials. From Table 1, metal powders are commonly used to produce implants by using powder bed fusion process because of their complex implant designs.

Currently, SLM biometallic implants are mostly focused on replacing tissue repair, dentistry, surgical tools as well as orthopedic. In upcoming future, the development of SLM printed metals will be further extended to form new biometallic applications for the implantable or metal bioelectronic [26]. SLM technique can print different types of materials, including metal, polymer, and metal combinations as well as metal-ceramic combinations. Due to its precision and near-density parts, it is widely used in medical applications to form complex structures implants based on anatomical structures. As SLM has becomes a main technology in the medical field, its stages in medical application is still in the initial phases prior to its clinical use [27]. This SLM technique is not as well established as those of the conventional method in the field of biomedical. The interaction between the metal powders, control of the residual stress, the external and internal defects and other technical problems still needed to be optimized to suit the microenvironment as well anatomic structure of human body [28]. The SLM accuracy is still insufficient as SLM adopted the layer-by-layer process, whereby the bond between each layer is compact, the defects affect the product density and strength, leading to a poor performance of the fabricated products.

Besides, in SLM fabrication, high quality raw materials are needed. These raw materials owing to various molding techniques either powdery or through filament to meet the specific requirement of the biomedical implants. These materials need to meet the requirement of implants in preventing any toxicity and biological risk. Then, for an implant to be used in clinical application, strict sterilization of implants is one of the crucial parts to ensure the success of implant. Sterilization of implant involves the placement of implant into the autoclave with high temperature of up to 130 °C. This is to ensure the implant is safe from the production of microorganisms, including bacteria, spores and fungi before implantation [29]. Commonly, the implant will be cleaned prior to the sterilization process. Thus, improper sterilization of the SLM implants will have a significant effect on the implant surface and properties. It is important to select the proper morphology and properties, especially to those of SLM implants with complex cellular structures [30,31].

This current review explained the previous strategies for the current trend of metallic SLM fabricated implant that have been used and identified their optimum parameters. Also, emphasized the most ideal alternative for the surface enhancement of the porous implant to be used in the medical field. The paper also presented the current challenges and limitations of AM manufacturing techniques *in vivo* and *in vitro* for the fabrication of AM implants. The successful AM implant would reduce stress shielding, enhance bone remodeling, and increase bacterial resistance to the antibiotic, which may be a major health concern after implantation.

**Table 1**
The materials used and clinical application of AM.

| Method | | Materials | Benefit | Drawback | Clinical Applications | Ref |
|---|---|---|---|---|---|---|
| Material Deposition | Material Extrusion (FDM) | Hydrogels, bioinks, ceramic, thermoplastic | Affordable, ease to find, biocomposite material, easily design | Time consuming, anisotropy, less resolution, high force of the nozzles impart | Bioprinting for cell culture, tissue and organ, rigid and soft models for surgical | [11,12] |
| | Directed Energy Deposition | Metallic metals | Fast, composite materials, high density | High cost, low resolution, needed post-processing | Limited use in clinical applications | [13,14] |
| | Material Jetting | Photopolymer, bio-inks | Good resolution, high cell proliferation, many cell/material deposition | Vey slow, high waste material, limited material selection, limited fabrication size | Bioprinting of soft tissue scaffolds for tissue and organ | [15–17] |
| Powder Based | Selective laser Sintering, Selective Laser Melting, Electron Beam Melting | Thermoplastics, metals powder, ceramic powders | High dense and strength parts, efficient, no needed of solvent | High cost, required post processing | Dental implant, orthopedic implant, wires, screw, rigid implant | [14, 18–20] |
| | Binder Jetting | Metal, polymer, ceramic, | Affordable, fast, comes in multicolor, no support | Low strength, required post processing, powders might cause hazard | Metallic implants of hard tissue | [21–23] |
| Liquid based | Stereolithography, Digital Light Processing | Ceramic resin, bio-resin, photopolymer, | High resolution, fast, high cell viability, no nozzle | Cause toxicity, limited material, uv might harm the DNA | Cell culture tissue and organ development | [12,24, 25] |

## 2. Classification of additive manufacturing in metallic implants

AM has been used in fabricating biomedical implants attributed to their precision and ability to fabricate complex shaped implant altered to the anatomical structure of human body. This advantage has piqued the interest of industrial organizations and researchers in expanding the use of AM. AM involves layer-by-layer fabrications which allows the fabrication of metal, ceramic, and polymers. AM processes are divided into seven groups by the American Society for Testing/International Organization for Standardization (ASTM/ISO) 52,900:2015 standard which and Materials American Society for Testing and ISO. As illustrated in Fig. 1, The powder-based AM methods, such as DED (Fig. 1(a)), BJ (Fig. 1(b)), EBM (Fig. 1(c)), laser engineered net shaping (LENS) (Fig. 1 (d)) and SLM (Fig. 1(e))are widely used in the fabrication of the packed and porous metallic implants as illustrated in**.** Nevertheless, other methods such as cold spraying, direct metal writing and diode-based processes have been proposed by researcher for the manufacture of metallic materials but are still under evaluation for their potential by

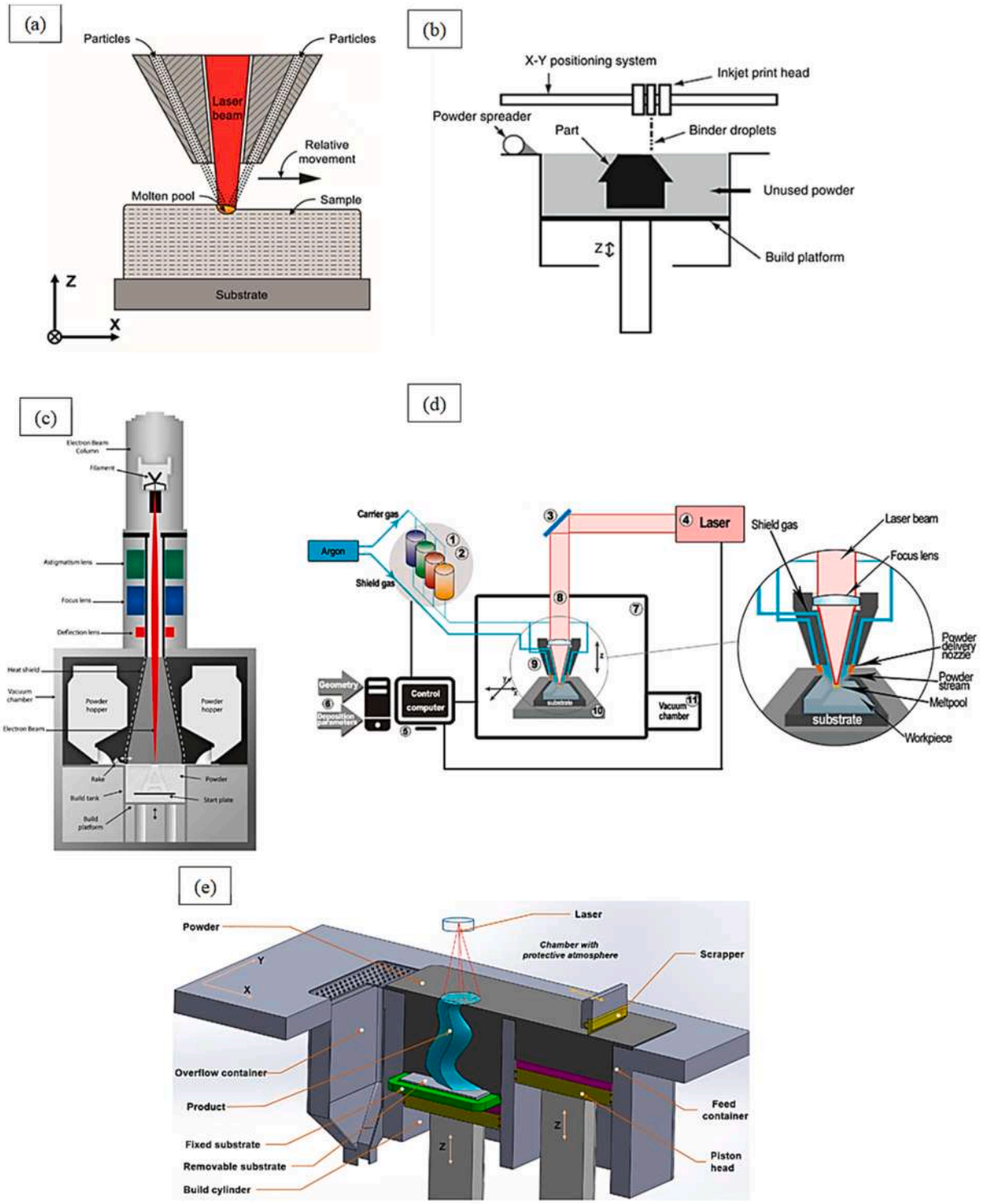


**Fig. 1.** Schematic illustration of current AM Processes (a) DED [32] (b) of binder jetting printing process [33] (c) electron beam melting process [34] (d) laser engineered net shaping (LENS) system [35] & selective laser melting [36].

ASTM to be recognized and classified in AM.

### 2.1. Directed energy deposition (DED)

DED is an AM process by transferring the energy between the fabricated material concurrently. DED is classified as electron beam AM due to its heat source is an electron beam. The fabricated materials are provided in the form of particles or wire, and a laser beam then melts the material on the desired surface in a vacuum chamber, as shown in Fig. 1 (a). The process commonly involves metal; however, it can still be used like ceramics. The type of gas utilized depends on the material, although argon is the most used to decrease oxidation in the molten pool. Compared to other AM methods, DED can be used as an addition or repairing the existing components. It also has the benefit of fabricating components with hybrid structures with of multiple materials of various compositions and structures [37]. DED has been previously employed for metallic implants, such as pure titanium (Cp-Ti) as well as porous structure for load bearing applications. The majority of the high cooling rates are attained during the DED process, which maintains the metastable β-phase of the Ti alloy intact. A study by Fisher et al. [38] found that these fast-cooling rates cause the laser deposited of beta-type Ti alloys of Ti-27.5Nb present an elastic modulus that almost similar to the cancellous bone. However, after the addition of oxygen content, the strength of the material decreases. This is due to the high reactivity of the oxygen which causes the martensitic phase transformations of Ti decreases with the increasing of oxygen content. Gonzalez et al. [32] fabricated DED of Ti–Nb and Ti–Zr–Nb and both of the sample demonstrated no apparent imperfections includes cracks or pores. However, there was formation of large, elongated columnar grain that grow parallelly to the building direction of the DED even after the sample has undergone polishing and etching with Kroll's reagent on the lower part (Fig. 2). These grains cause the DED sample to have a lower wear resistance. Another approach by Todaro et al. [39] utilized the high-intensity acoustic vibration in order to reduce the grain structure in the melt pool of DED-fabricated Ti6Al4V by stimulating the ultrasound. The microstructural analysis demonstrated the differences between the sample with and without ultrasound (Fig. 3). The sample without the ultrasound showed the formation of prior-β grains of ~0.5 mm in width, as shown in Fig. 3(a) and **(c)**. The sample with the ultrasound, on the other hand, exhibits a fine structure of prior-β grains of ~100μm in Fig. 3 (b) and **(d)**. The study concluded that the prior-β grain density increases with the ultrasound, indicating that the ultrasound enhances the nucleation during the DED solidification. The distribution of grain size and aspect ratio of prior-β grain on the sample drastically changed after ultrasound, demonstrating improved prior-B grain structure (Fig. 3(e) and (f)).

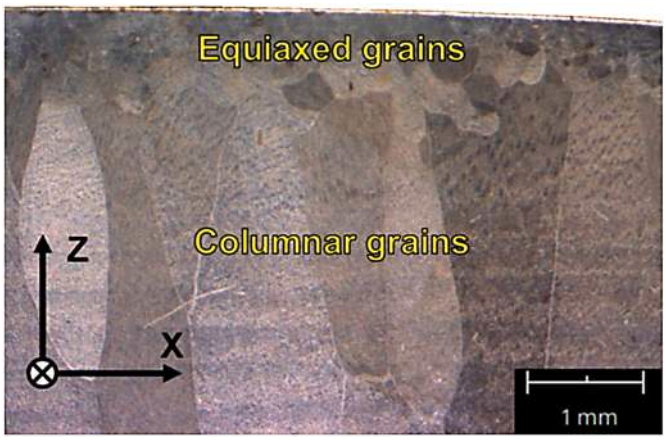


**Fig. 2.** Microstructure in the longitudinal XZ consist of elongated columnar prior beta grains parallel to the building directions [32].

### 2.2. Binder jet (BJ)

Binder Jet (BJ) printing is an AM method that printed liquid binding agent to generate a three-dimensional (3D) design on powder during manufacturing. It was first introduced in Massachusetts Institute of Technology (MIT) back in the early 90's [40]. The advantage of BJ is that it can be adapted to almost any type of metal power with a high production rate. It has broad range of technologies, including dynamic/powder interaction as well as post processing method. As shown in Fig. 1(b), BJ starts with applying a thin coating of powder to the printer bed. Next, the inkjet print head moves across the platform, depositing a droplet of binder in accordance with the data in the CAD file. Once the first layer has been printed out, the print head lowers the build platform, and the supply bed is lifted by one-layer thickness. However, this method demonstrates a reduction of the local temperature at a melt pool surface, which increases the presence of porosity due to the printing process that is performed at room temperature. This makes it impossible to produce metallic materials with high relative densities, leaving them unsuitable for use in biomedical implants for fracture fixation [41]. A previous study has reported on the use of BJ in fabricating biodegradable implant and scaffold, whereby they found that the BJ implant exhibit pores with positive benefits in *in vitro* degradation and cell adhesion. Chua et al. [42] combined the mixture of Fe-30 wt% with an open porosity of 36% that obtained through BJ. The corrosion rate of the implant sample was higher than the pure Fe by using potentiodynamic polarization test. The cytocompatibility showed an excellent cell infiltration on MC3T3-E1 pre-osteoblast cell line. These study were then followed by Hong et al. [43], whereby they utilized the Fe-35 wt% Mn with an addition of Calcium(Ca) and Magnesium(Mg). They confirmed the BJ sample showed that enhanced degradation of Ca was greater than that of the sintered compacted pellets. The MTT assays exhibited good live cells after 72 h of incubation.

### 2.3. Electron beam melting (EBM)

Electron beam melting (EBM) is an AM technology that holds potential in biomedical industries. The metal powder is melted by the electron beam in this powder bed fusion AM process to create complex parts. The materials fabricated in a vacuum chamber layer by layer, whereby the powder feedstock is supplied from the hopper in adjacent to the build chamber as shown in Fig. 1(c). EBM has the benefit of fabricating fine feature's part which involves mashes with internal structures. Typically, the direction of the lack-of-fusion faults is perpendicular to the build direction [44]. EBM showed pores on the surface of sample that caused from the leftover argon as trapped from the gas-atomization process that occurred in the powder during fabrications [44,45]. Researchers has been focused on the effect of EBM on the manufacturing, post processing as well the microstructure of the AM part. Szymczyk-Zio'łkowskaet et al. [46] demonstrated that the reduction of defects of EBM sample have a positive effects on the mechanical properties and their fatigue as well as elongation value once the EBM sample were treated by hot isostatic pressing (HIP). This is confirmed by Ahlfors et al. [47] that defects were reduced after HIP, whereby the sample showed 100% densities. This is attributed to the HIP process that allows the reduction of gas porosity as lack of fusion of the sample. Similar to Popov et al. [48] study's, whereby they demonstrated that the HIP treatment is able to close the pores on the sample. The result of the finalized sample demonstrated that the sample was free of unmelted surfaces due to the intense self-diffusion of the material at very high temperature of HIP. Therefore, it is crucial for EBM sample to undergo HIP treatment to ensure that the microstructure is appropriate for clinical applications.

### 2.4. LENS™ technique

LENS is method of 3D components fabrications from CAD file like

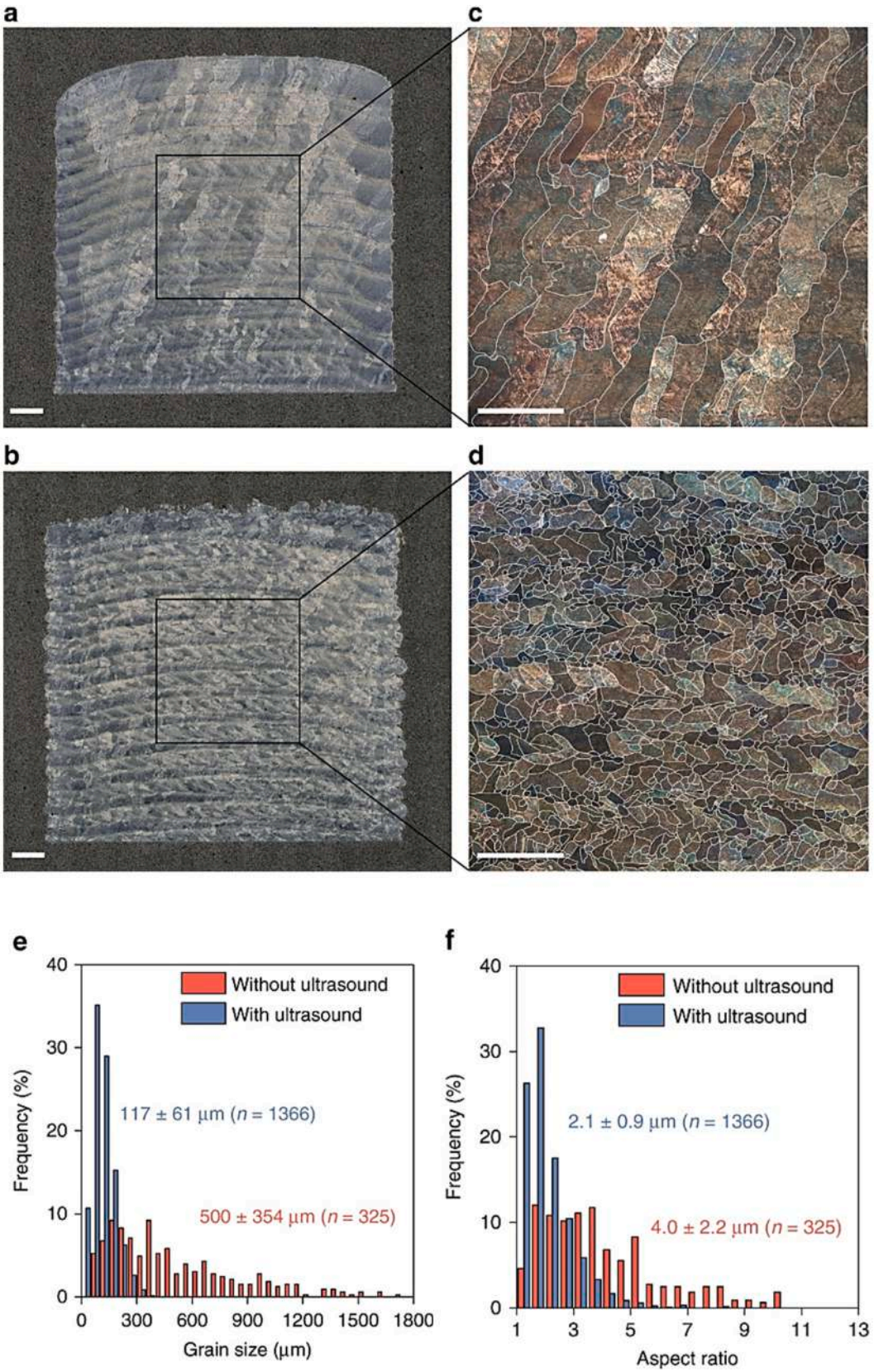


**Fig. 3.** SEM image Grain refinement of Ti6Al4V fabricated by DED by high-intensity ultrasound. (a) Sample without ultrasound,(b) sample with ultrasound (c) columnar grains formed on surface (d) fine equiaxed grains (e) Histogram of prior-β grains (e)grain size and (f) aspect ratio [39].

other AM techniques. As shown in Fig. 1(d), LENS process is a system, whereby metal powder is injected directly into the melt pool of continuous wave. LENS uses argon gas in maintaining the moisture level to be < 10 parts per million in preventing the oxidation of molten metals [49]. For this reason, powder with specific high reactivity can only be used in the production process. Generally, the LENS operates based on the selective deposition of metallic or ceramic powders and are melted with 500 W high-power fiber laser simultaneously. In comparison to other AM techniques, LENS uses powder with high purity as well as homogenous in the shape of spherical [35]. Mitra et al. [50] fabricated dense and porous Ta–Ti alloy composition with nanotube surface modification to enhance the Ti biocompatibility. Study demonstrated the increasing addition of Ta fabricated by LENS result into microstructural variations due to presence of α-Ti and martensite alpha' which result to higher hardness. Under *in vitro*, the percentage of Ta of 10% and 25% reveled higher osteoblast formed closely similar to the nanotube modification where there was more bone tissue attached with no gaps on the sample. Narayanan et al. [51] characterized the corrosion behavior of biomedical grade Co–Cr–Mo by using LENS technique, whereby they tested it under the Hank solution. The result demonstrated that the LENS sample surface showed micro-galvanic cells as well as a new crack feature which can act as active site for the localized dissolution of the alloy. Attributed to this, more studies are needed on the corrosion behavior of the LENS products to adapt the microenvironment of anatomical body fluid.

### 2.5. Selective laser melting (SLM)

SLM is one of the most popular powder bed AM techniques for creating structural parts without any geometry restrictions. "Selective" is defined as the processing of single or partial powder, while "laser" refers to the laser that is used for processing, and "melting" means the melting of the designated materials. SLM has a benefit of short production time with minimal processing steps than other AM methods [45]. As shown in Fig. 1(e), SLM method involves the use of metallic powder that are uniform on the build platform. Then, the powder is selectively melted by the energy source. The main advantage of SLM is that it can fabricate a wide range of metallic materials, including clinical grade of stainless steel (SS), cobalt-chromium (Co–Cr), titanium (Ti), and their alloys [15]. This is attributed to the complex shapes of anatomical structures, such as the knee, hip, skull as well as dental that requires precise design and accuracy to match the anatomical structure.

SLM has the capabilities of creating fine porous structures making it preferred for implant usage. These structures improve the cell adhesion between the human body and the implant part. Kelly et al. [52] adopted the sheet-based microstructure in fabricating SLM implant with a high permeability as well as increased the compressive and tensile fatigue behavior of the implant. A similar study by Xie et al. [53] fabricated scaffold with thicker-walled gyroid which result to excellent tensile strength. The sample is in the microarchitecture similar to the trabecular bone. Research on the metallic implant of SLM has acquire good attentions. It has showed evident from a previous study of developed interbody fusing cage of Ti6Al4V with compressive modulus of 4 GPa, which almost similar to the compressive modulus of trabecular and compact bone [45,54,55]. Yin et al. [56] customized Mg-based composite for enhancement of corrosion as well as cytocompatibility. They found that the SLM Mg composited with KZ30 and bioactive glass of 45S5 showed cell viability under *in vitro* test as well as cytocompatibility. Li et al. [57] found that the SLM sample of β Ti35Zr28Nb alloy exhibited elastic modulus of ~1 GPa which is in the range of trabecular bone. After 4 weeks of *in vitro* with osteoblast cell, the cell formed informing on the surface. This result conformed the integration between the cell and bone.

## 3. Advance metallic materials in SLM technology

Around 70%–80% of implants in the medical field are made of biometallic materials [58]. These biometallic materials are crucial for the reconstruction of failed hard tissue structure as well as to enhance the quality of life. The demands for these biometallic materials are increasing rapidly due to the increasing number of populations which includes high risk accident and elderly people who are prone to higher rich of anatomical failure. This biological and mechanical biocompatibility still needed many improvements for further use in biomedical applications. Commonly, the practical metallic clinical fields include stainless steel (SS), cobalt-based alloys, titanium (Ti) and its alloy as tabulated in Table 2. As for the SLM fabricated metallic alloy, the composition of the mostly used metallic material is as shown in Table 3.

### 3.1. Stainless steel

Stainless steel has been widely used in biomedical implants in fabricating stents, bone implant fixations and other devices attributed to its malleability, resistance to corrosion and fatigue. As compared to other biomedical implants, stainless steel comes in cheaper price, however, they are non-MRI compatible. Stainless steel generally exhibits a higher ductility and cyclic twist strength as compared to Co–Cr and Ti alloys. Stiffness is greatest for Co–Cr alloys, while it is the lowest for Ti alloys [45]. A previous study on their ability for fabricating biomedical implant has gain attentions, especially for the SLM process. Dwivedi et al. [72] fabricated the 316L and they found that the wetting and water contact angle of the sample were in the range of 60°–90°. This confirmed that the SLM 316 L has good permeability, allowing diffusion for the implant once implanted in the human body. Tekder et al. [73] determined the ability of 316L in the corrosion behavior. The samples were oxidized with ceramic-based of $TiO_2$. The corrosion was tested on the SBF solution and the result obtained were found that the plasma oxidized samples had higher corrosion resistance than the untreated 316L samples. The highest corrosion was found when the temperatures were at average of 700 °C.

### 3.2. Cobalt-base alloy

Cobalt-based alloy is a nonmagnetic and heat resistant alloy which is widely used in wear and tear-related application inherent to their high strength and corrosion resistance. Their corrosion resistance in generally adaptable to different environments. However, due to their different alloys in cobalt-based, the corrosion is dependent on the concentration, temperature as well as the acidic condition of the media. Cobalt-based alloys are originated from the solid-solution effect of chromium and molybdenum. Nevertheless, they are very hard to be fabricated, making them very limited to be used in the medical and industrial field due to its excellent resistant to degradation. The surface degradation and corrosion is mainly cause by the $H_2O_2$ present on the surface and as the concentration increases below the corrosion potential shifts, it will form the passive film. Hu et al. [74] fabricated CoCrMo with face-centered cubic (FCC) structure and they found that the alloy of the XY plane showed a lower degeneration compared to XZ plane due to the presence of precipitates consisting of grain boundaries. However, as more $H_2O_2$ were passed into the sodium chloride (NaCl) solution, the thickness of passive film increases, making them increase the chance of degradation and corrosion. Similarly, Gong et al. [75] studied the CoCrMo corrosion behavior in lactic acid concentration, whereby they found that the corrosion resistance of XZ plane is better than the XY plane. This is also stated by Kajima et al. [76] previously that the built XZ plane released more metal ions as compared to XY plane due to the large are of corroded pool boundaries. However, it is crucial for the CoCrMo alloy to undergo post-processing as stated by Axinte et al. [77] and Jangtap et al. [78] in order to increase the biocompatibility of SLM CoCrMo implant.

**Table 2**
Properties of material develop for orthopedic implant.

| Material | Melting Point (°C) | Yield Strength (MPa) | Tensile Strength (MPa) | Elastic Modulus (GPa) | Vickers hardness (HV) | Corrosion Resistance | Ref |
|---|---|---|---|---|---|---|---|
| SS | 1325–1500 | ≈250 | 450 | 200 | 275 | High | [59] |
| Iron | 1150–1600 | 130 | 350 | 200 | 30–80 | Good | [60–62] |
| CoCr Alloys | ≈1600 | 480–580 | ≈800 | ≥150 | 380–430 | Excellent | [63,64] |
| Ni Alloys | ≈1450 | ≈600 | ≈1000 | ≈150 | 300 | Good | [65–67] |
| Ti Alloys | 1670 | ≈750 | ≈900 | 120 | 350 | Average | [68,69] |
| Mg | 650 | ≈150 | ≈250 | ≈40 | 100 | Poor | [69] |
| Ta | 2980 | ≈230 | ≈260 | ≈185 | ≈1000 | Good | |
| Zn | 420 | 50–120 | 100–200 | ≈100 | 30 | Good | [70] |

**Table 3**
The chemical content of the SLM metallic materials [71].

| Materials | Al | V | Fe | Cr | Ni | Mo | Mn | Nb | Si | P | C | H | S | N | O | P | Ti |
|---|---|---|---|---|---|---|---|---|---|---|---|---|---|---|---|---|---|
| SS 316L ASTM A276 | | | Bal | 16.00 | 10.00 | 2.00 | 2.00 | | 1.00 | 0.045 | 0.03 | | 0.03 | | | | |
| Iron (Fe) ASTM A564 | | | Bal | 15.00 | 3.00 | 3.00 | 1.00 | | 0.07 | 0.15 | 0.07 | | 0.02 | 0.10 | 0.04 | 0.04 | |
| Ni ASTM B446 | | | 5.00 | 20.00 | Bal | 8.00 | | 3.15 | 0.50 | 0.015 | 0.10 | | 0.02 | | | 0.02 | |
| Ti6Al4V ASTM B348 | 5.50 | 3.50 | 0.25 | | | | | | | | 0.08 | 0.013 | | 0.03 | 0.13 | | Bal |

### 3.3. Titanium and titanium-base alloys

Ti alloys are currently an advancing material due to their predominant properties, exceptional mechanical characteristics, a high specific strength, outstanding corrosion resistance and good biocompatibility. Ti6Al4V is a desirable material for biomedical implants due of its distinct set of characteristics as it extensively used primarily in the aerospace and biomedical industries. Despite their high demand, Ti6Al4V is still expensive, large material waste as well as long lead time. Under these cases, AM offers the capability in the fabrication of Ti6Al4V with geometric complexities to be used in the medical field. Among the metallic biomaterials, Ti exhibits the highest biocompatibility, corrosion resistance and tensile strength as compared to stainless steel and cobalt chromium. Brandl et al. [79] stated previously that the wires deposited with Ti6Al4V achieved similar mechanical properties of wrought Ti6Al4V of AMS 4928. Suresh et al. [80] found that the elastic modulus of Ti–6Al–4V ELI is able to be reduced attributed to the porosity of ~15% and roughness. The cytocompatibility in the MC3T3-E1 showed no adherent toxicity and after 1 week of *in vitro* test, the proliferation rate was increased. Ji et al. [80] fabricated Ti–3Cu to determine the corrosion resistance and biocompatibility. The *in vitro* test in osteosarcoma cell MG63 showed good cell attachment. The antibacterial resistance under *E.coli* showed a stable highly-effective antibacterial rate with no cytotoxicity present.

### 3.4. Shape memory alloys – Ni–Ti alloy

Ni–Ti or also known as Nitinol is a type of alloy with composition combining of half nickel and Ti with composition of ~50% and they belong in shape memory alloys class. Attributed to their shape memory alloy, they are easily deformed at the low temperature as well as be able to retain to their initial shape even when exposed to high temperatures. This by the effect of its martensitic transformation on the surface of NiTi when expose at high temperatures. The Ni–Ti alloy is packed in an order of BCC structure which includes austenitic phase making them unable for twisting and bending. In biomedical field, Ni–Ti is commonly used in stent which can exhibit changes in diameter when inserted in human body, due to its austenitic phase at elevated temperature. Polozov et al. [81] fabricated NiTiNb shape alloy with a density of 99%. The yield strength obtained was up to 450 MPa with tensile strength of 706 MPa. The sample showed hysteresis of martensitic transformation once the temperature increased, demonstrating good mechanical properties. This study is similar to Yu et al. [82], whereby they found that SLM-NiTi showed ultra-high failure strength of up to 700 MPa and elongation of 10% under tensile conditions at room temperature.

### 3.5. Biodegradable metals – Mg based alloy

Magnesium (Mg) has gained attention in the medical field due to its appropriate mechanical properties, biocompatibility as well as lightweight. Mg is the highest positive charge in human body called cations, whereby mostly are stored in bone with composition up to 65% and soft tissues of 40% and mainly in muscle of 25% [83]. Mg plays important roles in synthetizing of protein from the mitochondria, known as the powerhouse of human body. The modulus of Mg ~40 GPa which is close to the cancellous bone modulus of 30 GPa [84,85]. These suitable properties make Mg a good choice for medical devices which preferred high compatibility of materials [86,87]. However, Mg exhibits the lowest corrosion resistance which attributed to the degradation of the implant after fixations, resulting to the premature loss and failed of mechanical properties [83]. The microenvironment of the human body fluid is between pH 7.4 and pH 7.6 that induce the local accumulation of ions, causing cytotoxic effect [88]. These effects are mainly attributed to the releasing of $H_2$ gases during degradation of Mg implant [89]. These issues are mainly the most primary issues for the limitation usage of Mg implants in clinical applications. Some study has focused on Mg doped with of rare elements that shows good resistance to corrosion [90]. Mg–Zn composites are much suitable for the biomedical field since Zn promotes bone mineralization as shown in a study by Shuai et al. [91], whereby they incorporated hydroxyapatite (HA) into Mg–Zn in order to slow down the degradation process. A good apatite layer was formed on the surface, encouraging good corrosion resistance. However, there was excessive HA content on the surface of the implant, leading to the pore formation. These pores eventually accelerated the bio-degradation. Nevertheless, SLM of Mg alloy is still it is challenge phase, largely owing to its high chemical activity and flammability even in bulk state [92].

### 3.6. Biodegradable metallic materials – zinc

Zinc (Zn) is a bioresorbable metal mostly designed to provide mechanical support for injured tissue [93]. Compared to Mg and Fe, Zn exhibits more biodegradation behavior to match the anatomical requirement. Zn is the second highest trace mineral in the human body which acts to maintain cardiomyopathy cardiac function and for the formation of new bone [94]. The lack of Zn in the human body is linked to the weaknesses and poor health of bone [95]. This allows zinc to be used as a new generation of orthopedic implant. However, zinc has a poorer mechanical strength and encourages localized deterioration which can lead to toxicity and implant failure. Thus, various studies have been done by alloying Zn with other elements. For example, Yang et al. [96] fused Zn element with Mg to improve the degradation and bone fracture healing. The study demonstrated that the Zn/Mg alloy showed ultimate tensile strength up to 650 ± 13 MPa, and in the *in vitro* study, the implant reduced its degradation behavior. Guillory et al. [97] evaluated the effect of Al element doped in the Zn on the increase activity of macrophages. Corrosion resistance of the Zn/Al implant after 20 months of *in vivo* in rat aorta and found that the degradation rate decreased with higher macrophages formed to engulf cells. A similar study was also reported by Drelish et al. [98] where they suggested that the pure Zn wire exhibits steady corrosion without any cytotoxicity. The bone remodeling rate increased, along with a decrease in inflammation *in vivo*. However, a buildup of passive corrosion on the implant was observed after 10 months of post-implantation. Recent study by Su et al. [99] found a uniform layer between the Zn and phosphate implant and the lumen tissue after 4 weeks on implantation *in vivo* of rabbit aorta as shown in Fig. 4. Connective tissues were observed between the material and host on the sample, demonstrating excellent biocompatibility to Zn implant to be used in clinical applications. However, the feasibility of SLM Zn in the medical field needs to be addressed before it is permanently used in anatomical structures to prevent its degradation.

### 3.7. A bioactive metal – Tantalum

Tantalum (Ta) is typically employed as an alloying element in Ti alloys to act as a beta-phase stabilizer, lowering the elastic modulus and preventing stress shielding effects. However, there has limited of study focusing on Ta as an alloying element due to its relatively expensive, high density and processing temperature (melting point of 3017 °C). Ti–Ta exhibit lower elastic modulus compared to the Ti6Al4V and easily detrimental to the surrounding bone tissue for long term implant applications. However, Brodie et al. [100] reported that Ti–25Ta and Ti–65Ta had the highest biocompatibility with bone, attributed to their lower elastic modulus (60–70 GPa) than conventional Ti6AL4V. Also, they demonstrated that the Ti–25Ta had the similar yield strength as the SLM Cp-Ti with a significant reduced in elastic modulus of 65 ± 5 GPa. There was a decrease in surface defects with randomly oriented α′ on the surface [101]. In addition, combination Ti with 25% of Ta, Brodie et al. [100] showed mineralization in an *in vitro* study with increased alkaline phosphatase activity. However, the lower Ta content exhibits an unpromising composition for an AM bone implant.

### 3.8. High entropy alloy – aluminum

Aluminum (Al) alloys have the merits of high specific strength, good casting capabilities, and low cost. However, their poor wear resistance, corrosion resistance, and incompatibility have hampered their application to be used in biomedical implants [102]. The high level of Al and their hypersensitivity may lead to a complicated health issue. Previously, Bowman et al. [103] used Al silicate to control bleeding in open reduction internal fixation surgery and found the Al was toxic at a minor level to the endothelial cell. Apart from the poor anti-corrosion and wide intrinsic friction coefficient, Al alloy can easily leach during a prolonged period. Thus, Al has barely been used in medical applications. Weng el al [104]. fabricated $Al_2O_3$ to enhance the biological response and antibacterial performance of Al. The antibacterial ratings were up to 99% for *S. aureus* with improved mechanical properties. However, as the duration of the immersion increases, the Al oxide is leaching out of the Al ions, increasing the sample corrosion rate.

## 4. Requirement for SLM printing in biomedical applications

### 4.1. Printability and structural performance

The implant that is fabricated using the SLM technique could vary in its microstructure, surface finish, and mechanical properties from the conventional techniques like casting and forging. The most noticeable features of these implants include the build direction of the morphology, embedded flaws, and high residual stress. It happens due to the non-uniform solidification in the melt pool [105], and the thermal stress distribution during the SLM process [106]. The rapid solidification (cooling rate at 105–106 K·s−1) can form a small grain size on the surface, which can change the functional properties and increase the requirement for the implant to undergo post-processing.

Despite biomedical implants attention to adopting SLM, it is crucial to overcome several problems, notably the formation of in-part defects [107]. For example, the lack of fusion can form voids due to the insufficient energy input during the fabrication process, whereby the prescribed volume of particle failed to fully melt [108]. Also, these inadequate amounts of energy tend to adhere irregular granules, which enclose the partially melted particles on the SLM sample. A study by Liverani et al. [109] fabricated Ti–Nb sample with melt pool of 2 μm, however there were defects formed on the surface caused by gas entrapment and void during the layer by layer process. Fig. 3 illustrates the schematic diagram of melt pool formation in the SLM process. As can be seen from Fig. 4, the adhered ((Fig. 5(a)) and partially melted particle (Fig. 5(b)) influenced the final surface roughness. Fig. 5(a) depicts a powder particle dispersed from a laser beam with surface damages generated by the staircase effect owing to layer-by-layer processing. The defect includes the balling, spatters or inadequate fusion that led to

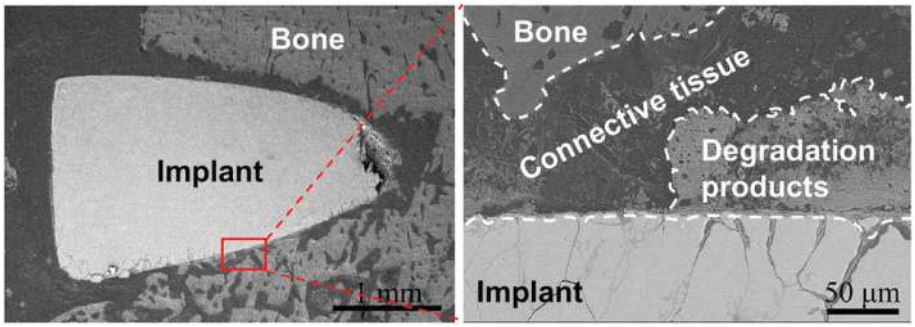


**Fig. 4.** Cross sectional of backscattered electron image of Zn implant after *in vivo* implantation in aorta of a rat after 18 weeks [99].

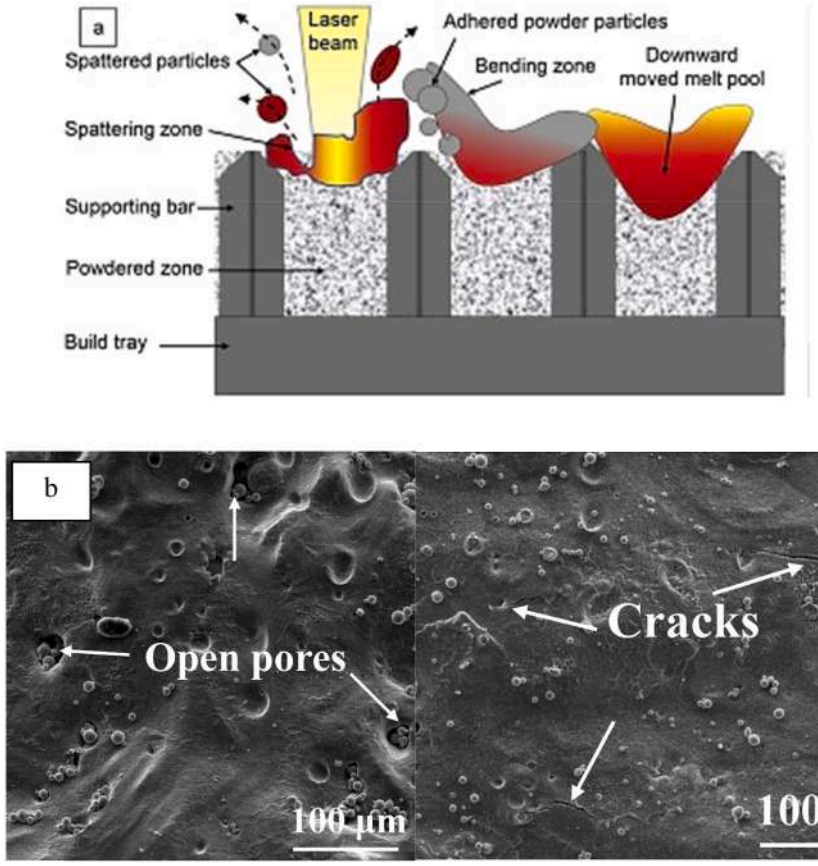


**Fig. 5.** Schematic diagram of (a) surface defects during layer by layer scanning [111], (b) SEM image of cross section of AM Sample [112].

irregular surface morphology due to high heat-shock. A high surface roughness can deteriorate the performance of parts to be used in biomedical implants. Fig. 5(b) shows the surface defect containing of open pores, which consist of partially melted and adhered powder particles. The implant surface characteristic plays an important role in the osseointegration which the cell attachment relies on the microscopic, mesoscopic and the nano structures of the implants [110]. However, when the energy input is high, the metal vaporizes and eventually creates gas bubbles that trap inside the sample. This trapped gas causes a rounded-shaped pore to form on the fabricated sample.

Attributed to these, SLM has made a significant advancement in the optimization of the processing parameters. The process parameters known as "energy density" Ev, can be defined as laser power (P), scanning at velocity (v), hatch spacing (h) and layer thickness (l) based on Equation (1).

$$Ev = \frac{P}{v.h.l} \tag{1}$$

Several studies have highlighted the correlation between input process parameters and mechanical properties of SLM components. Shipley et al. [113] **studied the effect of process parameters on mechanical properties and found a tolerable amount of compressive strength and acceptable microstructural composition.** It also demonstrated that the energy density plays a role in having a higher relative density of the SLM Ti6Al4V. Taban et al. [114] reported that the higher energy density increases the density of the sample Ti–Nb and as the density lowered, there were balling, porosity, and cracking defects. However, Dhansay et al. [115] suggested that a high level of energy input needs to be maintained during the process to prevent unwanted porosity and residual stress. They also stated that the scan direction should be in the range of 90° to reduce the presence of martensite on the surface. Similarly Yadroitsev et al. [116] stated that the slope angle alignment should be generated parallel to scanning directions in obtaining SLM samples with less than 1% of void. Moreover, King et al. [117] utilized the processing parameters to prevent the formation of large pores on the surface of the sample. They found that the laser power has a greater effect on the development of voids, and with increasing laser power, the crater formed was more prominent. For example, by using one factor at a time (OFAT), Kasperovich et al. [118] suggested the correlation between input parameters and the void as a fracture domain of SLM Ti6Al4V. As shown in Fig. 6, they mentioned that the scanning speed is the most dominate factor (Fig. 6(a)), followed by laser power (Fig. 6(b)) and the most least sensitive was hatch distance (Fig. 6(c)).

Also, the Ev is used to control the product void. The increase in void is produced by the high energy density, which occurs in SLM processing at high power and low velocity [119–121]. As tabulated in Table 4, cumulatively it can be understood as intermediate energy densities which are shown to have void formation. In exploring this outcome, Xu et al. [122] performed the SLM process by changing the layer thickness while keeping the other parameters intact. It was determined that the optimum layer thickness of 30 μm contributed the finest columnar with alpha martensite microstructure in comparison to values of 60 μm and 90 μm. The martensitic structure could lower the elongation, while α-β martensite eventually exhibits higher yield strength and improves tensile elongation to failure. However, a large powder particle of the martensitic structure could have the potential to produce large voids in the build sample. Salem et al. [123] fabricated lattice structure with various processing parameters and suggested that the laser power of 100 W with a scanning speed of 1600 mm/s reduced the void in the strut. Wen et al. [124] clarified processing parameters' impact on densification performance during the SLM technique. When power is set at 60 W, a lot of uneven pores are formed, which are the result of the unmelted material by the laser. On the other hand, Li et al. [125] came to the conclusion that a stronger laser power creates thermal strains in

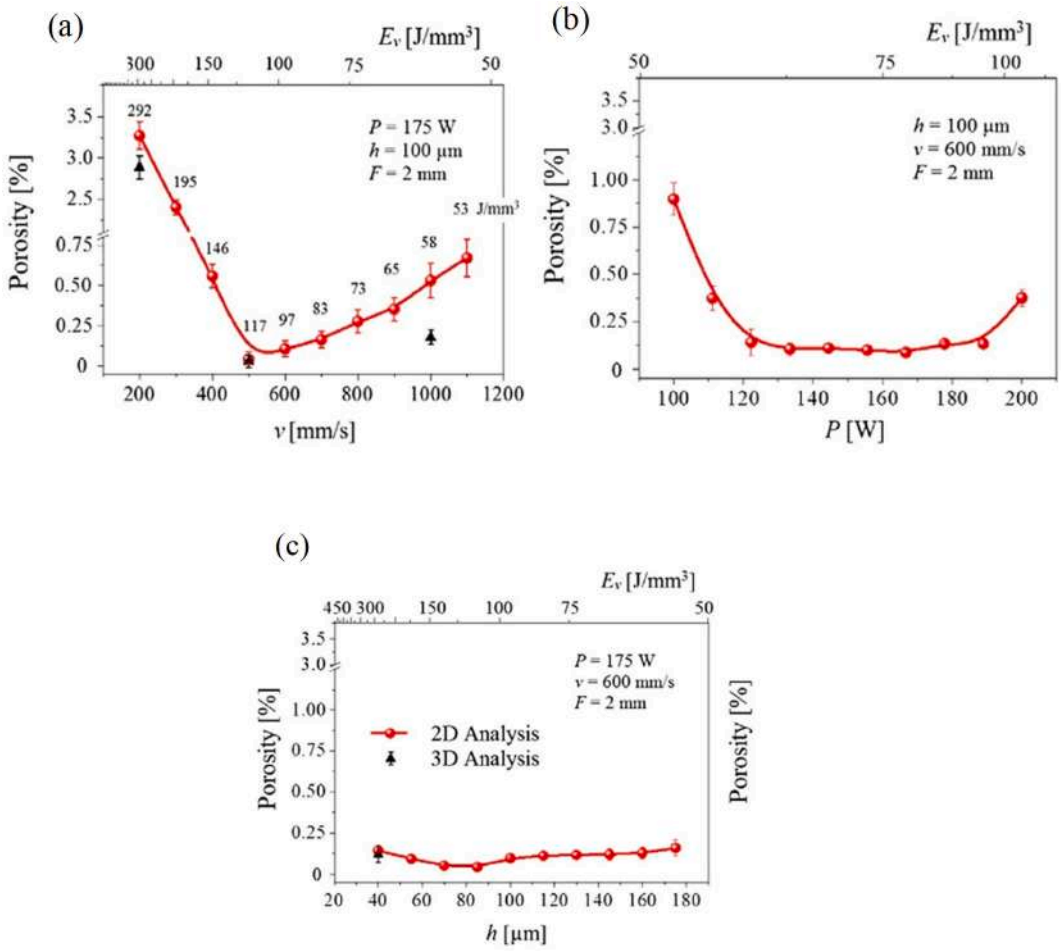


**Fig. 6.** The effect of energy density on void following varies of (a) scanning speed (b) power and (c) hatch distance [118].

**Table 4**
The optimization of process parameter of SLM metallic sample.

| Material | Power (P) | Scanning Speed (mm/s) | Layer thickness (um) | Hatch distance (um) | Remark | Reference |
|---|---|---|---|---|---|---|
| Ti6Al4V | 200 | 1250 | 30 | 0.80 | Surface roughness of SLM were lowered than the EBM caused by the initiation of fatigue crack | [126] |
| Ti6Al4V | 280 | 1200 | 84 | 0.14 | High laser power result to the increase in the porosity | [108] |
| Ti6Al4V | 200 | 1100 | 30 | 0.18 | Voids formed on the surface caused by the process overheating and insufficient fusion | [118] |
| 316L | 100 | 4000 | 50 | 0.13 | Void formed from the vapor cavity caused by the evaporation of the 316L | [117] |
| 316L | 100 | 250 | 50 | 0.114 | Sample of higher scanning speed demonstrated the highest densification and mechanical properties | [114] |
| 316L | 150 | 700 | 50 | 0.50 | Laser power influenced the density, higher laser power yield higher relative density | [109] |
| Ti6Al4V | 75 | 1000 | 250 | 0.77 | Microcracks formed on the surface caused by the melted powder particle | [111] |
| Ti6Al4V | 400 | 4000 | 30 | – | 400 W power showed the lowest internal porosity and defects on the structs design | [123] |
| Ti6Al4V | 200 | 1000 | 50 | 0.12 | The residual stress profile were affected by the process parameters | [121] |

the printed material, which causes to crack since there is insufficient power to melt the powder.

The mechanical characteristics, such as elastic modulus, elongation, and tensile strength are also influenced by those defects [126–129]. The existence of defects that are perpendicular to the loading direction results in the lowering of the mechanical properties of fabricated products. However, most metal alloys in biomedical technology offer a high level of strength as compared to human bone. It tends to introduce a stress-shielding effect when shear stresses arise due to mechanical properties mismatch between the bone and the implant. The decrease in bone density occurs as a consequence of an implant eliminating typical stress from the bone. In order to overcome this issue, many researchers have introduced porous structures or specially designed lattice scaffold to reduce the structural integrity of orthopedic implants. For example, Wang et al. [37] fabricated a medical implant using 316L stainless steel based on cubic, octet, and triply periodic minimal surface (TPMS) to determine their cytotoxicity via the SLM method. It was found that the pore sizes of these lattice struts ranged from 200 µm to 500 µm, resulting in Young's modulus comparable to anatomical bones. The cytotoxicity test showed a 30% cell viability enhancement on the surface with no

toxicity effect. Moreover, Wang et al. [38] mentioned that by modifying the SLM processing parameters, sintering temperature (1200 °C), and structural porosity ((between 3535 μm and 160,160 μm). The mechanical characteristics of 316L stainless steel were equivalent to cancellous bone. Also, Wally et al. [56] and Ran et al. [44] discovered that at a pore size of around 600 μm, the compression stiffness of SLM Ti6Al4V equivalent to bone and outperformed in osseointegration.

### 4.2. Corrosion resistance

The excessive corrosion of the metallic implant such as Ti6Al4V when exposed to the medium or any environment forms passive film consisting of $TiO_2$, $Al_2O_3$, and $V_2O_5$ [130]. These films degrade the surface due to the abrasion and oxidation formed from the relative motions of the implant after implantation. Furthermore, vanadium, which exists in both elemental form and as oxides ($V_2O_5$), is hazardous. Implants based on the Ti6Al4V alloy are reported to exhibit a decline in fatigue strength as a result of surface corrosion pit formation to the dissolution of $Ti^{2+}$ ions in body fluid. The toxic release of aluminium(Al) and vanadium ions can result in chronic disease including osteomalacia [131]. Whereas, Al ions on the surface of the implants during wear and tear might cause neurological disorders and Alzheimer's disease [132, 133]. In SLM, the rapid solidification and high rate of cooling during the fusion powder bed process result in α′-martensite and fine grain development in the microstructure. This is distinct from traditional processing methods like forging and machining. The changes may have an impact on the corrosion resistance on end-product. Table 5 summarizes the investigations of the corrosion properties of SLM in metallic implants. For instance, Dai et al. [134] mentioned that SLM Ti6Al4V had a lower corrosion resistance than the conventional grade 5 alloys because it had more acicular α′ phases and fewer β phases resultant in high cooling rate during the annealing processes in the melt pool bath. The α′ martensite phase easily cracks in a sufficient amount of oxygen and lowering the hardness of the material. Guo et al. [135] found that by mixing of Cu in a base metal of Ti6Al4V powder, it could improve structural porosity of the product. Beside doubling the frequency of β phases in the microstructure, the inclusion of Cu itself could strengthen the corrosion behavior of the structure [136]. Chi et al. [137] demonstrated that the corrosion rate also increased with the increasing of surface roughness. The higher surface roughness of the sintered powder can affect the oxidation kinetics, causing the sample to be easily oxidized when exposed to the simulated body fluid (SBF) [138,139]. The irregulating surface, consisting of pit and valley initiation sites, favors trapping a liquid and drastically dropping the pH value. It leads to the formation of localized corrosion by destabilizing the protective layer [140]. Chiu et al. [141] confirmed that the corrosion can accelerate in SLM Ti6Al4V

**Table 5**
The corrosion properties of the SLM metallic implants.

| Material | Assessment | Surface oxide/ precipitate/ ion | Remark | Ref | Year |
|---|---|---|---|---|---|
| Al–12Si | Effects of laser power on the corrosion resistance | He, Ar, $N_2$ | Pore clusters formed in the microstructure leading to corrosion | Wang et al. [144] | 2014 |
| CoCrMo | Electrochemical techniques and chemical analyses | Cr, O | Martensitic ε phase (hcp) formed on the surface increased the corrosion resistance | Hedberg et al. [145] | 2014 |
| Ti6Al4V | Corrosion resistance is determined in NaCl solution | $TiO_2$ | Corrosion resistance of the SLM caused by the high amount of acicular alpha' and low beta–Ti phase | Dai et al. [134] | 2016 |
| 316 L stainless steel | Grain boundaries and correlation to corrosion | MnS, oxide film | The sample sowed relatively low value of corrosion current density due to the increased of Cr and Mo content and a decrease of Ni in the grain boundaries. | Zietala et al. [68] | 2016 |
| AlSiMg | Volta potential analysis | Al oxide films $Al_2P$ | Larger and coarser microstructure regions showed significantly better potential difference between the phases. | Revilla et al. [146] | 2016 |
| Ti6Al4V-xCu | Effects of Cu content on phase constitution and corrosion resistance | $Ti_2Cu$ | Trapped gas porosity exhibits a limited effect on the corrosion resistance. | Guo et al. [135] | 2017 |
| 316 L stainless steel | Role of MnS in corrosion | MnS, TiN and Al2O3 | Superior corrosion resistance relative to wrought form | Chao et al. [147] | 2017 |
| Ti6Al4V | Effect of heat treatment on the SLM sample | $TiO_2$ | Both horizontal and vertical specimens that have been heat-treated exhibit improved corrosion resistance. | Chandramohan et al. [142] | 2017 |
| 316L Stainless | Different laser scan speed | MnS | The corrosion characteristics of the SLM printed 316L were also revealing higher pitting potentials compared with wrought 316L | Sander et al. [148] | 2017 |
| Ti6Al4V | Corrosive environment of Ringer's simulated body solution | $VO^{2+}$ $Ti^{3+}$ $OH^-$, $Cl^-$ | Corrosion were mainly caused by the formation of passive film during wear and tear | Chiu et al. [141] | 2018 |
| 316L Stainless Steel | NaCl solution and SBF based on the protein albumin. | MnS | 316L Stainless Steel showed higher corrosion compared to the wrought materials attributed to higher surface area covered by voids caused by the AM process | Stendhal et al. [149] | 2018 |
| CoCr | Effect of different laser power on corrosion resistance, and crystalline structure | Passive film, $Cr_2O_3$,CrO $Cr^{3+}$, $Cr^{2+}$ | High laser powers facilitate the formation of complex oxide films, the fast cooling rate which result in the crystalline phase transformation from γ to ε | Wang et al. [150] | 2018 |
| 316L stainless steel | Effects of Phosphate buffered saline on corrosion resistance | Cr oxide film, $Cl^-$, $OH^-$ | SLM sample had a more passive region and higher charge transfer resistance (Rt) SLM 316L SS outperformed the conventional wrought 316L SS | Al-Mamun et al. [151] | 2018 |
| AlSi10Mg | Effect of HIP on the corrosion of SLM sample | Si, $Cl^-$ | Untreated specimens showed superficial corrosion with microcrack formation | Rubben et al. [152] | 2019 |
| AlSi10Mg | Microstructure of the melt pools of SLM sample | Si precipitate, oxide film | Grain size, Al-dendrite, and coarser eutectic-Si network developed melt pool caused by slower solidification rate. | Fathi et al. [153] | 2019 |
| Ti6Al4V | The effect of 12 wt% HCl polish on corrosion resistance | Oxide film, $TiO_2$ | Polishing the surface of the Ti–6Al–4 V alloy enhance the corrosion resistance attributed to the decrease in roughness | Chi et al. [137] | 2020 |
| 7075 Al | Effect of heat treatment on the corrosion of SLM sample | $Al_2Cu$ precipitate | Si phases and θ phases precipitated at the grain boundary has a significant effect to improve the hardness and corrosion properties | Liu et al. [154] | 2020 |

Abbreviation: He-helium, Ar-argon, N2-nitrogen, Cr-chromium, O-oxide, $TiO_2$-titanium dioxide, MnS- manganese(II) sulfide, TiN- titanium nitride, $Al_2O_3$- Aluminum oxide $VO^{2+}$- oxovanadium(IV) cation, $OH^-$-Hydroxide, $Cl^-$- chlorine ion $Cr_2O_3$ -chromium(III) oxide, γ-gamma, ε-dielectric.

samples, due to the mechanical attrition following the tribo-corrosion assessment in *in vitro* of simulated body fluid and chloride solutions. As a result, the rougher surface has the potential to severely increase the kinetics of corrosion and form cracks on the oxide layer that forms to protect titanium alloys. Furthermore, Chandramohan et al. [142] mentioned that the corrosion of the SLM fabricated Ti6Al4V sample was superior in the media solution containing chloride ion due to the less formation of vanadium oxide ($V_2O_5$) on the SLM sample. The insufficient resistance to corrosion of SLM Ti6Al4V was obtained when passive films of $TiO_2$, $Al_2O_3$, and $V_2O_5$ were formed as an exposure effect to a corrosive environment. These films degrade the surface, resultant of oxidation formed from the relative motions of the implant after fixation. However, the oxidation of these elements vary according to the phase-type of α elements (Al) and β elements (V) that diffuse into α and β phases, respectively, which causes an electrochemical difference in the sample. In conclusion, a higher α+β morphology can increase interfacial boundary regions between those phases and finally trigger the sample to corrode. A recent study by Ciliveri et al. [143] demonstrated that the Ti3Al2V produced by the reduction of Al and V in Ti6Al4V showed a reduction in compressive strength of up to 18%. This is attributed to the Al and V elements that formed the β-Ti phase in the Ti6Al4V sample.

One most employed biomaterial is cobalt-chromium(CoCr) alloy, consists of nickel (Ni) and molybdenum (Mo) [155]. The corrosion of CoCr are more prominent in the wet and high ions of the human body where the CoCr releases toxins into the body, forming of cancerous tumors [156]. The corrosion behavior of dental alloys mostly depends on numerous factors, including composition, pH level, post-processing treatment, and clinical circumstances simulation [157]. Like CoCrMo, the main constituent phases consist of γ-austenite and brittle ε-martensite, which are stable at both low and high temperatures; however, the stress interfacial area between these phases can facilitate crack initiation and corrosion [158,159]. Previously, Guoqing et al. [145] studied the corrosion behavior of SLM CoCrMo in PBS and they found that the metal ion released was lower than the cast sample regardless the duration of immersion time. The enhanced resistance to corrosion of SLM CoCrMo mainly caused by the presence of Mo's segregation to the fine cellular boundaries of mainly micron size carbon and the ε-martensite phase. Wang et al. [150] observed that SLM CoCr sample had a superior corrosion resistance after polishing the surface. This is due to the oxides on the inner and outer layer that play essential role in influencing the corrosion resistance.

The corrosion studies of SLM Al alloys (Al–Si alloys) mainly rely on features of surface texture, layer microstructure, residual stress and electrolyte concentrations [154,160,161]. The surface of SLM Al has various grain boundaries and passive film which increase the corrosion [162]. It is self-stable and has good corrosion resistance with neutral solutions; however, when exposed to open air containing chloride ions (pH $<$ 7.0) of neutral body pH, the pitting polarization increased, making it susceptible to corrosion [163]. In general, SLM Al is better corrosion-resistant than the casting products. Several studies have focused on segregating the SLM Al via a coated sample with Mg, Si, and Fe, which are essential to cellular life and improve corrosion resistance. For example, Revilla et al. [146] coated the SLM Al and pure Al samples with silicon-magnesium and submerged them in 0.1 M of sodium chloride (NaCl) to assess their corrosion resistance. The SLM Al demonstrated less Si–Mg segregation than the pure Al counterpart. Similarly, Leon et al. [161] noticed a lower Fe–Mn segregation in the SLM sample; however, several local galvanic cell formations on the pure Al were obtained due to high corrosion of Al, inappropriate to be used in clinical application. According to Rubben et al. [152], the coarser grain that formed in SLM Al–Si sample offered superior corrosion resistance than the cast sample. Fathi et al. [153] evaluated the effect of laser parameters influence on the corrosion resistance of SLM AlSi10Mg by using a 3.5 wt% NaCl immersion similar to bodily fluid. They found that the increased laser energy density reduced the surface roughness by forming cyclic small-to-large melt-pool structures, as shown in Fig. 7. SLM

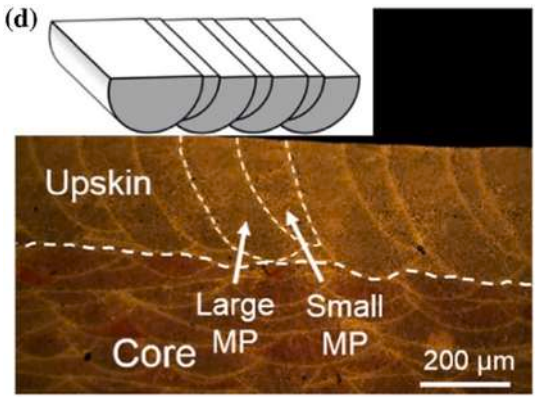


**Fig. 7.** Cyclic melt-pool structure[153].

AlSi10Mg corrosion was dependent on the rate of melt-pool solidification; surfaces with a higher solidification rate contain finer Si precipitates and Al dendrites, which reduces the occurrence of pitting corrosion. A recent study by Liu et al. [154] found a small amount precipitated at the grain boundary and these boundaries significantly improved the hardness and corrosion properties of SLM Al alloys, allowing to be used in biomedical implants.

SS application in biomedical industries has well address. The release of metallic ions of the SS can fasten the corrosion which may cause inflammatory reactions, severe ache and the repercussions of surgery [164]. Following SLM fabrication, austenitic stainless steels like 304L and 316L show an austenitic phase [165]. The high corrosion on SLM 316L was mainly cause by the absence of manganese sulfide (MnS) and the formation of carbon grain structure. Stainless steel is vulnerable to localized corrosion caused by decreased sulfur compounds and chloride ions [166]. Sander et al. [148] stated this pitting is due to the annihilation of MnS. MnS oxidized during pit initiation attracts the concentrated Cl ions. This ion can hasten pit growth and inhibit surface layer repassivation. Zietala et al. [68] and Chao et al. [147] stated that the presence of chloride and absence of MnS during the corrosion evaluation of the 316L sample in electrolyte causes the lower passive current density and higher pitting leading to the corrosion. Chao et al. [147] observed oxide/hydroxide layers in the passive film with higher charge transfer resistance in phosphate buffered saline causes by the absence of MnS. The passive film formation as reported by Al-Mamun et al. [151] found that higher corrosion potential ($E_{corr}$) breakdown potential in SLM SS 316L were three times higher than their wrought counterparts. A recent study by Karimi et al. [167] displayed that the SLM SS 316L can obtained superior corrosion resistance by tailoring the crystallographic texture at low energy density. This is supported by the study by Stendhal et al. [149] and Wang et al. [144] that the superior corrosion resistance in SLM SS 316L were attributed to the refined grains formed on the surface.

### 4.3. Osseointegration of SLM metallic implants

SLM has attracted various medical fields for the manufacturing of metallic structures as tabulated in Table 6. In bone implant, SLM has focused on 316L stainless steel [168–170], Ti6Al4V [171–179], Ti35Zr28Nb [57], $Fe_{81}Ga_{19}$ [180], Pure Zn [124], NiTi [181] and Co–Cr–Mo [182]. As for dental implant, AM focused on Ti6Al4V–5Cu [183], and Co–Cr [184,185].

Orthopedic implants are used for fixation, providing mechanical support and biological integration for the human body once osseointegration is achieved. For instance, stainless steel 316L implants are the most often utilized in the orthopedic industry for treating bone fractures and ruptures due of its affordability and minimal weight to form bone to implant contact. Wang et al. [168] studied the octet gyroid lattice

**Table 6**
Common techniques to enhance the biological properties of the SLM metallic implant from earlier work.

| Material | Implant | Assessment | Yield Strength (Mpa) | In vitro/In Vivo | Remark | Ref |
|---|---|---|---|---|---|---|
| 316L stainless steel | Bone implant | Porous structure | 520.8 | SBF | Porosity 160–35 μm and 58–28% match with those of cancellous bone. | Xie et al. [169] |
| Co–Cr | Dental implant | Porous structure | 300.5 | X-ray testing | Presence of porosity on the sandblasted sample, demonstrating biocompatibility | Al Jabbari et al. [185] |
| Co–Cr–Mo | End prosthetic ankle device | Process optimization | 874.0 | Stereophotogrammetric system | Custom-fit articular surfaces and able to contract as natural joint motion | Liverani et al. [182] |
| Ti6Al4V | Bone Implant | Compatibility | 47.6 | SBF | Apatite formed uniformly on surface after 14 days of immersion | Yan et al. [177] |
| Ti6Al4V | Bone implant | Porosity | 252.1 | *in vitro* cell and white rabbits | 600 μm porosity showed highest bone to implant contact compared to 500 μm and 700 μm | Ran et al. [175] |
| 316L SS | Bone implant | Compatibility | 290.0 | SBF | Poor performance and unstable during long-term experiments in simulated body fluid. | Kong et al. [170] |
| CoCr | Implant | Bone-replicating CoCr porous scaffolds | 252.1 | MG63 | 15–100 μm of irregularities and macro alterations were observed on the porous scaffolds | Caravaggi et al. [186] |
| Ti6Al4V | THR | Modulus of elasticity | 122.8 | | The coated sample showed higher modulus than the cortical bone | Peng et al. [178] |
| Ti6Al4V | Dental | Porosity | 204.0 | MLO-A5 cell seeding | Pore size between 250 and 650 μm are favorable for cell attachment after 28 days. | Wally et al. [187] |
| Ti35Zr28Nb | Bone Implant | Scaffold porosity | 200.0 | SAOS-2 | MTS assay revealed that SLM implant the scaffolds had cell viability Osteoblast adhered on the implant after 4 weeks of *in vitro* | Li et al. [57] |
| Ti6Al4V and Ta | Bone Implant | Porosity | – | Rat distal femur | After 12 weeks in in vivo, there were higher osteoid present on the implant | Bandyopadhyay et al. [179] |
| Ti6Al4V–5Cu | Dental implant | Microstructure and composition | – | Simulated saliva | The specific wear rate of Ti6Al4V–5Cu alloy was about 6.55 times better than that of the TC4 | Zong et al. [183] |
| Ti6Al4V | Implant | Post processing | 760.0 | SAOS-2 | Acid etched sample showed higher biological performance | Jamshidi et al. [174] |
| NiTi | Bone Implant | Modulus | 170.5 | SBF | NiTi structures etched with $H_2O$, $HNO_3$ and HF exhibit elastic moduli that match that of bone tissue | Bartolemeu et al. [181] |
| Ti6Al4V | Bone Implant | Compatibility | – | MC3T3-E1 | HA coated surface sample showed an increased in the metabolic activity on the | Fazel et al. [176] |
| Ti6Al4V | Bone Implant | Coating with HA and cell proliferation | 200.0 | rBMSCs | HA formed on surface, increase the proliferation and enhances cell differentiation | Pei et al. [173] |
| Co–Cr–Mo | Implant | Coating | 180.0 | In vitro femur Wistar rat | Enhanced osseointegration after 12 week of implantation | Latecola et al. [188] |
| Ti6Al4V | Bone Implant | Chemical Treatment | 147.0 | SBF | Apatite formed uniformly under SEM after 7 days of SBF immersion. | Aufa et al. [171] |
| Ni–Ti | Implant | *in vivo* Compatibility | 220.0 | Pig | After 16 weeks *in vivo*, more bone to implant contact on the surface | Naujokat et al. [189] |
| Co29Cr9W3Cu | Joint implant | Porosity | | Rat | Early bone ingrowth into the bone contacts porous surface of the ankle joint | Lu et al. [190] |

Abbreviation: SBF-simulated body fluid, MG63-male osteosarcoma cell, MLO-A5- murine osteoblast to osteocyte-like cell, SAOS-2- female osteosarcoma cell, $HNO_3$-nitric acid, HF-hydrofluoric acid, MC3T3-E1-murine calvarial cell, rBMSCs-mesenchymal stem cells, SEM-scanning electron microscopy.

structure made of 316L stainless steel to determine the appropriate bone cell mitigation and ingrowth via *in vitro* assessment. They demonstrated that this structure offered the highest osseointegration with a good degree of osteoblasts stability attached to the struts. The cytotoxicity test showed 25% cell viability, and the sample was safe even at a high toxicity test concentration (900 μg/mL). Similarly, Xie et al. [169] revealed that the struts structural performance of SS 316L with 28%–58% porosity matches that of the cancellous bone with increased osteoclast in the MC3T3-E1 cell. Kong et al. [170] fabricated SS 316L by using SLM and evaluated apatite formation following simulated body fluid and MC3T3-E1 cells. The F-actin cells, the main components of the cytoskeleton, were heavily spread on the surface sample under the fluorescent test and proliferated into osteoblast cells to form tiny bones. Also, the presence of chloride (Cl), calcium (Ca), and sodium (Na) were obtained after 288 h in the SBF immersion, proven the main build-up of apatite on the sample.

Several studies were conducted to investigate the osseointegration of SLM Ti6Al4V. Ran et al. [175] evaluated the cell attachment on SLM Ti6Al4V, which consists of a variety of circular pores by using *in vivo* rabbit femurs. It was demonstrated that the optimum structure for bone ingrowth was a scaffold with pore sizes of 600 μm. Peng et al. [178] fabricated SLM Ti6Al4V with porosity ranging between 60% and 65%, suggesting that increasing porosity increases the bone-to-implant contact. In contrast, the diamond-shaped unit cell from Ti6Al4V materials was fabricated by Wally et al. [187] by using SLM. The compression stiffness of this novel structure was closely related to cancellous bone, and massive cell viability proliferation was also observed to the strut surfaces after 28 days. However, the implant did not support maximal calcium deposition due to the complex strut structure. Bandyopadhyay et al. [179] fabricated porous Ti and Ta with 30% volume fraction porosity, and after 12 weeks of *in vivo* in rat distal femur, there were higher osteoid formations on both implant surfaces. "The scanning electron microscopy result confirmed that the volume fraction porosity influenced the osseointegrations of the Ta and Ti implants. Furthermore, Jamshidi et al. [174] measured mechanical properties of SLM Ti6Al4V sample in x and y build up directions by using the universal testing machine. Due to the needle-like alpha' martensite structure, a higher Young's modulus and ultimate tensile strength in vertical direction were obtained. The cellular affinity of the sample was improved with increased bone to implant integration after post processing with etching,

as indicated in Fig. 8. An increased cellular activity on the surfaces were obtained, whereby the chemically etched surfaces demonstrated higher biological response with more SAOS-2 cells deposited after 14 days of immersion (Fig. 8(a) and (b)). Bandyopadhyay et al. [191] fabricated Ti3Al2V with reduced Al and V content with different orientation of 0°, 45° and 90° and they found that the compressive yield strength was reduced up to 18% which is 968 MPa compared to Ti6Al4V (1178 MPa) at 90° build orientation. The cyclic loading of Ti6Al4V fabricated at 90° on the other hand were the highest limit of 250 MPa which able to withstand the cycling multiaxial loading during the contraction and relaxation of the anatomical muscle.

Currently, Co–Cr is used in biomedical implants; however, the repetitive force and dynamic exerted on the teeth resulted in fatigue damage to these dental prostheses. For example, Latecola et al. [188] fabricated an implant from SLM Co–28Cr–6Mo and placed it in the rat femur for 12 weeks. Excellent bone integrity, good tissue integration without infection, and no sign of osteonecrosis were elucidated. The sample with 56% of porosity showed the highest bone remodeling proliferation. Another study by Lu et al. [190] produced an ace-centered cubic (FCC), and hexahedron (HCP) of Co29Cr9W3Cu with 65% of porosity to evaluate the bone ingrowth behavior. Both samples were implanted *in vivo* in goats for 12 weeks, and outstanding biocompatibility and osseointegration bone growth inside the pores were obtained. From the *in vitro* study of BMSCs, those samples excellently exhibited cell proliferation and non-cytotoxic under fluorescence staining. Similarly, by Caravaggi et al. [186] found that most of the CoCr strut scaffolds showed cell viability and high ALP; however, unstructured pore size had a reduced effect on the on cell vialibility and adhesion while smallest pore size structure demonstrated the least bone remodeling for the formation of anatomical bone.

Naujokat et al. [189] printed the nickel–titanium (NiTi) which belongs to the group of shape-memory alloys (SMAs). The clinical plantation demonstrated that there was no sign of local inflammation, or any wound healing disturbance *in vivo* of pigs. The implant which has direct contact with the pig showed well connective tissue between the struts and the bone overgrowth with nearly complete coverage of the implants.

### 4.4. Antibacterial

Implant infection caused by bacteria, also known as osteomyelitis (OM), is a serious issue in the field of biomedical implants that may result in bone loss known as osteolysis. These contaminations develop through the inflammatory response of the human body against microbials that spread through the bloodstream toward the implant. Then, the amount of antimicrobial on the surface of AM implants has been increasing due to the resistance of microbials to antibiotics [192]. The microbial can colonize the surface of AM implants by forming a thin film known as biofilm. Fig. 9 shows the biofilm formation process of bacterial on the SLM surface. It begins with the microorganisms attach to a surface via van der Waals interactions and then the bacteria colonized to the implant surface [193]. During colonization, collagen-binding adhesive proteins known as polysaccharides between the bacteria cause stronger hydrophobic/hydrophilic interactions [194]. Then, the bacteria develop, and the cells are accumulated through proliferation. A stable formation of bacteria that underwent mitosis is divided, followed by the maturation phase, which is distributed around the sample [195].

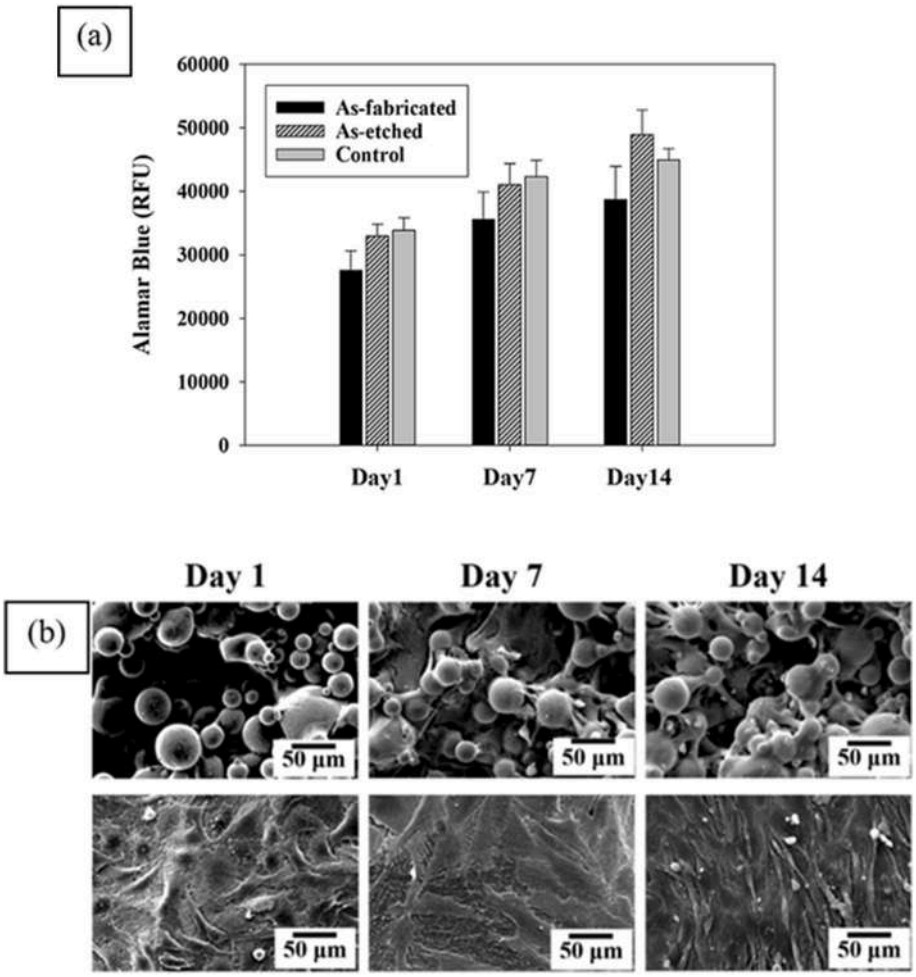


**Fig. 8.** Assessing the SAOS-2 cells' metabolic activity after seeded on the prefabricated Ti6Al4V surface [174].

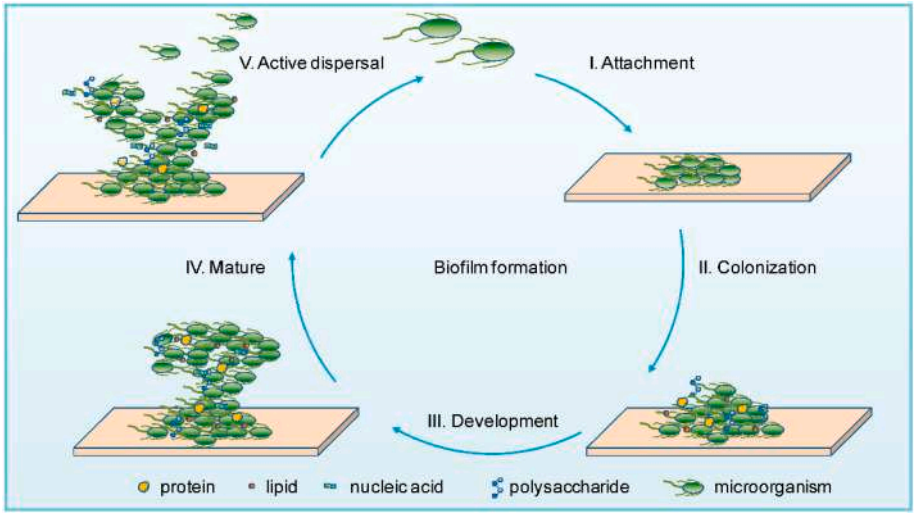


**Fig. 9.** Stages of biofilm formation on the surface of implants [199].

During the active dispersal, the bacteria evolve in multiple layers, then forming a thick layer of biofilm [194]. Finally, the bacteria divide into multiple levels of biofilm formation, including initiation, maturation, and dispersal, colonizing on other location [196]. They are usually known as *Staphylococcus aureus (S. aureus)* and *Escherichia coli (E. coli)*, both are gram-negative bacteria and highly resistant to most medicine and antibiotics [197]. It has been shown that microbial activity is responsible for more than 20% of overall implant failure and causes billions of dollars in damages each year [198]. Microbial infection is acknowledged to be one of the main causes of implant failure in biomedical industries. Table 7 summarized the methods to reduce the implant infections and toxicity from the previous study.

A study has been conducted to improve the antimicrobial mechanism via copper (Cu)-bearing which an important ion in living organism act as an bactericidal element. Therefore, developing a new method in SLM for incorporating different elements into the alloy and maintaining its mechanical properties and biocompatibility is crucial. The new strategy in developing new alloys has been promoted back in 2004 by Cantor et al. [216] and Yeh et al. [217], whereby they proposed multicomponent of materials that exhibited the "core" properties of high entropy, lattice, and slug diffusion. These are known as entropy alloys or multicomponent ions. Using this method, the Cu is able to be designed with good antibacterial properties and excellent mechanical properties. A recent study by Zhou et al. [218] showed that the new type of antibacterial implant containing Cu exhibits good antimicrobial than the common 316L implant in the market. Similarly, Wang et al. [219] indicated the

**Table 7**
Method to reduce implant infections and toxicity.

| Material | *In Vitro*/Antimicrobial Technique | Yield Strength (MPa) | Remark | Ref | Year |
|---|---|---|---|---|---|
| CoCrCu | *E. Coli* (ATCC25922) and *S. aureus* (ATCC 25923) | 565.0 | CoCrCu alloys have effective antibacterial and antibiofilm properties. | Ren et al. [200] | 2016 |
| Ti6Al4V | MRSA strain AMC201 and hMSCs | 636.5 | SLM PEO silver-releasing implants demonstrated significant antibacterial efficacy, with no evidence of cytotoxicity. | Hangel et al. [201] | 2017 |
| Ti6Al4V–Ag | *E. Coli* (ATCC25922) | 860.0 | Ag exhibit moderate antibacterial capability compared to Cu | Macpherson et al. [202] | 2017 |
| Ti6Al4V-xCu | *S. aureus*, (ATCC 6538) and *E. coli* (ATCC 2592) | – | Stronger antibacterial properties were demonstrated by SLMed Ti6Al4V alloys containing 4 and 6 wt% Cu. | Guo et al. [203] | 2017 |
| CoCrWCu | *E. coli.* (ATCC 25922) | 540.0 | The SLMed CoCrWCu alloy had outstanding antibacterial action of *E. coli.* | Lu et al. [204] | 2018 |
| Ti6Al4V | MG-63 | – | Ti6Al4V alloys with 6 wt% Cu content exhibit good cytocompatibility. | Luo et al. [205] | 2018 |
| Ti6Al4V | MC3T3-E1 | 850.0 | Samples containing zinc showed inhibitory effects *on S.sanguinis.* | Wu et al. [206] | 2019 |
| ZK30-Cu | *S. aureus* (ATCC25923) | – | As Cu content increased, the colonies of *S. aureus* decreased | Xu et al. [207] | 2019 |
| Ti6Al4V–TiO2/ Ag | *E.Coli* (MG 1655) | 1110.0 | Ceramics strengthened with titanium had a markedly impaired antibacterial action. | Rahmani et al. [208] | 2019 |
| 316L | BMSCs, *E. coli* (ATCC 25922 and *S. aureus* (ATCC 25923) | 470.0 | stainless steel 3D printed with zeolite coatings containing silver have improved antibacterial activity | Qing et al. [209] | 2020 |
| Fe–xCu | *E. coli* (ATCC 25922) | – | The SLMed Fe-2.3Cu exhibits significant antibacterial activity. | Guo et al. [210] | 2021 |
| ZK30-Cu-Mn | MG63 and *S. aureus*, (ATCC 25923) | 730.0 | The cells adhered on the SLMed with spindle and round shape according to the cell morphologies. No detection of S.aureus after 72 h | Xie et al. [211] | 2021 |
| Ti-xCu | MG63 *E. coli* (ATCC 25922) | 760.0 | A continuous, very potent antimicrobial rate (antibacterial rate>99%) was demonstrated by the SLMed Ti–3Cu. | Ji et al. [212] | 2021 |
| Ti6Al4V | MC3T3-E1 *S. aureus* (ATCC 25923) | 880.0 | Increased alkaline phosphatase levels and pre-osteoblast metabolic activity | Fazel et al. [176] | 2021 |
| CoCrCuFeNi | *E. coli* (ATCC 25922) and *S. aureus* (ATCC 25923) | 516.0 | Excellent antibacterial properties of the CoCrFeCuNi HEA suitable for use in medical applications | Gao et al. [213] | 2022 |
| Ti6Al4V | MG63 and S.aureus (ATCC 25923) | 950.0 | $Ca^{2+}$ ions with anatase $TiO^2$ layer increased the bioactivity and adhesion of the scaffold | Rajendran et al. [214] | 2022 |
| Ti6Al4V–Ag | *E. coli* (ATCC 25922) and *S. aureus* (ATCC 25923) | 890.0 | The antibacterial capabilities increased after 12 days against *S. aureus and E. coli* | Sedaghat et al. [215] | 2024 |

Abbreviation: MRSA-methicillin-resistant *Staphylococcus aureus*, and hMSCs PEO- Plasma electrolytic oxidation MG-63- human osteosarcoma cell, MC3T3-E1- murine calvarial cell line.

copper bearing of 316L results, whereby there was no cytotoxicity effect on rat mesenchymal stem cell and excellent antimicrobial against *E.Coli* and *S. aureus* after 24 h of incubation. This is attributed to the Cu that homogenously distributed on the microstructure of the sample. However, the *in vivo* test did not demonstrate anti-infection under mesenchymal stem cell.

Many attempts have been made to use antibacterial alloys and reduce the colonization of biofilm. For example, Chen et al. [220] evaluated the performance of blended powder, based on CoCrFeMnNi as a high entropy alloy (HEA) fabricated utilizing SLM technique. This study found that the HEA alloy can release more Cu2+, preventing biofilm formation. Also, Gao et al. [213] fabricated antibacterial CoCrCuFeNi HEA alloy via SLM to determine the antibacterial capability and biofilm formation. After 24 h of immersion in the bacterial colony of *S. aureus* and *E. coli*, the sample possessed antibacterial rates against *S. aureus* and *E. coli*, almost 95% and 80%, respectively. A thin biofilm was formed with more dead bacteria on the surface, indicating an excellent antibiofilm formation capability. It is due to the release of Cu ions and the act of microphage that engulf the bacteria.

Many studies have explored CoCr material in SLM as base metal coping due to their favorable properties, including excellent mechanical strength, ductility, corrosion resistance, and biocompatibility. For instance, Ren et al. [200] fabricated novel metal copings of CoCrCu alloy by using SLM and proved that the addition of Cu increased the antibacterial and antibiofilm capabilities. Also, Lu et al. [69] used a highly dense CoCrWCu alloy to fabricate dental restoration following the ISO standard. A fine microstructure with a columnar grain was obtained, and the *E. coli* attached to the CoCrWCu were fewer after 24 h than the control group.

Currently, researchers have explored the optimum surface roughness to prevent microbial attachment on the surface of biomedical implants. Moore et al. [221] suggested that a fine surface roughness can resist the *S. aureus* attachment on the hip-stem SLM implant. Fig. 9 compares the gram-negative bacteria *S.aureus* attachment between a fine and rougher surface of the SLM implant. It was found that the Ra value of the hip stem, 78.440 ± 4.85 μm showed higher biofilm colonization (Fig. 10(a)) in comparison to its smoother counterpart, of 17 ± 0.42 μm (Fig. 10(b)). *S.aureus* is the most common pathogen of periprosthetic joint infections that prefers the creases, shard edges or ridges on the implant's surface. These fasten the delivery of nutrients from both sides of the biofilm, encouraging bacterial growth and leading to infections.

Currently, Ti-based alloy has been modified by mixing some alloys like Cu or Ni to provide a strong antibacterial resistance in biomedical implant [203,205]. Guo et al. [203] doped Cu into Ti6Al4V powder while producing the implant by using SLM (Mlab-R, Conceptlaer). The effect on microstructure, phase constitutions, antibacterial properties and cytotoxicity of samples were observed. The Cu element is effectively fused from Ti6Al4V, resulting in stable properties of antibacterial activity against *E.coli* and *S. aureus*. An excellent cytocompatibility from an *in vitro* test by using BMSc was obtained; however, the density of the implant gradually decreased as the Cu content increased, attributed to the presence of micropores. Another study by Luo et al. [205] suggested that 6% of Cu added into SLM Ti6Al4V exhibited good cytocompatibility *in vitro* MG-63. The SEM and fluorescent staining demonstrated excellent cell morphology and adhesion on the sample. The most recent study by Bandyopadhyay et al. [222] manufactured a Ti3Al2V custom alloy with the addition of 10 wt% Ta and 3 wt% Cu to investigate the antibacterial resistance against *P. aeruginosa* and *S. aureus* at the initial stage of osseointegration. The bone implant contact was the highest and showed no gaps on the sample, and the presence of Cu increased the osteoid formation, which filled the pores of the Ti3Al2V implant. *S. aureus* and *P. aureus* decreased with the duration of the agar plate counting after 36 and 48 h compared to the conventional CpTi and Ti6Al4V implants, as shown in Fig. 11. This is attributed to the antibacterial effect of the $TiO_2$. Photocatalytic property that results in the lysis of the bacterial cell membrane.

Surface modification or coating on the surface of SLM implants is one as an effective method to enhance the bioactivity of Ti6Al4V. Rajendran et al. [214] treated the surface of SLM Ti6Al4V with silver nitrate ($AgNO_3$), an inorganic compound to enhance the bioactivity as well as antibacterial capability. The SLM Ti6Al4V was coated for 1 h at a temperature of 600 °C and demonstrated good bioactivity in the simulated body fluid (SBF), which corresponded to a higher number of $Ca^{2+}$ and anatase $TiO_2$ layers. A good Ca:Ag ratio of 9.9:0.1 for the prevention of attachment of bacterial in *S.aureus* immersion was observed. Similarly, Fazel et al. [176] used silver nanoparticles (AgNP) to coat the SLM sample containing $Ca^{-}$ and $P^{-}$ ions by using the PEO method. The result showed a spindle-like hydroxyapatite(HA) formed which allow the anchorage of osteoblast and osteoclast cell for bone remodeling process. There was a higher level of alkaline phosphatase activity (ALP) in *in vitro*

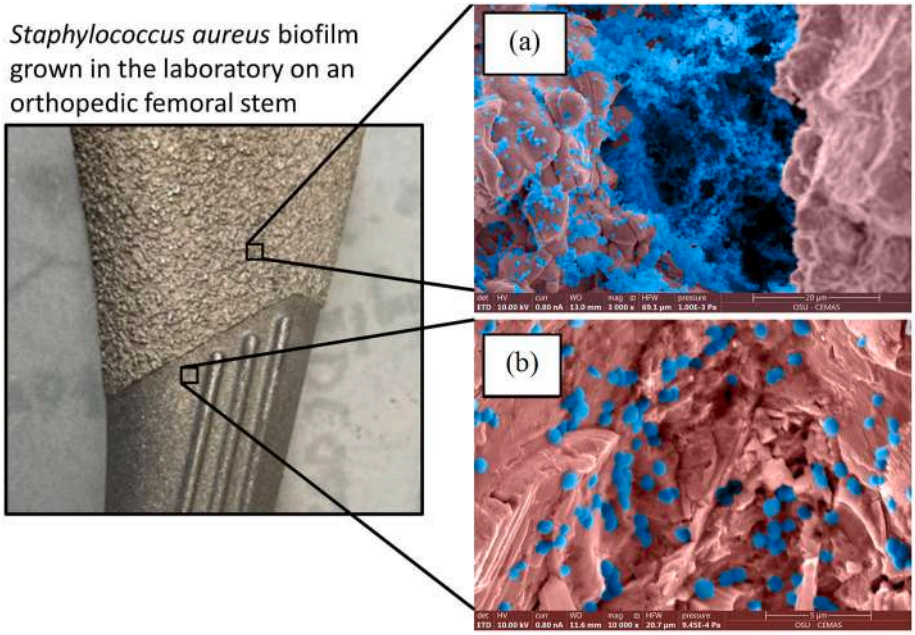


**Fig. 10.** SEM images of bacteria adhered to surfaces with different roughness on femoral hip stem of (a) smooth counterpart and (b) rough counterpart [221].

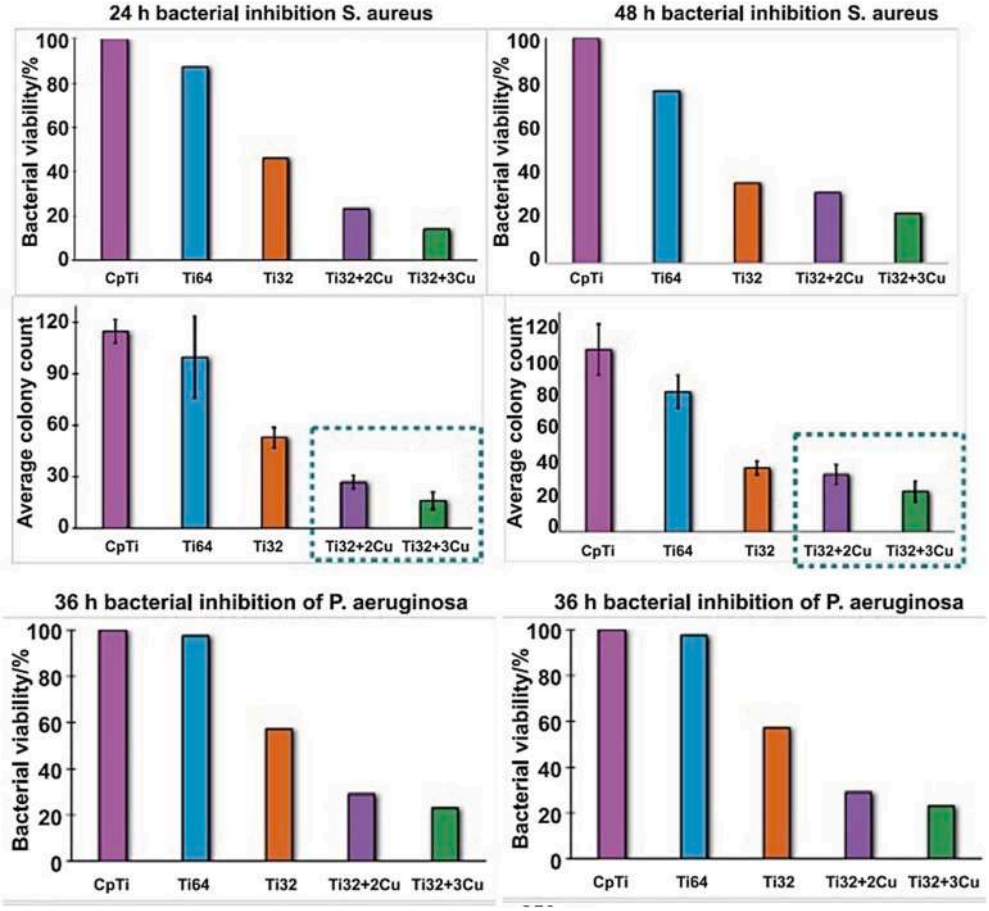


**Fig. 11.** Bacterial viability and bacterial colonies on the CpTi, Ti6Al4V and Cu addition Ti3Al2V [222].

study, as well as a crystalline transition of the Ca–P compound formed on the surface. After 8 h of culture in *S. aureus*, the trace amount of AgNPs in the PEO layers significantly increased (***p < 0.001), improving their antibacterial activity. This is due to the embedded AgNPs that release the Ag ions, which prevents the bacteria from attaching and colonizing the implant surface. Recent study by Sedaghat et al. [223] doped AgNPs with Ti6Al4V and tested the antibacterial efficacy for a duration of 12 days in *S. aureus* and *E. coli*.There was an increase in the mineralization of MSCs attached to the AgNP-coated implant ($p < 0.05$). The *S. aureus* and *E. coli* bacterial properties decreased within 96 h, and after 288 h, *S. aureus* possessed a thicker peptidoglycan layer compared to *E. coli*, which acted as a protective barrier that prevented the penetration of antimicrobial agents. The On the other hand, Chen et al. [224] deposited Ag composite coating on the surface of the SLM implants with a varied time from 0.5 h to 4 h to evaluate the antibacterial rate. As the spraying time increased, the antibacterial rate of the *E. coli* on the implant increased to 60%. This corresponds to the higher release of Ag ions that generate reactive oxygen species (ROS) when in contact with human cells.

Alloying Ag with Ti is an alternative to increasing antibacterial capabilities and localizing antibiotics during implantation. A study by Xu et al. [225] demonstrated that the addition of Ag to Ti–Mo showed a minimal effect on cell viability compared to the control group. The cytotoxicity study indicates that the Ag exhibits no cytotoxicity to the Ti alloy, where the cells are clustered in a circular shape and connected by pseudopods. On the other hand, the antibacterial behavior of the Ti–Ag decreased up to 85%, attributed to the increase in Ag concentration. A similar study by Macpherson et al. [226] ound that Ag-containing Ti showed moderate antibacterial properties with a 300% increase in ductility. They concluded that it could be caused by the low alloying content of Ti6Al4V. Lowther et al. [226] assessed the Ti–Ag alloys that were fabricated by the powder blend method. The high Ti–Ag content, up to 35% intermetallic, showed an insignificant change in antimicrobial action compared to the control sample. However, Ag precipitate formed, attributed to the increased diffusion at the grain boundaries. In an *in vivo* study, Liu et al. [227] fabricated a Ti–Ag alloy with a nanotube coating and implanted the sample on the right femoral of a rat. There was an increase in alkaline phosphatase expression, and the highest cell attached to 4% of the Ag content. As for the low toxicity, the 2% content of Ag was optimal. The study was consistent with a previous study where it was demonstrated that 2% wt Ag–TiO2 exhibited the highest cell attachment [228,229].

Titania ($TiO_2$) is a ceramic material catalyst containing manganese and rhenium, which is used as a thin film or additive in composites to fasten the chemical reaction between the sample and the active coating site [230]. However, it has limitations to be used due to its high brittleness and low fracture toughness (2–3 MPa $m^{1/2}$) [231]. Rahmani et al. [208] fabricated lattice structure made of Ti6Al4V and coating with $TiO_2$-2.5% Ag by using plasma spark sintering. The result suggested that there was no significant effect on the antibacterial activity of *E. coli* after the addition of TiO2-2.5% Ag.

Among Mg alloys, ZK30 also known as Mg–3Zn-0.5Zr has attracted attention in biomedical field due to their good biodegradation resistance and mechanical properties. The antibacterial properties of ZK30 can be improved by alloying with any antimicrobial metal. Xu et al. [207] studied on the antibacterial and biodegradation resistance of ZK30 with the addition of antimicrobial Cu. The grain size of the ZK30 decreased, and the hardness increased with the increasing amount of Cu content. The antibacterial effect of *S. aureus* increased as the soaking time increased, attributed to the increase in surrounding pH that degraded

Cu-ZK30. A recent study by Xie et al. [211] evaluated the combination of Cu-ZK30 with Mn, known as an essential element in body microenvironment to enhance the biodegradation and antibacterial of Cu-ZK30. After 7 days of MG63 cell culture, the number of stain cells on the surface increased, suggesting the SLM sample is cytocompatibility, and the colonies of *S. aureus* were none after 72 h of immersion in a pH 7.2 environment. The sample of the highest Mn content (8 wt%) demonstrated the strongest antibacterial ability and good cytocompatibility. However, The micro-galvanic corrosion between the Cu-containing intermetallic compounds and the alloy matrix causes Cu-containing ZK30 to erode in the 7.0 pH conditions [232–234].

Table 8 demonstrates the previous study of modifications done on the SLM metallic biomedical implants prior to their clinical application on their osseointegration, antibacterial, corrosion, and mechanical properties. Generally, this table provides a valuable study on the relationship between the modifications and their biocompatibility. It is important to recognize the limitations, of the SLM metallic implant like the high elastic modulus and corrosion resistance. However, due to their superior bone remodeling and antibacterial capabilities, Ti6Al4V and Cp-Ti dominated the SLM-fabricated implants used in the biomedical field. Thus, further study, such as further modification and alloying processes, needed to be done on other metallic implants to enhance their reliability prior to clinical application.

## 5. Post processing

In improving the antibacterial, biocompatibility, corrosion resistance, and clinical properties of SLM metallic to meet the appropriate applications and treatments, various surface modification technologies have emerged. The post-process modification techniques are divided into four categories: mechanical, physical, chemical, and biological modification, as shown in Table 9.

### 5.1. Mechanical and physical modification of SLM implants

The mechanical and physical modification of the implant is a method of exposing the surface to charge, laser, or plasma to improve their performance by altering the topography of the metallic substrate. These two techniques do not change the chemical composition and properties of the SLM metallic implant. They are commonly known as plasma spray [239], plasma immersion [240], and physical vapor deposition [241]. In order to improve crack resistance of implant, Li et al. [242] employed plasma spray ceramic coatings of $Al_2O_3$, $ZrO_2$, and $Al_2O_3$–$ZrO_2$ composite on SLM CoCrMo alloy. The coating adhesion reached 238 MPa and there were morphology enhancement with fewer microcrack and higher corrosion resistance. This is due to the melting temperature of $Al_2O_3$ (2050 °C) and $ZrO_2$ (2680 °C) below the melting temperature, which led to few porosity and micro-cracks upon solidification. In addition, the conventional mechanical techniques, such as machining, grinding, polishing [243,244], sandblasting [245] and friction stir has been widely explored to modify the surface of SLM fabricated sample. Likewise, Liang et al. [243] used the laser polished technique on SLM-built Ti6Al4V and found that the roughness of the sample reduced from 10.2 μm to 2.1 μm. The lowest roughness sample exhibited the highest cell attachment in *in vitro* of MC3T3E1. Besides, eliminating the partially melted powders, Zhao et al. [244] suggested a reduction of 75% of the roughness of SLM-fabricated SS 304L following electrochemical polishing of the sample. Similarly, Obeidi et al. [246] found that the surface roughness of SLM fabricated SS 316L was reduced from 10.4 μm to 2.7 μm after laser polishing, enhancing the apatite formation after 72 h of immersion in a pH 7.2 environment. Nevertheless, Bai et al. [247] demonstrated formation of oxide on the top surface of SLM SS 316L caused by the heated particles during polishing. Li et al. [248] polished the sample of Inconel 718 of temperature 1683 K and cooling of 2.46 × 106 K/s that showed reduction of porosity up to 65%, mainly caused by the equiaxed columnar grain formed on the surface.

Sandblasting involves the abrasive modification that is fed at high air flow directed to the substrate at high pressure. It is a common method to clean or to smooth and clean the surface of SLM implant. Yang et al. [249] employed sandblasting on SLM Ti and demonstrated a sample lowest water contact angle. It showed the osteoclast differentiation and bone osteoclastogenesis in *in vitro* study, reducing the bone resorption after implantation. Lv et al. [250] removed the spheroidized particles and corrosion cracks on SLM SS 316L sample surface. The pores formed after sandblasting inhibit the $Ca^{2+}$ and $P^{-}$ attachment under the SBF. Baciu et al. [251] polished the dental implant of SLM CoCr alloy by using three stages of sandblasting and found that a roughness of sample approximately 4.34 μm. The lamellar like cell of keratinocyte was observed on the surface. The physical and mechanical methods from previous study have shown simple technique to improve the surface of implant. However their ability in optimizing the surface of SLM metallic implants is limited yet inadequate for complex shapes of implants.

A chemical vapor deposition method called plasma vapor deposition is used to deposit a thin films originating from a gas vapor [252]. It has increased applications in engineering field for its ability to control temperature, deposition, and distance rate, allowing the substrate to be protected against wear, corrosion, and damage. Lassegue et al. [253] deposited CrZr on SLM Cu to enhance the optical absorption, however, the coating was oxidized causing it to leach. On the other hand, Wozniak et al. [254] coated SLM Cp-Ti with CrN and TiN, whereby the sample showed best pitting corrosion resistance with transpassivation potential of 3052 ± 143 mV and a maximum charge transfer resistance of 1132 $k\Omega cm^2$ in the charge transfer resistance. This is attributed to the plasma vapor coating that formed double layer consisting of compact and a porous external layer. Nevertheless, there is still lack of study in plasma vapor deposition in biomedical field.

### 5.2. Chemical modification of SLM implants

Chemical modification method refers to the various processes that involve the alteration of the chemical composition or structure with the presence of a new substance to improve the performance of the metallic implant. These methods are mainly classified as chemical vapor deposition, electrochemical treatment, sol-gel, etc. The most common is chemical vapor deposition, whereby a solid material is deposited from a vaporization by chemical reactions. Konalov et al. [255] modified the surface of Ti-6.5Al–1Mo–1V–2Zr with Ni-based superalloy Ni–16Co–11Cr powder with coating thickness of 70 μm–130 μm and surface layer and the substrate is wave-shaped (Fig. 12). As shown in Fig. 12, microcracks started to appear throughout the coating due to mismatch between the substrate and the coatings coefficient of thermal expansion (CTE). Sitek et al. [256] modified the surface of nickel superalloy IN 718 with the participation of $AlCl_3$ vapor at a temperature of 1040 °C, and lasted 8 h at a reduced pressure of 150 kPa. Nevertheless, the IN 718 showed degradation in mechanical properties with visible microcracks after the aluminizing process. The reduction in mechanical properties was mainly caused by the brittle fracture on the sample.

The sol-gel method occurs in a solution based. Macera et al. [257] prepared silica sol-gel coating to enhance the corrosion resistance of SLM Al6061. The sample showed pH values ranging between pH 6.9 and pH 7, demonstrating a good corrosion resistance. Koo et al. [258] prepared sol-gel dense SiO2 insulation into SLM Fe-6.5 wt% alloy, whereby the coating is able to preserve the shell thickness of 2.2 mm. Xu et al. [237] improved the biological and bone regeneration of SLM Ti6Al4V through subsequent alkali treatment. Thus, previous study has stated that the development of surface modification technique of SLM metallic implant to satisfy the clinical needs. The chemical mechanism of these modifiers is relatively complex and expensive and often used in the preparation of complex samples.

**Table 8**
Summary of the SLM metallic implant's modification, osseointegration, antibacterial, corrosion, and mechanical properties.

| Material | In vitro/In Vivo Studies | Modification | Osseointegration | Antibacterial/ Toxicity | Corrosion | Tensile strength (MPa), Yield strength (MPa) and Young Modulus (GPa) | Ref |
|---|---|---|---|---|---|---|---|
| Ti6Al4V | rMSCs | Reinforced with growth factor BMP-2 | The sample's cell growth was higher than that of the uncoated group. | | | | Lv et al. [235] |
| Zn | MG63 | Al | There was an increase in macrophage labeling and fibrous encapsulation. | | The least amount of corrosion is inhibited by lower Al concentration. | 37, NR, 95 | Guillory et al. [97] |
| Ti6Al4V | L-929 fibroblast cell | Simvastatin/ poloxamer 407 hydrogel | Improved neovascularization under *in vitro* study | Poloxamer 407 showed the lowest toxicity and weak immunogenicity. | | 960,NR, 90 | Liu et al. [236] |
| CoCrCu | rMSCs | Cu | The addition of Cu increases cell adhesion and decreases biofilm formation on the sample. | On the surface of SLMCoCr alloys, 98% of *E. coli* and 92% of *S. aureus* survived. | | 991,636.5220 | Ren et al. [200] |
| Ni | Dorsal sides of mice | Doped with zirconium (Zr) | After 4 days, the tissue was excised from the sample with no inflammation response. | A thin layer of biofilm formed on the sample. | When immersed in the PBS, the sample exhibits the least amount of corrosion. | | Sonofuchi et al. [155] |
| Zn | HUVECs | Pure Zinc and Zinc Alloy | After four days of incubation, the Zn alloy had the highest cell viability. | Severy cytotoxicity of the pure Zn | The galvanic effect caused the release of higher Zn ions during corrosion. | 225,130,85 | Wang et al. [64] |
| SS 316L | rMSCs | Doped with Cu | The MTT assay demonstrated no cytotoxic effect *in vitro*. | The sample with Cu doping showed the highest antimicrobial activity against *E. coli.* | | NR,45.2,20.9 | Wang et al. [219] |
| Ti6Al4V | MC3T3-E1 | Modified with HF and $HNO_3$ which of acid etching | After 8 weeks of *in vivo*. The etched sample exhibits a higher bone-to-implant contact, up to double that of the untreated sample. | | | 900,850, 78 | Xu et al. [237] |
| Zn | MC3T3-E1 | | Despite the release of passive corrosion products, no toxicity was evident after up to 20 months of implantation. | | Zinc oxide, phosphate, and carbonate are the primary factor for the Zn implant's corrosion. | 430, 325, 105 | Drelish et al. [98] |
| Ti6Al4V | BMSCs | Cu | Higher Cu exhibits cytocompatibility when implanted *in vitro.* | A higher Cu content exhibits stable antibacterial capability against *E. coli* and *S. aureus.* | The corrosion of the Cu-doped sample was lower than that of the Cu-free sample. | 80 | Guo et al. [203] |
| Fe | Rabbit abdominal aorta | Nitride | The mass loss of the Nitride Fe sample was twice as high as that of the Fe sample, indicating that Fe is biocompatible for use as an implant. | | The PBS study showed insoluble corrosion products were safe and were cleared by the macrophages. | 92 | Lin et al. [69] |
| Ti6Al4V | | Cu and Ag | | Cu's antibacterial capabilities were higher than Ag's. | | 930,860,113 | Macperson et al. [202] |
| Mg–Zn | SBF | HA | Bone-like apatite formed a stable layer of $MgCl_2$ after 1 week of immersion. | | The grain refinement that formed on the SBF hindered hydrogen degeneration, resulting in decreased biodegradation. | | Shuai et al. [91] |
| Ti6Al4V | hMSCs | AgNPs | In rat femurs with greater bone-to-implant contact, samples show no cytotoxicity. | The Ag sample exhibited antibacterial activity against pathogens and reduced inhibition of surface microbial growth. | | 900,790,110 | Hangel et al. [201] |
| Ti6Al4V | Beagle | | Osteoblast cells in the sample increased after 4 weeks of implantation. | | TiO crevices formed on the sample due to the argon ion bombardment, increasing corrosion. | | Zhao et al. [172] |
| SS 316L | SBF | Quenched | A globular and thick layer of apatite formed on the 316L sample compared to the quenched sample. | | After 288 h in SBF, the passive current and corrosion current showed a higher corrosion potential on the 316L sample than the quenched sample. | 614.3470.8,55 | Kong et al. [170] |
| CoCr | *E.coli* | Cu and Mo | Cell attachments were higher on the Cu sample, specifically | Compared to Mo, Cu-bearing CoCr exhibits excellent | | 951,503, 215 | Lu et al. [204] |

(*continued on next page*)

**Table 8** (*continued*)

| Material | In vitro/In Vivo Studies | Modification | Osseointegration | Antibacterial/ Toxicity | Corrosion | Tensile strength (MPa), Yield strength (MPa) and Young Modulus (GPa) | Ref |
|---|---|---|---|---|---|---|---|
| | | | on the cellular and columnar structures. | antibacterial capabilities against *E. coli*. | | | |
| CoCr | MG63 | Cu | The alkaline phosphatase activity was higher in the Cu-doped sample, promoting cell proliferation. | 90% antibacterial activity against E. Coli and *S. aureus* was demonstrated by 4% Cu, while up to 99% antibacterial activity was demonstrated by 6% Cu. | Compared to 2% and 4%, 6% of Cu showed the least corrosion. | | Lou et al. [205] |
| SS 316L | L929 | HA | The HA-coated sample showed higher biocompatibility and exhibited no cell cytotoxicity. | | | 730,NR, 214 | Lou et al. [238] |

Abbrevation: rMSCs-rat mesenchymal stem cells, BMP-2- Human Bone morphogenetic protein 2, Zn-zinc, MG63-human osteosarcoma cell, Al-aluminuium, L-929-fibroblast cell, hMSCs-human mesenchymal stem cells, *E.Coli- Escherichia coli, S.aureus-Staphylococcus aureus*, Ni-nickel, Zr-zirconium, HUVECs- Human umbilical vein endothelial cells, MTT assay- (3-[4,5-dimethylthiazol-2-yl]-2,5 diphenyl tetrazolium bromide) assay, MC3T3-E1- murine calvarial cell line, HF- hydrofluoric acid, $HNO_3$- nitric acid, Fe-iron, PBS-phosphate buffered saline, SBF- simulated body fluid, HA-hydroxyapatite, AgNPs-silver nanoparticles, TiO-titanium(II) oxide, Mo-molybdenium, L929-mouse fibroblast cell.

**Table 9**
Surface modification categories to improve SLM based implants.

| Mechanical | Physical | Chemical | Biological |
|---|---|---|---|
| • Grinding<br>• Blasting<br>• Polishing<br>• Machining<br>• Shot peening | • Physical Vapor deposition,<br>• Chemical polishing<br>• Ion Implantation<br>• Thermal Spray<br>• Microwave | • Alkaline<br>• Acid<br>• Hydrogen peroxide<br>• Sol gel<br>• Chemical Vapor Deposition<br>• UV Irradiation | • Biomimetic<br>• Cross-linking<br>• Cell seeding<br>• Chemical conjunction |

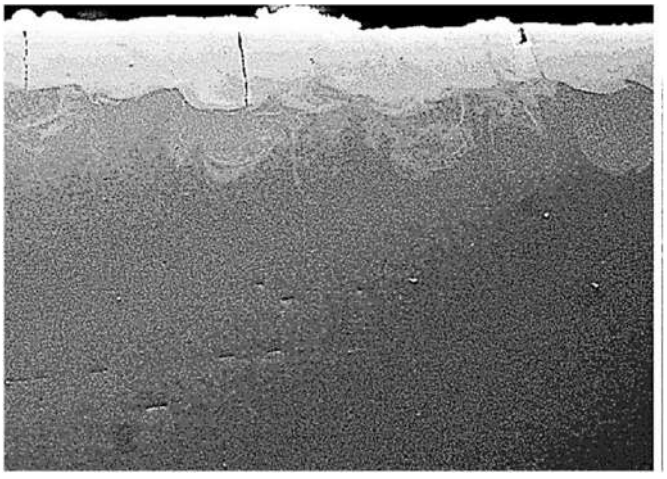

**Fig. 12.** The cross-section view of the material's microstructure [255].

### 5.3. Biological modification SLM implants

For the SLM-fabricated metallic implant to be used in human body, the substrate should be able to promote bone-to-implant contact with high biocompatibility, ensuring a long-term usage with efficacy. A common used biomodifications method is by coating the SLM metallic surface with a biological coatings, such as HA [238] and biomimetic coating [259,260]. Yan et al. [177] used biomimetic mineralization duplex treatment as a biomimetic coating on SLM Ti6Al4V sample. It demonstrated that a crystalline bone-like apatite and a thick titanate layer formed after SBF immersion. The titanate layer led to the formation of Ti–OH consisting of negatively charged $PO^{3-}$ to form Ca–P layer. Lou et al. [238] coated the SLM 316L with HA coating with thickness of 7.50 μm and the SEM morphological surface showed no redundant agglomerated HA particles on the coating area. The sample exhibited no cell cytotoxicity and highest relative growth rate RGR than the virgin sample. Fig. 13 shows the HA coating on SLM SS 316L sample. To promote the collagen synthesis by osteoblast, Gu et al. [259] fabricated

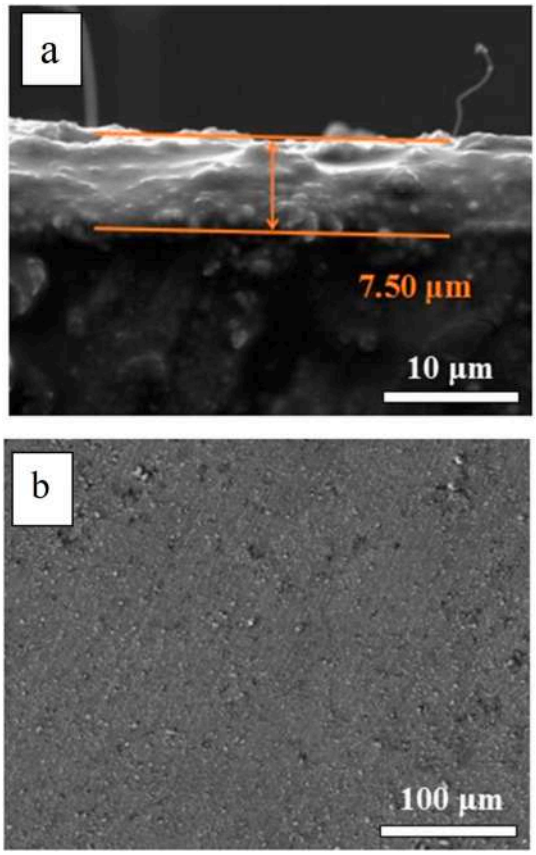


**Fig. 13.** SEM imaging of SLM fabricated SS 316L coating with (a) 7.50 μm and (b) surface morphology of the sample [238].

porous SLM Ti6Al4V similar to cancellous bone and used biomimetic calcium phosphate as a carrier to attach on bone protein. The biomimetic coating induced the osteogenesis and promoting the new bone formation in *in vivo* dog model evaluation. Sun et al. [260] employed the bioactive glass nanosphere coating (MBG) on SLM Ti6Al4V implant surface through the sol-gel process to obtain micro- and nano-topography. The hydrophilic water-to-implant contact angle of the sample was increased, and adhesion osteogenic differentiation was enhanced as compared to commercial CP-Ti in *in vitro* pre-osteoblast cells. The process-inherent appropriate surface roughness and cellular scaffold showed higher implant-bone contact for osseointegration. However, there is still lack of study in biological modification for SLM metallic implant which of Co–Cr, Mg and Zinc. Thus, more research are needed in SLM metallic to integrate the bone-to-implant for clinical application in the future.

### 5.4. Coating of pharmaceutical

Drug delivery is a technology used to safely incorporate pharmaceutical or drug into the host for a specific therapeutic effect. These incorporation of drugs into human body acts as active materials to the site of actions and it is one of a challenges approaches. In reducing the restenosis rate of the implant, the implants are coated with drugs such as bioactive compounds [235,261–265]. The Ti implants are also deposited by using the and polymer coating to improve their biocompatibility [266,267]. These implants are modified and coated with different techniques, such as dip, spray or spin coating or even solvent casting as summarized in Table 10.

Surface modification of implant by using bioactive compound or also known as biomolecules enhance the surface of the implant and making them biocompatible which can act as a good drug delivery. Fina et al. [269] presented a study, whereby they employed SLM with a single step with an elevated resolution during the fabrication process. Then, paracetamols were loaded into the SLM sample and found that the paracetamols were released accordingly in the acidic environment of human stomach acid. Vaithilingam et al. [261] attached the paracetamols by using the immersion technique for a duration of 1 h. Prior to immersion, the sample was polished to improve the surface for drug attachment. The result demonstrated an improved wettability of up to 95° angle. This high wettability is due to the presence of oxides on implant surface. After four weeks of *in vitro* test, the Ti6Al4V demonstrated a stable layer of paracetamol, indicating that the drug can be efficiently used as a coating for implant to enhance the biocompatibility and reducing the post-implant complications. Another study by Lv et al. [235], whereby they doped the surface of Ti6Al4V with growth doped fibrin glue to enhance the angiogenesis and osteogenesis in cases of bone defect. Their study focused on the controlled released of drug Bone-morphogenic protein-2 (BMP-2) and vascular endothelial growth factor (VEGF) which contributed to the main bone defect after implantation. The *in vitro* cell viability assay indicated there were no presence of toxicity to the cell, whereby there were an improvement of cell viability on Ti6Al4V scaffold surface.

Antibiotic is a well-known for the treatment of bacterial infections, whereby it helps in killing bacteria as well as preventing their growth in human body. Vancomycin is a well-known antibiotic and is recommended as a treatment for the skin infections as well as bone infections. Bezuidenhout et al. [263] and Zhang et al. [268] utilized the effectiveness of vancomycin in treating bone infections. Bezuidenhout et al. [263] incorporated vancomycin into Ti6Al4V implant and confirmed that there was an enhancement in antimicrobial activity against the *S. aureus*. The drug delivery of the vancomycin was also evaluated, whereby they found that the implant contact angle significantly improved the permeability of the implant surface. These allow the release of the vancomycin after implantation. On the other hand Zhang et al. [268] demonstrated that structure containing vancomycin had a good antibacterial effect on *E. coli* and *S. aureus*. They found that there was an increased osteogenic expression of MC3T3-E1 cell attach on the surface after *in vitro* cell culture.

Drug releasing implant requires an appropriate surface modification. Polymers are available in two types, such as synthetic and natural. The natural polymers occurs in nature and can be extracted naturally. The most common biocompatible and biodegradable polymers are chitosan, poly(ε-caprolactone) and poly(3-hydroxybutyrate), and can be deposited on implant surface by spin coating or adsorption. Micheletti et al. [266] rinsed the SLM sample with acetone and kept in air-dried, pen--strep were used for the loading of antibiotics. They found that the release of the antibiotics was about 17% for a single-layer polymer and was double percentage rate for the two-layer polymer. The *in vivo* study in rat model demonstrated that the polymer is able to modify the drug release pattern in rat model. Similarly, Chudinova et al. [267] used the method of adsorption on Ti6Al4V surface by using poly (allylamine hydrochloride) loaded with calcium carbonate. The *in vitro* test demonstrated that the cell growth pattern on the implant surface showed the cell grew normally on the surface in spindle shape. The drug release of the sample showed increase in percentage after 1 week of implantation. However, there are some limitations in using polymeric

**Table 10**
Biological modification of SLM metallic implant on drug delivery techniques.

| Enhancement Technique | Drug Delivery | *In Vitro/In Vivo* | Remark | Ref | Year |
|---|---|---|---|---|---|
| Immersion deposition | Paracetamol | 3T3-L1 | Not an ideal drug for immobilization as there were contaminant present on surface of sample | Vaithilingam et al. [261] | 2015 |
| Injection | Reinforcement with growth factor doped fibrin | rMSCs | Biocompatible and provide slow release of the bioactive growth factors. The angiogenesis were enhance with the addition of growth factor. | Lv et al. [235] | 2015 |
| Custom-made gel chamber | Simvastatin/ poloxamer 407 thermosensitive hydrogel | White rabbits | Sample with simvastatin demonstrated higher bone mineral density, and composition. | Liu et al. [236] | 2016 |
| Integrated permeable structure | Vancomycin | *E.Coli* and *S. aureus* | Controlled release of the antibiotics the exhibit the periprosthetic joint infections | Bezuidenhout et al. [263] | 2018 |
| Electrochemical Anodization | MTANi | hMSCs | Enhance ALP and antibacterial formed firm film, preventing biofilm formation | Li et al. [265] | 2020 |
| micro-arc oxidized (MAO) | Vancomycin | E.Coli and S. aureus | Scaffold with vancomycin exhibit least of bone infection | Zhang et al. [268] | 2020 |
| Spin coating | Biodegradable polymers | – | Presence of polymers modified the pen-strep release under the *in vitro* test of rat model | Micheletti et al. [266] | 2021 |
| Adsorption | PSS and PAH | 3T3-L1 | The surface modification affected cell morphology *in vitro*. No cytotoxicity and improved cell adhesion | Chudinova et al. [267] | 2021 |

Abbreviation: 3T3-L1-mouse embryonic fibroblast, rMSCs-rat mesenchymal stem cells, *E.Coli- Escherichia coli, S.aureus-Staphylococcus aureus,* MTANi-Methylthioadenosine nucleosidase inhibitor, hMSCs-human mesenchymal stem cells, PSS-polystyrene sulfonate, PAH-poly(allylamine)hydrochloride, 3T3-L1-mouse embryonic fibroblast.

carriers for biomedical applications, includes surface fractures and coating waviness, which can cause inflammatory and hypersensitivity reactions as well as unequal medication distribution.

## 6. Applications

Currently, SLM printed biometallics are mainly focused in producing implants for tissue repair, dentistry, orthopedic including cranial, dental, total hip replacement as well as prosthesis. This is due to their ability of tailoring to anatomical structure, lightweight and ease of handling during clinical applications. There are various applications of SLM printed materials in biomedical applications, including skull, joint and hip replacement, and dental.

### 6.1. Skull

Trauma, inflammatory diseases, or malignancies are the main causes of mandibular and craniofacial bone abnormalities. These defects cause patients to suffer from speech, mastication, and aesthetic issues as they alter the bone structure, resulting in the need for implants [270]. Mohammed et al. [271] fabricated a lower jaw to replace the patient's fractured mandible by using the Ti6Al4V SLM technique. The patient underwent a CT scan to obtain the shape of the lower jaw, and the results demonstrated that the implant was able to support the patient's contraction and relaxation during speech. In addition, Peel et al. [272] used Ti6Al4V to fabricate a porous orbital floor for treating a post-traumatic zygomatic osteotomy patient. The implant offered a high bending stiffness to weight ratio, which improved the patient's facial symmetry and enhanced the ability to fully close the eyelid.

Head trauma including cranial defects is one of the arduous task for most craniomaxillofacial surgeons. Previous study has demonstrated the application of SLM technique for the cranial prosthesis to restore the skulls' integrity, ensure adequate protections and functionality of the underneath brain. Likewise, Sharma et al. [273] created a biomimetic patient-specific cranial prosthesis with an interconnected strut to fit the patient's skull of head trauma by using SS 316L. It was fabricated in a vertical direction; however, this complex structure was overhanging between the interconnected network (Fig. 14(a)). The combination of flange (Fig. 14(b)) and angular fixation (Fig. 14(c)) was used to fix the problem. This design of lightweight (30 g) biomimetic pattern prostheses was fit to the anatomical biomodel (Fig. 14(d)).

### 6.2. Joint and hip replacement

Generally, the mass productions of implants fabricated by the conventional method can serve the most of the patients population. However, due to the complex structure of anatomical, the ready-made conventional implant does not fit the clinical applications scenario, such as hip and severe joint surgery. The problem related to total hip replacement, which entailed the acetabular cup dislocated or loosened, has been shown in earlier research. Thus, SLM patient-specific implants has shown as a valuable method for addressing the most common causes of hip replacements. Colen et al. [274] fabricated custom-made reinforcement ring by using SLM for the trabecular surface of the acetabular cup to increase long term stability and to encourage bone ingrowth. The cortex screws were also used to achieve a maximum balance, and after 10 months of radiological follow-up, there was good attachment of bone cells around the porous acetabular cup. In addition, Baauw et al. [275] fabricated acetabular components by using Ti6Al4V for 16 patients with Paprosky Type 3 defects to determine the accuracy and stability of the implant. Under CT data, the implant demonstrated good position of inclination, anteversion and center of rotation as compared to the pre-operative data. Wang et al. [276] fabricated the femoral neck of a Ti6Al4V implant for severe hip arthroplasties. The 24 months of clinical data showed that the implant postoperative weight bearing was better than that of the conventional, attributed to a higher femoral neck anteversion angle. The implant demonstrated good stability with the physiological and anatomical structures of the patients.

Treatment of complex acetabular fracture and defects can also get benefit from the SLM technology. The fabricated implants could also

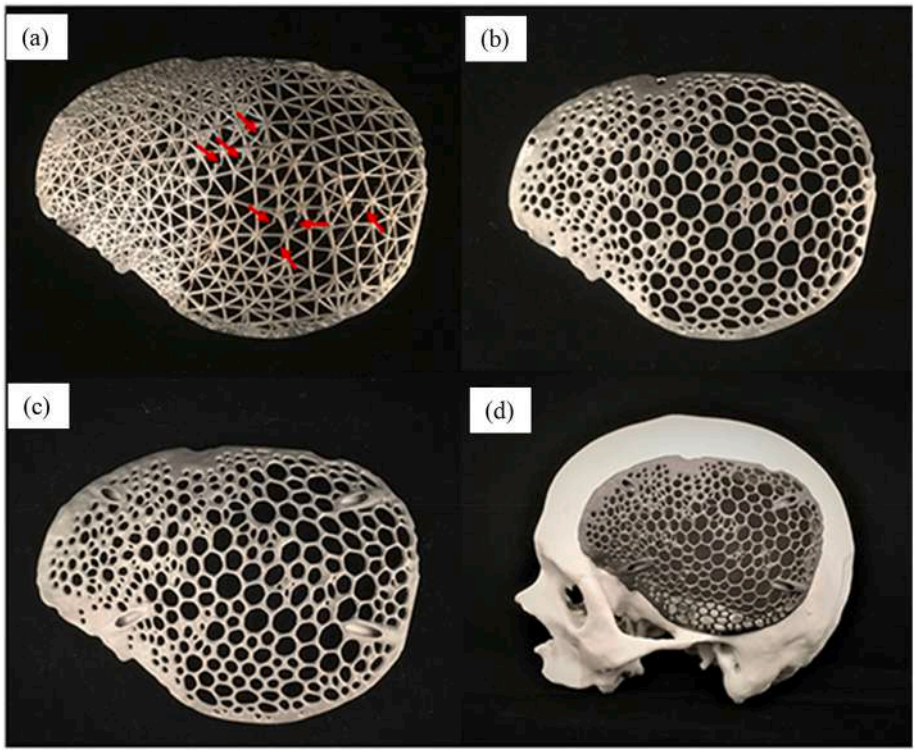


**Fig. 14.** Biomimetic cranial prostheses and a skull biomodel tailored patient (a) wireframe pattern prosthesis highlighting issues with structural printing (red-arrows) (b) prosthesis with screw fixing points on a flange (c) prosthesis with points for angular screw fixing and (d) cranial biomodel [273].

customized to the shape of the pelvis and acetabular fracture [277]. Weiβmann et al. [278] manufactured different struts type of acetabular cup from Ti6Al4V. It was demonstrated that the mechanical strength was depended on the struts to fit the prosthesis and the implants were matched to the anatomical features of the patients with porous structure that enhance osseointegration. Femoral implants were also constructed by using CoCrMo SLM by Song et al. [279], and they demonstrated a surface roughness of 7.9 μm on the planate surface and 16.8 μm on the curved surface, allowing the attachment of bone cells. The implant exhibited good corrosion resistance and biocompatibility.

### 6.3. Dental

Oral health and dental hygiene play a crucial and significant role in overall human health. Tooth wear occurs naturally because teeth are exposed to loosening, fracture, harnessing, overall chemical stressors, including damage, misalignment, and discoloration [280]. Thus, taking care of it is important for preventing any cavities or plugs. AM has come a long way in fabricating medical implants by leveraging pioneering science and engineering technology, as well as in the field of dental implants. Biocompatibility of the dental implants for the implantations for the prolong time is the most critical factor, including other characteristics of resistance to corrosion, fracture, and material strength. In fabricating a dental implant, the corrosive nature of the materials may lead to harmful events due to the acidic pH of the saliva and may corrode the surface of the dental. The natural microenvironment of saliva, which consists of 99% water, proteins, and electrolytes, may as well cause ion interchange, leading to the corrosive behavior of the dental implant [281]. Thus, in order to replicate tooth wear and simulate real-world oral cavity interactions, researchers have created artificial saliva by chemical formulation.

Dental implant prosthetics are used in replacing missing teeth as well as treating partially or fully damaged teeth. The primary types of dental implant, including endosteal or endosseous, subperiosteal, and transosteal [282]. Endosteal dental implants are inserted within the mandible of the skeletal face, as shown in Fig. 15(a). Subperiosteal dental prosthetics are positioned at the jawbone's gum while are fastened through bone remodeling and osseointegration. It applications include the common dentures, which are fixed and removable. As for transosteal implants, they needed sufficient bone support from the mandible commonly used for patients with severe resorption and jaw damage [282]. Screws were used to pierce through the jawbone and bolted through the lower mandible to support the metal rods, which acts as a support beam as shown **in Fig. 15(b)**. The common type of implants used are the Cp-Ti [283] for the base of the implants, however, Ti6Al4V [284] and Ti-Zi [285,286] are mainly used for these kind of implants due to their excellent corrosion resistance.

SLM dental implants mostly depend on the two factors of porosity and part density, which are mainly determined by the energy density input. Low energy input may be attributed to the imperfection on the surface of sample, which is the molten layer that eventually results in the large pores. Zhang et al. [287] analyzed the corrosion behavior of dental implant SLM Ti6Al4V under the environment of the artificial saliva of pH 2, pH 4 and pH 6. The corrosion test revealed that the SLM sample of the Ti6Al4V had lower corrosion than the wrought sample. On the other hand, Kim et al. [288] assessed the Co–Cr alloy mechanical characteristics and microstructure under *in vitro* study and they found that all the samples of casting, milling and milling/post-sintering showed excellent crystallinity under XRD examination (Fig. 16). Nevertheless, the CoCr alloy exhibit dominant γ-FCC and it showed that the SLM has the highest superior mechanical properties due to the full local melting and rapid solidification that minimizes the porosity.

## 7. Way forward and challenges

The current AM technologies require the recognising the obstacles and comprehending the reliable technologies, as well as their future impacts, at an early stage in the procedure for making decisions [289]. Therefore, this section addresses the current and crucial challenges in the adoption of SLM technologies in the market, which involve the standard design, selection of material, manufacturing, and trial for biomedical applications. The microstructure has been hindered by the lack of simulation-based printing processes, which has reduced the mechanical characteristics of the manufactured parts [290].

As stated earlier, the current SLM metallics are still limited in their ability to obtain the appropriate properties to the anatomical structure. This manufactured implant's strength remains greater than that of the

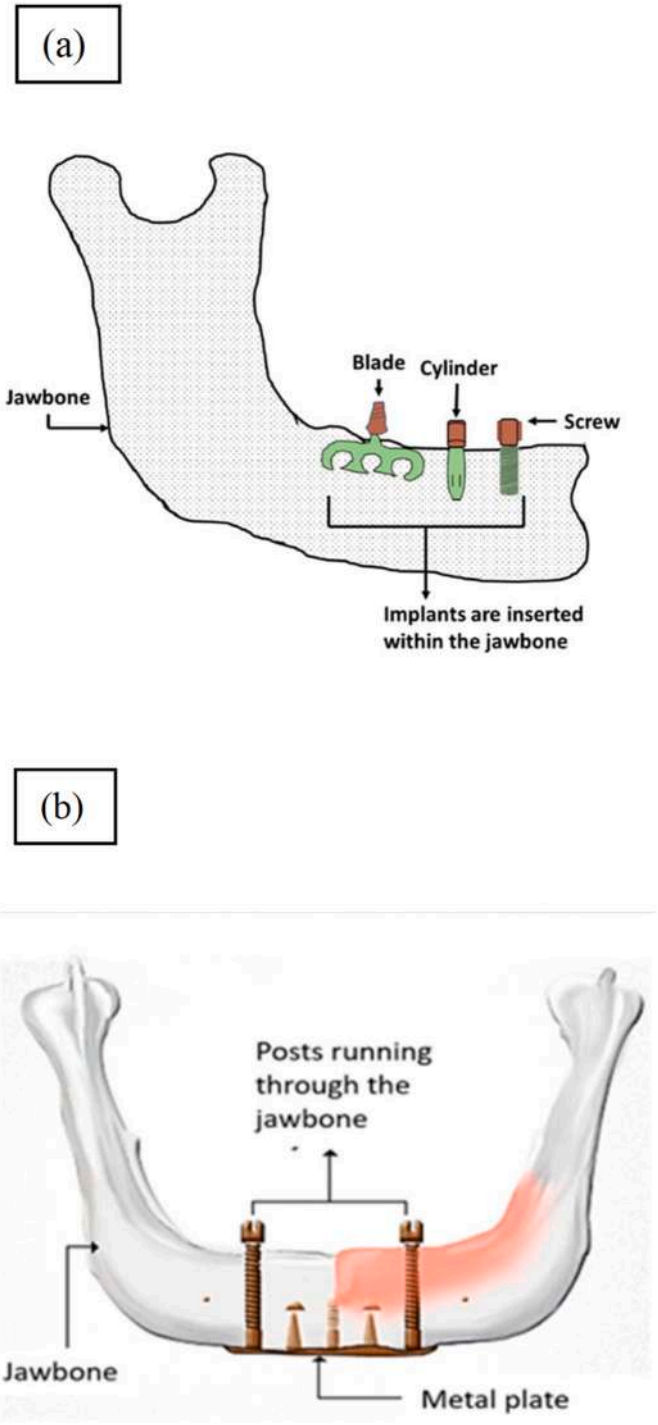


**Fig. 15.** Schematic Dental implant consisting of (a) Endosteal dental implants and (b) a transosteal implant [3].

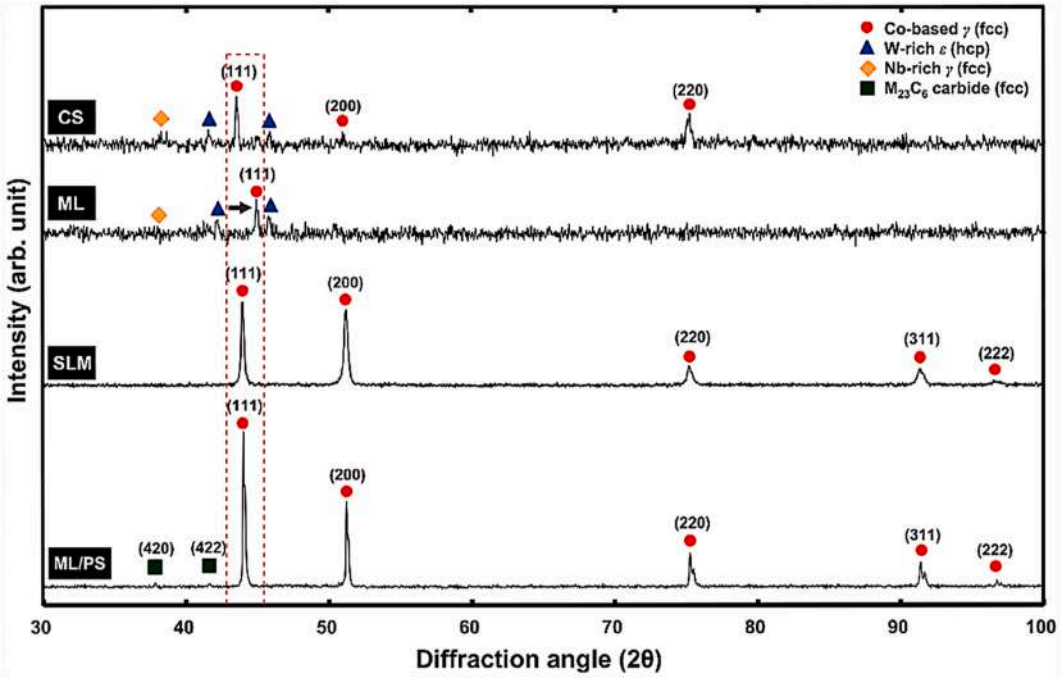


**Fig. 16.** The XRD analysis of the CoCr alloy with different manufacturing process [288].

bone tissues. For instance, the SLM metallic implant (density 1.63 g/cm$^3$) and porosity of 65% demonstrated more strength than anatomical bone [291]. Thus, it is worth developing topological optimization to control the load transfer to mimic the bone implant in the future. This geometrical modeling structure can be determined by using the finite element softwares, such as Abaqus and Ansys. The ideal shape can also be assessed before being used as a biomedical implant by validating the structural performance using von Mises failure criteria.

The metallic implant fabrication by the SLM needed more research due to the particular geometric constraint and the stringent requirements for producing the quality of the struts [292]. In this sense, the best build geometry with the required quality that ought to be generated can be optimal by using the SLM parameters. This means that the pore and the lack of fusion defects can be avoided during the fabrication. The internal porosity could be reduced by using the pore-free feedstock, and the lack of fusion defects could also be minimized by thoroughly controlling the SLM process [293,294]. In addition, The topology optimization can also be used and formulated to study bone internal architecture and provide optimal topological structure of the fabricated sample. This limitation necessitates manual involvement and a less-than-ideal design approach, adding needless complexity, danger, and expense to the manufacturing process of biomedical implants.

Apart from these challenges and limitations, the cracks and void formation of the metallic material fabricated by SLM significantly lowered its tensile performance [295]. The formation of voids leads to lack of interfacial bonding between the adjacent layers on the sample, results in the layer delamination upon printing. These will result in a discernible difference between the interior material and the edges of the layers, leading to the creation of anisotropic microstructures [296]. These problems are the major causes of the formation of cracks to occurs, reducing the mechanical strength of the metallic SLM sample. To overcome these problems, adjusting the input parameters throughout the SLM process. The hatching distance, laser power, scan speed, hatch distance, and layer thickness needed to be carefully addressed. Prior to the experimental study, optimization techniques such as the Taguchi method and the response surface method can be used to enhance the design.

The tensile property of the SLM-fabricated metallic wear is lowered due to the rough strut surface, internal defects, and incomplete decomposed alpha' martensitic microstructure [297]. In general, the brittle fracture of the implants still remains a great concern for the wider applications and needs to be appropriately addressed prior to implantation in the human body. Post-processing operations may improve the as-fabricated sample, which includes powder removal, stress relief, and eliminating or lowering print-induced flaws including porosity and lack of fusion [297]. HIP is mostly used on the SLM to reduce the build sample's porosity, enhance mechanical qualities, and relieve stresses [298]. This process involves high temperatures and applies to the sample in an inert environment. According to the research, the microstructure changes caused the interior porosity and tensile strength to decrease after the HIP treatment.

Recent research has shown the significant micro- and nanoscale porous materials are for the adhesion, differentiation, migration, and proliferation of cells. The integration of SLM and dealloying with other metals, such as Cu, Ti, Na, and Tb has the potential to produce structures and surfaces that replicate the properties of anatomical structures at the macro-to nanoscale [299–301]. However, the effect of dealloying on an implant's mechanical properties has not yet been explored. Metallic implants are bio-inert, and the survival of cells is still a main issue. It has been shown that surface treatment and modification can enhance the biological activity of SLM implant, leading to easier fixation and improving long-term stability. The antibacterial properties of SLM metallic implant could be improved by the introduction of silver, antihistamines, and antibiotics, as discussed previously [302,303]. These coatings prevent the implant from with a wide range microorganisms that causes infections without affecting its characteristics. However, the surface coating may result in surface leaching, which would reduce implant integrity [304]. Thus, it is great to achieve access to a novel exploration in the future.

As for the load-bearing application, especially in the orthopaedic field, which includes multiple compressions, tensions, and bending applied during contraction and the relaxation of muscles tissue [305]. This main scenario is crucial for the SLM-fabricated metallic implant. Therefore, further study is needed to enhance the reliability of the SLM-fabricated parts and prevent the unfavorable effects caused by the

SLM on surface roughness and cell proliferation. In addition, the product cost of SLM is higher in comparison to conventional manufacturing of similar geometries and has been determined to be among the most overburdening elements. The large environmental impact mostly is caused by the high amount of waste powder. By using different grades according to the melt flow rate of the recycled powder, the material quality and the usage of fresh powder can be used efficiently. Thus, more optimal recycling and reusing the metallic implants from the SLM fabrication could reduce the cost to both patients and the clinical industry. In addition, the consumption of compressed air of nitrogen from the external reservoir might as well cause significant environmental impact. To avoid this, by sealing the process chamber appropriately so there is no longer needed of continuous filling of the chamber. The total production cost of the metal SLM should be reduced based on the optimal topological optimization of SLM in reducing material, labor, power, and equipment costs.

## 8. Conclusions

Metallic implants fabricated by SLM method have been manufactured and utilized in different medical procedures due to their excellent biocompatibility and non-toxicity. The surface modification on the treatment has broaden the usage of the SLM metallic in treating the fracture and bone diseases, particularly for load bearing applications. Therefore, this review article had summarized and demonstrated the previous works on the widely used powder-based SLM method of metallic implant fabrication. A large amount of research has been focused regarding how the parameters of the process relate to the characteristics of the final product, such as scanning speed, hear course, product microstructure, mechanical properties, corrosion, and defects. The SLM method used in clinical applications has also emerge, including surface modification, drug development, biomaterials and tissue engineering. Also, this review has demonstrated some attempts made in the evolution of SLM fabricated metallic implant to offer more understanding of the methods, parameters, properties of the fabricated parts including their structures. Thus, acquiring knowledge in producing a defect free product efficiently and sustainably. The innovations in the powder materials can as well be explored since the powder of unique properties have the potential to broaden the scope of applications.

Therefore, more research and development on process optimizations of SLM metallic implant is necessary in the future. Current SLM implants yet to focus on the material, printed quality, processing complexities and mechanical properties that has been discussed in this paper. Some of the future directions include the usage of composite and alloy powders can be uncovered due to the immense number of combinations. Then more focus on the post processing surface modification as well as the Z-directional printing as it can reduce the martensite and anisotropy of the implant. Another method for reducing the chances of nozzle clogging and the cost of the feedstock, using multi-nozzles during SLM fabrications, would be interesting to explore. Finally, combining various printing lasers with a high deposition rate could increase productivity with good accuracy. This involves the re-melting process and post-processing in reducing and repairing the defective parts on the sample.

## Declaration of competing interest

The authors declare that they have no known competing financial interests or personal relationships that could have appeared to influence the work reported in this paper.

## Acknowledgments

The financial support for this project was financed through “Geran Universiti Penyelidik” UTMFR Scheme Q.K130000.3809.23H19 under Universiti Teknologi Malaysia.

## References

[1] Davis R, Singh A, Jackson MJ, Coelho RT, Prakash D, Charalambous CP, Ahmed W, da Silva LRR, Lawrence AA. A comprehensive review on metallic implant biomaterials and their subtractive manufacturing. Int J Adv Des Manuf Technol 2022;120:1473–530.
[2] Tom T, Sreenilayam SP, Brabazon D, Jose JP, Joseph B, Madanan K, Thomas S. Additive manufacturing in the biomedical field-recent research developments. Result Eng. 2022:100661.
[3] Saha S, Roy S. Metallic dental implants wear mechanisms, materials, and manufacturing processes: a literature review. Materials 2022;16.
[4] Noronha J, Qian M, Leary M, Kyriakou E, Almalki A, Brudler S, Brandt M. Additive manufacturing of Ti-6Al-4V horizontal hollow struts with submillimetre wall thickness by laser powder bed fusion. Thin-Walled Struct 2022;179.
[5] Mirzaali MJ, Moosabeiki V, Rajaai SM, Zhou J, Zadpoor AA. Additive manufacturing of biomaterials—design principles and their implementation. Materials 2022;15:5457.
[6] Shekhawat D, Singh A, Bhardwaj A, Patnaik A. A short review on polymer, metal and ceramic based implant materials. In: IOP conference series: materials science and engineering. IOP Publishing; 2021, 012038.
[7] Dhoonooah N, Moussaoui K, Monies F, Rubio W, Zitoune R. Challenges in additive manufacturing: influence of process parameters on induced physical properties of printed parts. In: Additive manufacturing of bio-implants: design and synthesis. Springer; 2024. p. 1–31.
[8] Kumar R, Kumar M, Chohan JS. The role of additive manufacturing for biomedical applications: a critical review. J Manuf Process 2021;64:828–50.
[9] Mobarak MH, Islam MA, Hossain N, Al Mahmud MZ, Rayhan MT, Nishi NJ, Chowdhury MA. Recent advances of additive manufacturing in implant fabrication–A review. Appl Surf Sci Adv 2023;18:100462.
[10] Standardization I. Additive manufacturing: general: principles. Terminology 2015;640.
[11] Avcu E, Baştan FE, Abdullah HZ, Rehman MAU, Avcu YY, Boccaccini AR. Electrophoretic deposition of chitosan-based composite coatings for biomedical applications: a review. Prog Mater Sci 2019;103:69–108.
[12] Ahangar P, Cooke ME, Weber MH, Rosenzweig DH. Current biomedical applications of 3D printing and additive manufacturing. Appl Sci 2019;9:1713.
[13] Buciumeanu M, Bagheri A, Silva FS, Henriques B, Lasagni AF, Shamsaei N. Tribocorrosion behavior of NiTi biomedical alloy processed by an additive manufacturing laser beam directed energy deposition technique. Materials 2022;15:691.
[14] Jang T-S, Kim D, Han G, Yoon C-B, Jung H-D. Powder based additive manufacturing for biomedical application of titanium and its alloys: a review. Biomed Eng Lett 2020;10:505–16.
[15] Bandyopadhyay A, Ghosh S, Boccaccini AR, Bose S. 3D printing of biomedical materials and devices. J Mater Res 2021:1–12.
[16] Bezek LB, Chatham CA, Dillard DA, Williams CB. Mechanical properties of tissue-mimicking composites formed by material jetting additive manufacturing. J Mech Behav Biomed Mater 2022;125:104938.
[17] Gülcan O, Günaydın K, Tamer A. The state of the art of material jetting—a critical review. Polymers 2021;13:2829.
[18] Murr L. Metallurgy principles applied to powder bed fusion 3D printing/additive manufacturing of personalized and optimized metal and alloy biomedical implants: an overview. J Mater Res Technol 2020;9:1087–103.
[19] Allavikutty R, Gupta P, Santra TS, Rengaswamy J. Additive manufacturing of Mg alloys for biomedical applications: current status and challenges. Curr Opin Biomed Eng 2021;18:100276.
[20] Vignesh M, Ranjith Kumar G, Sathishkumar M, Manikandan M, Rajyalakshmi G, Ramanujam R, Arivazhagan N. Development of biomedical implants through additive manufacturing: a review. J Mater Eng Perform 2021;30:4735–44.
[21] Ziaee M, Crane NB. Binder jetting: a review of process, materials, and methods. Addit Manuf 2019;28:781–801.
[22] Li M, Du W, Elwany A, Pei Z, Ma C. Metal binder jetting additive manufacturing: a literature review. J Manuf Sci Eng 2020;142:090801.
[23] Mostafaei A, Elliott AM, Barnes JE, Li F, Tan W, Cramer CL, Nandwana P, Chmielus M. Binder jet 3D printing—process parameters, materials, properties, modeling, and challenges. Prog Mater Sci 2021;119:100707.
[24] Nikfarjam N, Ghomi M, Agarwal T, Hassanpour M, Sharifi E, Khorsandi D, Ali Khan M, Rossi F, Rossetti A, Nazarzadeh Zare E. Antimicrobial ionic liquid-based materials for biomedical applications. Adv Funct Mater 2021;31:2104148.
[25] Calignano F, Galati M, Iuliano L, Minetola P. Design of additively manufactured structures for biomedical applications: a review of the additive manufacturing processes applied to the biomedical sector. J Healthcare Eng 2019;2019.
[26] Pei X, Wu L, Lei H, Zhou C, Fan H, Li Z, Zhang B, Sun H, Gui X, Jiang Q. Fabrication of customized Ti6AI4V heterogeneous scaffolds with selective laser melting: optimization of the architecture for orthopedic implant applications. Acta Biomater 2021;126:485–95.
[27] Park HS, Nguyen DS, Le-Hong T, Van Tran X. Machine learning-based optimization of process parameters in selective laser melting for biomedical applications. J Intell Manuf 2022;33:1843–58.
[28] Hu Q, Chen C, Liu M, Chang C, Yan X, Dai Y. Improved corrosion resistance of magnesium alloy prepared by selective laser melting through T4 heat treatment for biomedical applications. J Mater Res Technol 2023;27:813–25.
[29] Park JH, Olivares-Navarrete R, Baier RE, Meyer AE, Tannenbaum R, Boyan BD, Schwartz Z. Effect of cleaning and sterilization on titanium implant surface properties and cellular response. Acta Biomater 2012;8:1966–75.

[30] Brogini S, Sartori M, Giavaresi G, Cremascoli P, Alemani F, Bellini D, Martini L, Maglio M, Pagani S, Fini M. Osseointegration of additive manufacturing Ti-6Al-4V and Co-Cr-Mo alloys, with and without surface functionalization with hydroxyapatite and type I collagen. J Mech Behav Biomed Mater 2021;115:104262.

[31] Dzogbewu TC, du Preez WB. Additive manufacturing of titanium-based implants with metal-based antimicrobial agents. Metals 2021;11.

[32] Arias-González F, Rodríguez-Contreras A, Punset M, Manero JM, Barro Ó, Fernández-Arias M, Lusquiños F, Gil FJ, Pou J. In-situ laser directed energy deposition of biomedical ti-nb and ti-zr-nb alloys from elemental powders. Metals 2021;11:1205.

[33] Mirzababaei S, Pasebani S. A review on binder jet additive manufacturing of 316L stainless steel. J Manufact Mater Process 2019;3.

[34] Lancaster R, Davies G, Illsley H, Jeffs S, Baxter G. Structural integrity of an electron beam melted titanium alloy. Materials 2016;9.

[35] Antolak-Dudka A, Platek P, Durejko T, Baranowski P, Malachowski J, Sarzynski M, Czujko T. Static and dynamic loading behavior of Ti6Al4V honeycomb structures manufactured by laser engineered net shaping (LENS(TM)) technology. Materials 2019;12.

[36] Nguyen D-S, Park H-S, Lee C-M. Applying selective laser melting to join Al and Fe: an investigation of dissimilar materials. Appl Sci 2019;9:3031.

[37] Bandyopadhyay A, Traxel KD, Lang M, Juhasz M, Eliaz N, Bose S. Alloy design via additive manufacturing: advantages, challenges, applications and perspectives. Mater Today 2022;52:207–24.

[38] Fischer M, Laheurte P, Acquier P, Joguet D, Peltier L, Petithory T, Anselme K, Mille P. Synthesis and characterization of Ti-27.5Nb alloy made by CLAD(R) additive manufacturing process for biomedical applications. Mater Sci Eng C Mater Biol Appl 2017;75:341–8.

[39] Todaro C, Easton M, Qiu D, Zhang D, Bermingham M, Lui E, Brandt M, StJohn D, Qian M. Grain structure control during metal 3D printing by high-intensity ultrasound. Nat Commun 2020;11:142.

[40] Wang Y, Zhao YF. Investigation of sintering shrinkage in binder jetting additive manufacturing process. Procedia Manuf 2017;10:779–90.

[41] Mostafaei A, Stevens EL, Hughes ET, Biery SD, Hilla C, Chmielus M. Powder bed binder jet printed alloy 625: densification, microstructure and mechanical properties. Mater Des 2016;108:126–35.

[42] Chou D-T, Wells D, Hong D, Lee B, Kuhn H, Kumta PN. Novel processing of iron–manganese alloy-based biomaterials by inkjet 3-D printing. Acta Biomater 2013;9:8593–603.

[43] Hong D, Chou D-T, Velikokhatnyi OI, Roy A, Lee B, Swink I, Issaev I, Kuhn HA, Kumta PN. Binder-jetting 3D printing and alloy development of new biodegradable Fe-Mn-Ca/Mg alloys. Acta Biomater 2016;45:375–86.

[44] Sames WJ, List F, Pannala S, Dehoff RR, Babu SS. The metallurgy and processing science of metal additive manufacturing. Int Mater Rev 2016;61:315–60.

[45] Aufa AN, Hassan MZ, Ismail Z. Recent advances in Ti-6Al-4V additively manufactured by selective laser melting for biomedical implants: prospect development. J Alloys Compd 2021;896.

[46] Szymczyk-Ziółkowska P, Ziółkowski G, Hoppe V, Rusińska M, Kobiela K, Madeja M, Dziedzic R, Junka A, Detyna J. Improved quality and functional properties of Ti-6Al-4V ELI alloy for personalized orthopedic implants fabrication with EBM process. J Manuf Process 2022;76:175–94.

[47] Eklund A, Ahlfors M, Bahbou F, Wedenstrand J. Optimizing HIP and printing parameters for EBM Ti-6Al-4V. Key Eng Mater 2018;770:174–8.

[48] Popov V, Katz-Demyanetz A, Garkun A, Muller G, Strokin E, Rosenson H. Effect of hot isostatic pressure treatment on the electron-beam melted Ti-6Al-4V specimens. Procedia Manuf 2018;21:125–32.

[49] Onuike B, Heer B, Bandyopadhyay A. Additive manufacturing of Inconel 718—copper alloy bimetallic structure using laser engineered net shaping (LENS™). Addit Manuf 2018;21:133–40.

[50] Mitra I, Bose S, Dernell WS, Dasgupta N, Eckstrand C, Herrick J, Yaszemski MJ, Goodman SB, Bandyopadhyay A. 3D Printing in alloy design to improve biocompatibility in metallic implants. Mater Today 2021;45:20–34.

[51] Narayanan D, Liu M, Kuttolamadom M, Castaneda H. Identification and development of a new local corrosion mechanism in a Laser Engineered Net Shaped (LENS) biomedical Co-Cr-Mo alloy in Hank's solution. Corrosion Sci 2022;207.

[52] Kelly CN, Francovich J, Julmi S, Safranski D, Guldberg RE, Maier HJ, Gall K. Fatigue behavior of As-built selective laser melted titanium scaffolds with sheet-based gyroid microarchitecture for bone tissue engineering. Acta Biomater 2019;94:610–26.

[53] Xie W, Zheng M, Wang J, Li X. The effect of build orientation on the microstructure and properties of selective laser melting Ti-6Al-4V for removable partial denture clasps. J Prosthet Dent 2020;123:163–72.

[54] Aufa AN, Hassan MZ, Ismail Z. The fabrication of titanium alloy biomedical implants using additive manufacturing: a way forward. J Min Metal Mater Eng 2021;7:39–48.

[55] Liu S, Shin YC. Additive manufacturing of Ti6Al4V alloy: a review. Mater Des 2019;164:107552. 107552.

[56] Yin Y, Huang Q, Liang L, Hu X, Liu T, Weng Y, Long T, Liu Y, Li Q, Zhou S. In vitro degradation behavior and cytocompatibility of ZK30/bioactive glass composites fabricated by selective laser melting for biomedical applications. J Alloys Compd 2019;785:38–45.

[57] Li Y, Ding Y, Munir K, Lin J, Brandt M, Atrens A, Xiao Y, Kanwar JR, Wen C. Novel β-Ti35Zr28Nb alloy scaffolds manufactured using selective laser melting for bone implant applications. Acta Biomater 2019;87:273–84.

[58] Niinomi M, Nakai M, Hieda J. Development of new metallic alloys for biomedical applications. Acta Biomater 2012;8:3888–903.

[59] Lerebours A, Vigneron P, Bouvier S, Rassineux A, Bigerelle M, Egles C. Additive manufacturing process creates local surface roughness modifications leading to variation in cell adhesion on multifaceted TiAl6V4 samples. Bioprinting 2019;16.

[60] Sadeghpour S, Abbasi S, Morakabati M, Kisko A, Karjalainen L, Porter D. A new multi-element beta titanium alloy with a high yield strength exhibiting transformation and twinning induced plasticity effects. Scripta Mater 2018;145:104–8.

[61] Marinelli G, Martina F, Ganguly S, Williams S. Microstructure, hardness and mechanical properties of two different unalloyed tantalum wires deposited via wire+ arc additive manufacture. Int J Refract Metals Hard Mater 2019;83:104974.

[62] Fu Y, Zhang Y, Zhou H, Li D, Liu H, Qiao H, Wang X. Timely online chatter detection in end milling process. Mech Syst Signal Process 2016;75:668–88.

[63] Krystýnová M, Doležal P, Fintová S, Březina M, Zapletal J, Wasserbauer J. Preparation and characterization of zinc materials prepared by powder metallurgy. Metals 2017;7:396.

[64] Wang C, Yang H, Li X, Zheng Y. In vitro evaluation of the feasibility of commercial Zn alloys as biodegradable metals. J Mater Sci Technol 2016;32:909–18.

[65] Ghasali E, Alizadeh M, Shirvanimoghaddam K, Mirzajany R, Niazmand M, Faeghi-Nia A, Ebadzadeh T. Porous and non-porous alumina reinforced magnesium matrix composite through microwave and spark plasma sintering processes. Mater Chem Phys 2018;212:252–9.

[66] Tonelli L, Fortunato A, Ceschini L. CoCr alloy processed by selective laser melting (SLM): effect of laser energy density on microstructure, surface morphology, and hardness. J Manuf Process 2020;52:106–19.

[67] Nor MM, Salleh Z, Masdek N, Taib Y, Abu M. Electrodeposition of Co-Ni-Fe on stainless steel bolts. Int J Eng Technol 2018;7:221–5.

[68] Zięłala M, Durejko T, Polański M, Kunce I, Płociński T, Zieliński W, Łazińska M, Stępniowski W, Czujko T, Kurzydłowski KJ. The microstructure, mechanical properties and corrosion resistance of 316 L stainless steel fabricated using laser engineered net shaping. Mater Sci Eng, A 2016;677:1–10.

[69] Lin W, Qin L, Qi H, Zhang D, Zhang G, Gao R, Qiu H, Xia Y, Cao P, Wang X. Long-term in vivo corrosion behavior, biocompatibility and bioresorption mechanism of a bioresorbable nitrided iron scaffold. Acta Biomater 2017;54:454–68.

[70] Sukhodub L, Sukhodub L, Kumeda M, Panda A, Baron P. ZnO coatings on Ti6Al4V substrate: structural and antibacterial properties in literature review and research. Manag Syst Prod Eng 2020;28:318–24.

[71] Lee J-Y, Nagalingam AP, Yeo S. A review on the state-of-the-art of surface finishing processes and related ISO/ASTM standards for metal additive manufactured components. Virtual Phys Prototyp 2021;16:68–96.

[72] Dwivedi S, Dixit AR, Das AK. Wetting behavior of selective laser melted (SLM) bio-medical grade stainless steel 316L. Mater Today Proc 2022;56:46–50.

[73] Tekdir H, Yetim T, Yetim AF. Corrosion properties of ceramic-based TiO2 films on plasma oxidized Ti6Al4V/316L layered implant structured manufactured by selective laser melting. JBE 2021;18:944–57.

[74] Hu Y, Dong C, Kong D, Ao M, Ding J, Ni X, Zhang L, Yi P, Li X. Degradation behaviour of selective laser melted CoCrMo alloys in H2O2-containing chloride solutions. Corrosion Sci 2022;195:109981.

[75] Gong X, Li Y, Nie Y, Huang Z, Liu F, Huang L, Jiang L, Mei H. Corrosion behaviour of CoCrMo alloy fabricated by electron beam melting. Corrosion Sci 2018;139:68–75.

[76] Kajima Y, Takaichi A, Kittikundecha N, Htat HL, Cho HHW, Tsutsumi Y, Hanawa T, Wakabayashi N, Yoneyama T. Reduction in anisotropic response of corrosion properties of selective laser melted Co–Cr–Mo alloys by post-heat treatment. Dent Mater 2021;37:e98–108.

[77] Axinte D, Guo Y, Liao Z, Shih AJ, M'Saoubi R, Sugita N. Machining of biocompatible materials—recent advances. CIRP Annals 2019;68:629–52.

[78] Pawade KAJRS. Experimental investigation on surface roughness of face turned Co-Cr-Mo biocompatible alloy followed by polishing. 2017.

[79] Brandl E, Palm F, Michailov V, Viehweger B, Leyens C. Mechanical properties of additive manufactured titanium (Ti–6Al–4V) blocks deposited by a solid-state laser and wire. Mater Des 2011;32:4665–75.

[80] Suresh S, Sun C-N, Tekumalla S, Rosa V, Nai SML, Wong RCW. Mechanical properties and in vitro cytocompatibility of dense and porous Ti–6Al–4V ELI manufactured by selective laser melting technology for biomedical applications. J Mech Behav Biomed Mater 2021;123:104712.

[81] Polozov I, Popovich A. Microstructure and mechanical properties of NiTi-based eutectic shape memory alloy produced via selective laser melting in-situ alloying by Nb. Materials 2021;14.

[82] Yu Z, Xu Z, Guo Y, Xin R, Liu R, Jiang C, Li L, Zhang Z, Ren L. Study on properties of SLM-NiTi shape memory alloy under the same energy density. J Mater Res Technol 2021;13:241–50.

[83] Xu L, Liu X, Sun K, Fu R, Wang G. Corrosion behavior in magnesium-based alloys for biomedical applications. Materials 2022;15:2613.

[84] Luffy SA, Wu J, Kumta PN, Gilbert TW. Evaluation of magnesium alloys for use as an intraluminal tracheal for pediatric applications in a rat tracheal bypass model. J Biomed Mater Res B Appl Biomater 2019;107:1844–53.

[85] Kiani F, Wen C, Li Y. Prospects and strategies for magnesium alloys as biodegradable implants from crystalline to bulk metallic glasses and composites-A review. Acta Biomater 2020;103:1–23.

[86] Steigmann L, Jung O, Kieferle W, Stojanovic S, Proehl A, Gorke O, Emmert S, Najman S, Barbeck M, Rothamel D. Biocompatibility and immune response of a newly developed volume-stable magnesium-based barrier membrane in

combination with a PVD coating for guided bone regeneration (GBR). Biomedicines 2020;8.
[87] Zhu B, Xu Y, Sun J, Yang L, Guo C, Liang J, Cao B. Preparation and characterization of aminated hydroxyethyl cellulose-induced biomimetic hydroxyapatite coatings on the AZ31 magnesium alloy. Metals 2017;7.
[88] Tian L, Sheng Y, Huang L, Chow DH, Chau WH, Tang N, Ngai T, Wu C, Lu J, Qin L. An innovative Mg/Ti hybrid fixation system developed for fracture fixation and healing enhancement at load-bearing skeletal site. Biomaterials 2018;180:173–83.
[89] Wang J, Wu Y, Li H, Liu Y, Bai X, Chau W, Zheng Y, Qin L. Magnesium alloy based interference screw developed for ACL reconstruction attenuates peri-tunnel bone loss in rabbits. Biomaterials 2018;157:86–97.
[90] Nam SW. High temperature properties and recent research trend of Mg-RE alloys. Kor J Metals Mater 2017;55:213–21.
[91] Shuai C, Zhou Y, Yang Y, Feng P, Liu L, He C, Zhao M, Yang S, Gao C, Wu P. Biodegradation resistance and bioactivity of hydroxyapatite enhanced Mg-Zn composites via selective laser melting. Materials 2017;10:307.
[92] Dasgupta S, Singh YP. Additive manufacturing techniques used for preparation of scaffolds in bone repair and regeneration. In: Advances in additive manufacturing artificial intelligence, nature-inspired, and biomanufacturing. Elsevier; 2023. p. 103–27.
[93] Su Y, Fu J, Zhou J, Georgas E, Du S, Qin Y-X, Wang Y, Zheng Y, Zhu D. Blending with transition metals improves bioresorbable zinc as better medical implants. Bioact Mater 2023;20:243–58.
[94] Hernández-Escobar D, Champagne S, Yilmazer H, Dikici B, Boehlert CJ, Hermawan H. Current status and perspectives of zinc-based absorbable alloys for biomedical applications. Acta Biomater 2019;97:1–22.
[95] Hussain M, Ullah S, Raza MR, Abbas N, Ali A. Recent developments in Zn-Based biodegradable materials for Biomedical Applications. J Funct Biomater 2022;14:1.
[96] Yang H, Jia B, Zhang Z, Qu X, Li G, Lin W, Zhu D, Dai K, Zheng Y. Alloying design of biodegradable zinc as promising bone implants for load-bearing applications. Nat Commun 2020;11:401.
[97] Guillory RJ, Bowen PK, Hopkins SP, Shearier ER, Earley EJ, Gillette AA, Aghion E, Bocks M, Drelich JW, Goldman J. Corrosion characteristics dictate the long-term inflammatory profile of degradable zinc arterial implants. ACS Biomater Sci Eng 2016;2:2355–64.
[98] Drelich AJ, Zhao S, Guillory II RJ, Drelich JW, Goldman J. Long-term surveillance of zinc implant in murine artery: surprisingly steady biocorrosion rate. Acta Biomater 2017;58:539–49.
[99] Su Y, Yang H, Gao J, Qin YX, Zheng Y, Zhu D. Interfacial zinc phosphate is the key to controlling biocompatibility of metallic zinc implants. Adv Sci 2019;6:1900112.
[100] Brodie EG, Robinson KJ, Sigston E, Molotnikov A, Frith JE. Osteogenic potential of additively manufactured TiTa alloys. ACS Appl Bio Mater 2021;4:1003–14.
[101] Brodie E, Medvedev A, Frith J, Dargusch M, Fraser H, Molotnikov A. Remelt processing and microstructure of selective laser melted Ti25Ta. J Alloys Compd 2020;820:153082.
[102] Al-Moameri HH, Nahi ZM, Rzaij DR, Al-Sharify NT. A review on the biomedical applications of alumina. J Eng Sustain Dev 2020;24:28–36.
[103] Bowman PD, Wang X, Meledeo MA, Dubick MA, Kheirabadi BS. Toxicity of aluminum silicates used in hemostatic dressings toward human umbilical veins endothelial cells, HeLa cells, and RAW267. 4 mouse macrophages. J Trauma Acute Care Surg 2011;71:727–32.
[104] Weng Y, Liu H, Ji S, Huang Q, Wu H, Li Z, Wu Z, Wang H, Tong L, Fu RKY, Chu PK, Pan F. A promising orthopedic implant material with enhanced osteogenic and antibacterial activity: Al2O3-coated aluminum alloy. Appl Surf Sci 2018;457:1025–34.
[105] Catchpole-Smith S, Aboulkhair N, Parry L, Tuck C, Ashcroft IA, Clare A. Fractal scan strategies for selective laser melting of 'unweldable' nickel superalloys. Addit Manuf 2017;15:113–22.
[106] Rodrigues TA, Duarte V, Avila JA, Santos TG, Miranda RM, Oliveira JP. Wire and arc additive manufacturing of HSLA steel: effect of thermal cycles on microstructure and mechanical properties. Addit Manuf 2019;27:440–50.
[107] Stef J, Poulon-Quintin A, Redjaïmia A, Ghanbaja J, Ferry O, De Sousa M, Goune M. Mechanism of porosity formation and influence on mechanical properties in selective laser melting of Ti-6Al-4V parts. Mater Des 2018;156:480–93.
[108] Gordon JV, Narra SP, Cunningham RW, Liu H, Chen H, Suter RM, Beuth JL, Rollett AD. Defect structure process maps for laser powder bed fusion additive manufacturing. Addit Manuf 2020;36:101552.
[109] Liverani E, Toschi S, Ceschini L, Fortunato A. E ff ect of selective laser melting (SLM) process parameters on microstructure and mechanical properties of 316L austenitic stainless steel. J Mater Process Technol 2017;249:255–63.
[110] Singh S, Ramakrishna S. Biomedical applications of additive manufacturing: present and future. Curr Opin Biomed Eng 2017;2:105–15.
[111] Pal S, Lojen G, Hudak R, Rajtukova V, Brajlih T, Kokol V, Drstvenšek I. As-fabricated surface morphologies of Ti-6Al-4V samples fabricated by different laser processing parameters in selective laser melting. Addit Manuf 2020;33:101147.
[112] Shuai C, Yang Y, Wu P, Lin X, Liu Y, Zhou Y, Feng P, Liu X, Peng S. Laser rapid solidification improves corrosion behavior of Mg-Zn-Zr alloy. J Alloys Compd 2017;691:961–9.
[113] Shipley H, McDonnell D, Culleton M, Coull R, Lupoi R, O'Donnell G, Trimble D. Optimisation of process parameters to address fundamental challenges during selective laser melting of Ti-6Al-4V: a review. Int J Mach Tool Manufact 2018;128:1–20.
[114] Larimian T, Kannan M, Grzesiak D, AlMangour B, Borkar T. Effect of energy density and scanning strategy on densification, microstructure and mechanical properties of 316L stainless steel processed via selective laser melting. Mater Sci Eng, A 2020;770.
[115] Dhansay NM, Tait R, Becker T. Fatigue and fracture toughness of Ti-6Al-4V titanium alloy manufactured by selective laser melting. Adv Mater Res 2014;1019:248–53.
[116] Yadroitsev I, Thivillon L, Bertrand P, Smurov I. Strategy of manufacturing components with designed internal structure by selective laser melting of metallic powder. Appl Surf Sci 2007;254:980–3.
[117] King WE, Barth HD, Castillo VM, Gallegos GF, Gibbs JW, Hahn DE, Kamath C, Rubenchik AM. Observation of keyhole-mode laser melting in laser powder-bed fusion additive manufacturing. J Mater Process Technol 2014;214:2915–25.
[118] Kasperovich G, Haubrich J, Gussone J, Requena G. Correlation between porosity and processing parameters in TiAl6V4 produced by selective laser melting. JMADE 2016;105:160–70.
[119] Ding L, Tan S, Chen W, Jin Y, Zhang Y. Manufacturability analysis of extremely fine porous structures for selective laser melting process of Ti6Al4V alloy. Rapid Prototyp J 2021;27:1523–37.
[120] Mukherjee T, Zuback J, De A, DebRoy T. Printability of alloys for additive manufacturing. Sci Rep 2016;6:19717.
[121] Yakout M, Elbestawi M, Veldhuis SC. A study of the relationship between thermal expansion and residual stresses in selective laser melting of Ti-6Al-4V. J Manuf Process 2020;52:181–92.
[122] Xu W, Brandt M, Sun S, Elambasseril J, Liu Q, Latham K, Xia K, Qian M. Additive manufacturing of strong and ductile Ti–6Al–4V by selective laser melting via in situ martensite decomposition. Acta Mater 2015;85:74–84.
[123] Salem H, Carter LN, Attallah MM, Salem HG. Influence of processing parameters on internal porosity and types of defects formed in Ti6Al4V lattice structure fabricated by selective laser melting. Mater Sci Eng, A 2019;767.
[124] Wen P, Jauer L, Voshage M, Chen Y, Poprawe R, Schleifenbaum JH. Densification behavior of pure Zn metal parts produced by selective laser melting for manufacturing biodegradable implants. J Mater Process Technol 2018;258:128–37.
[125] Li X, Kang C, Huang H, Sercombe T. The role of a low-energy–density re-scan in fabricating crack-free Al85Ni5Y6Co2Fe2 bulk metallic glass composites via selective laser melting. Mater Des 2014;63:407–11.
[126] Fousová M, Vojtěch D, Doubrava K, Daniel M, Lin C-F. Influence of inherent surface and internal defects on mechanical properties of additively manufactured Ti6Al4V alloy: comparison between selective laser melting and electron beam melting. Materials 2018;11:537.
[127] Singla AK, Banerjee M, Sharma A, Singh J, Bansal A, Gupta MK, Khanna N, Shahi AS, Goyal DK. Selective laser melting of Ti6Al4V alloy: process parameters, defects and post-treatments. J Manuf Process 2021;64:161–87.
[128] Honarvar F, Varvani-Farahani A. A review of ultrasonic testing applications in additive manufacturing: defect evaluation, material characterization, and process control. Ultrasonics 2020;108:106227.
[129] Zhou X, Dai N, Chu M, Wang L, Li D, Zhou L, Cheng X. X-ray CT analysis of the influence of process on defect in Ti-6Al-4V parts produced with Selective Laser Melting technology. Int J Adv Des Manuf Technol 2020;106:3–14.
[130] Afrouzian A, Bandyopadhyay A. 3D printed silicon nitride, alumina, and hydroxyapatite ceramic reinforced Ti6Al4V composites - tailored microstructures to enhance bio-tribo-corrosion and antibacterial properties. J Mech Behav Biomed Mater 2023;144:105973.
[131] Igbokwe IO, Igwenagu E, Igbokwe NA. Aluminium toxicosis: a review of toxic actions and effects. Interdiscipl Toxicol 2019;12:45.
[132] He Z, Han S, Zhu H, Hu X, Li X, Hou C, Wu C, Xie Q, Li N, Du X, Ni J, Liu Q. The protective effect of vanadium on cognitive impairment and the neuropathology of Alzheimer's disease in APPSwe/PS1dE9 mice. Front Mol Neurosci 2020;13:21.
[133] Manivasagam G, Dhinasekaran D, Rajamanickam A. Biomedical implants: corrosion and its prevention - a review. Recent patents on corrosion. Science 2010;2:40–54.
[134] Dai N, Zhang L-C, Zhang J, Chen Q, Wu M. Corrosion behavior of selective laser melted Ti-6Al-4 V alloy in NaCl solution. Corrosion Sci 2016;102:484–9.
[135] Guo S, Lu Y, Wu S, Liu L, He M, Zhao C, Gan Y, Lin J, Luo J, Xu X. Preliminary study on the corrosion resistance, antibacterial activity and cytotoxicity of selective-laser-melted Ti6Al4V-xCu alloys. Mater Sci Eng C 2017;72:631–40.
[136] Khan HM, Özer G, Yilmaz MS, Koç E. Corrosion of additively manufactured metallic components: a review. Arabian J Sci Eng 2022;47:5465–90.
[137] Chi G, Yi D, Liu H. Effect of roughness on electrochemical and pitting corrosion of Ti-6Al-4V alloy in 12 wt.% HCl solution at 35 C. J Mater Res Technol 2020;9:1162–74.
[138] Zhang Y, Liu F, Chen J, Yuan Y. Effects of surface quality on corrosion resistance of 316L stainless steel parts manufactured via SLM. J Laser Appl 2017;29.
[139] Nandwana P, Elliott AM, Siddel D, Merriman A, Peter WH, Babu SS. Powder bed binder jet 3D printing of Inconel 718: densification, microstructural evolution and challenges. Curr Opin Solid State Mater Sci 2017;21:207–18.
[140] Wang X, Mercier D, Danard Y, Rieger T, Perrière L, Laurent-Brocq M, Guillot I, Maurice V, Marcus P. Enhanced passivity of Cr-Fe-Co-Ni-Mo multi-component single-phase face-centred cubic alloys: design, production and corrosion behaviour. Corrosion Sci 2022;200:110233.
[141] Chiu T-M, Mahmoudi M, Dai W, Elwany A, Liang H, Castaneda H. Corrosion assessment of Ti-6Al-4V fabricated using laser powder-bed fusion additive manufacturing. Electrochim Acta 2018;279:143–51.

[142] Chandramohan P, Bhero S, Obadele BA, Olubambi PA. Laser additive manufactured Ti–6Al–4V alloy: tribology and corrosion studies. Int J Adv Des Manuf Technol 2017;92:3051–61.
[143] Ciliveri S, Bandyopadhyay A. Understanding the influence of alloying elements on the print quality of powder bed fusion-based metal additive manufacturing: Ta and Cu addition to Ti alloy. Virtual Phys Prototyp 2023;18:e2248464.
[144] Wang X, Zhang L, Fang M, Sercombe TB. The effect of atmosphere on the structure and properties of a selective laser melted Al–12Si alloy. Mater Sci Eng, A 2014;597:370–5.
[145] Hedberg YS, Qian B, Shen Z, Virtanen S, Wallinder IO. In vitro biocompatibility of CoCrMo dental alloys fabricated by selective laser melting. Dent Mater 2014;30:525–34.
[146] Revilla RI, Liang J, Godet S, De Graeve I. Local corrosion behavior of additive manufactured AlSiMg alloy assessed by SEM and SKPFM. J Electrochem Soc 2016;164:C27.
[147] Chao Q, Cruz V, Thomas S, Birbilis N, Collins P, Taylor A, Hodgson PD, Fabijanic D. On the enhanced corrosion resistance of a selective laser melted austenitic stainless steel. Scripta Mater 2017;141:94–8.
[148] Sander G, Thomas S, Cruz V, Jurg M, Birbilis N, Gao X, Brameld M, Hutchinson C. On the corrosion and metastable pitting characteristics of 316L stainless steel produced by selective laser melting. J Electrochem Soc 2017;164:C250.
[149] Stendal J, Fergani O, Yamaguchi H, Espallargas N. A comparative tribocorrosion study of additive manufactured and wrought 316L stainless steel in simulated body fluids. J Bio-and Tribo-Corros 2018;4:1–10.
[150] Wang W, Yung K, Choy H, Xiao T, Cai Z. Effects of laser polishing on surface microstructure and corrosion resistance of additive manufactured CoCr alloys. Appl Surf Sci 2018;443:167–75.
[151] Al-Mamun NS, Deen KM, Haider W, Asselin E, Shabib I. Corrosion behavior and biocompatibility of additively manufactured 316L stainless steel in a physiological environment: the effect of citrate ions. Addit Manuf 2020;34:101237.
[152] Rubben T, Revilla RI, De Graeve I. Influence of heat treatments on the corrosion mechanism of additive manufactured AlSi10Mg. Corrosion Sci 2019;147:406–15.
[153] Fathi P, Rafieazad M, Duan X, Mohammadi M, Nasiri A. On microstructure and corrosion behaviour of AlSi10Mg alloy with low surface roughness fabricated by direct metal laser sintering. Corrosion Sci 2019;157:126–45.
[154] Liu P, Hu J-y, Li H-x, Sun S-y, Zhang Y-b. Effect of heat treatment on microstructure, hardness and corrosion resistance of 7075 Al alloys fabricated by SLM. J Manuf Process 2020;60:578–85.
[155] Sonofuchi K, Hagiwara Y, Koizumi Y, Chiba A, Kawano M, Nakayama M, Ogasawara K, Yabe Y, Itoi E. Quantitative in vivo biocompatibility of new ultralow-nickel cobalt–chromium–molybdenum alloys. J Orthop Res 2016;34:1505–13.
[156] Sasikumar Y, Indira K, Rajendran N. Surface modification methods for titanium and its alloys and their corrosion behavior in biological environment: a review. J Bio-and Tribo-Corros 2019;5:1–25.
[157] Malik A, Rouf S, Haq MIU, Raina A, Puerta APV, Sagbas B, Ruggiero A. Tribo-corrosive behavior of additive manufactured parts for orthopaedic applications. J Orthop 2022;34:49–60.
[158] Qi J, Ma L, Gong P, Rainforth W. Investigation of the wear transition in CoCrMo alloys after heat treatment to produce an HCP structure. Wear 2023;518:204649.
[159] Xiao J, Shang X, Hou J, Li Y, He B. Role of stress-induced martensite on damage behavior in a metastable titanium alloy. Int J Plast 2021;146:103103.
[160] Kale AB, Kim B-K, Kim D-I, Castle E, Reece M, Choi S-H. An investigation of the corrosion behavior of 316L stainless steel fabricated by SLM and SPS techniques. Mater Char 2020;163:110204.
[161] Leon A, Aghion E. Effect of surface roughness on corrosion fatigue performance of AlSi10Mg alloy produced by Selective Laser Melting (SLM). Mater Char 2017;131:188–94.
[162] Pal S, Basak D. Interaction of an ultrathin zinc surface passivation layer with a room temperature-deposited Al-doped ZnO film leading to highly improved electrical transport properties. J Phys Chem C 2023;127:14439–49.
[163] Aboulkhair NT, Maskery I, Tuck C, Ashcroft I, Everitt NM. The microstructure and mechanical properties of selectively laser melted AlSi10Mg: the effect of a conventional T6-like heat treatment. Mater Sci Eng, A 2016;667:139–46.
[164] Lodhi MK, Deen KM, Greenlee-Wacker M, Haider W. Additively manufactured 316L stainless steel with improved corrosion resistance and biological response for biomedical applications. Addit Manuf 2019;27:8–19.
[165] Man C, Dong C, Liu T, Kong D, Wang D, Li X. The enhancement of microstructure on the passive and pitting behaviors of selective laser melting 316L SS in simulated body fluid. Appl Surf Sci 2019;467:193–205.
[166] Al-Mamun NS, Haider W, Shabib I. Corrosion resistance of additively manufactured 316L stainless steel in chloride− thiosulfate environment. Electrochim Acta 2020;362:137039.
[167] Karimi MS, Yeganeh M, Zaree SA, Eskandari M. Corrosion behavior of 316L stainless steel manufactured by laser powder bed fusion (L-PBF) in an alkaline solution. Opt Laser Technol 2021;138:106918.
[168] Wang N, Meenashisundaram GK, Chang S, Fuh JYH, Dheen ST, Senthil Kumar A. A comparative investigation on the mechanical properties and cytotoxicity of Cubic, Octet, and TPMS gyroid structures fabricated by selective laser melting of stainless steel 316L. J Mech Behav Biomed Mater 2022;129:105151.
[169] Xie F, He X, Cao S, Qu X. Structural and mechanical characteristics of porous 316L stainless steel fabricated by indirect selective laser sintering. J Mater Process Technol 2013;213:838–43.
[170] Kong D, Ni X, Dong C, Lei X, Zhang L, Man C, Yao J, Cheng X, Li X. Bio-functional and anti-corrosive 3D printing 316L stainless steel fabricated by selective laser melting. Mater Des 2018;152:88–101.
[171] Aufa AN, Hassan MZ, Ismail Z, Harun N, Ren J, Sadali MF. Surface enhancement of Ti–6Al–4V fabricated by selective laser melting on bone-like apatite formation. J Mater Res Technol 2022;19:4018–30.
[172] Zhao B, Wang H, Qiao N, Wang C, Hu M. Corrosion resistance characteristics of a Ti-6Al-4V alloy scaffold that is fabricated by electron beam melting and selective laser melting for implantation in vivo. Mater Sci Eng C Mater Biol Appl 2017;70:832–41.
[173] Pei X, Wu L, Lei H, Zhou C, Fan H, Li Z, Zhang B, Sun H, Gui X, Jiang Q, Fan Y, Zhang X. Fabrication of customized Ti6AI4V heterogeneous scaffolds with selective laser melting: optimization of the architecture for orthopedic implant applications. Acta Biomater 2021;126:485–95.
[174] Jamshidi P, Aristizabal M, Kong W, Villapun V, Cox SC, Grover LM, Attallah MM. Selective laser melting of Ti-6Al-4V: the impact of post-processing on the tensile, fatigue and biological properties for medical implant applications. Materials 2020;13.
[175] Ran Q, Yang W, Hu Y, Shen X, Yu Y, Xiang Y, Cai K. Osteogenesis of 3D printed porous Ti6Al4V implants with different pore sizes. J Mech Behav Biomed Mater 2018;84:1–11.
[176] Fazel M, Salimijazi HR, Shamanian M, Minneboo M, Modaresifar K, van Hengel IAJ, Fratila-Apachitei LE, Apachitei I, Zadpoor AA. Osteogenic and antibacterial surfaces on additively manufactured porous Ti-6Al-4V implants: combining silver nanoparticles with hydrothermally synthesized HA nanocrystals. Mater Sci Eng C Mater Biol Appl 2021;120:111745.
[177] Yan C, Hao L, Hussein A, Wei Q, Shi Y. Microstructural and surface modifications and hydroxyapatite coating of Ti-6Al-4V triply periodic minimal surface lattices fabricated by selective laser melting. Mater Sci Eng C Mater Biol Appl 2017;75:1515–24.
[178] Peng WM, Liu YF, Jiang XF, Dong XT, Jun J, Baur DA, Xu JJ, Pan H, Xu X. Bionic mechanical design and 3D printing of novel porous Ti6Al4V implants for biomedical applications. J Zhejiang Univ - Sci B 2019;20:647–59.
[179] Bandyopadhyay A, Mitra I, Shivaram A, Dasgupta N, Bose S. Direct comparison of additively manufactured porous titanium and tantalum implants towards in vivo osseointegration. Addit Manuf 2019;28:259–66.
[180] Gao C, Zeng Z, Peng S, Shuai C. Magnetostrictive bulk Fe-Ga alloys prepared by selective laser melting for biodegradable implant applications. Mater Des 2022;220.
[181] Bartolomeu F, Costa MM, Alves N, Miranda G, Silva FS. Engineering the elastic modulus of NiTi cellular structures fabricated by selective laser melting. J Mech Behav Biomed Mater 2020;110:103891.
[182] Liverani E, Fortunato A, Leardini A, Belvedere C, Siegler S, Ceschini L, Ascari A. Fabrication of Co–Cr–Mo endoprosthetic ankle devices by means of Selective Laser Melting (SLM). Mater Des 2016;106:60–8.
[183] Zong W, Zhang S, Zhang C, Ren L, Wang Q. Design and characterization of selective laser-melted Ti6Al4V–5Cu alloy for dental implants. Mater Corros 2020;71:1697–710.
[184] Wu M, Dong X, Qu Y, Yan J, Li N. Analysis of microstructure and fatigue of cast versus selective laser-melted dental Co-Cr alloy. J Prosthet Dent 2022;128:218 e211–e218 e217.
[185] Al Jabbari YS, Koutsoukis T, Barmpagadaki X, Zinelis S. Metallurgical and interfacial characterization of PFM Co-Cr dental alloys fabricated via casting, milling or selective laser melting. Dent Mater 2014;30:e79–88.
[186] Caravaggi P, Liverani E, Leardini A, Fortunato A, Belvedere C, Baruffaldi F, Fini M, Parrilli A, Mattioli-Belmonte M, Tomesani L. CoCr porous scaffolds manufactured via selective laser melting in orthopedics: topographical, mechanical, and biological characterization. J Biomed Mater Res B Appl Biomater 2019;107:2343–53.
[187] Wally ZJ, Haque AM, Feteira A, Claeyssens F, Goodall R, Reilly GC. Selective laser melting processed Ti6Al4V lattices with graded porosities for dental applications. J Mech Behav Biomed Mater 2019;90:20–9.
[188] Iatecola A, Longhitano GA, Antunes LHM, Jardini AL, Miguel EdC, Béreš M, Lambert CS, Andrade TN, Buchaim RL, Buchaim DV. Osseointegration improvement of Co-Cr-Mo alloy produced by additive manufacturing. Pharmaceutics 2021;13:724.
[189] Naujokat H, Gokkaya AI, Acil Y, Loger K, Kluter T, Fuchs S, Wiltfang J. In vivo biocompatibility evaluation of 3D-printed nickel-titanium fabricated by selective laser melting. J Mater Sci Mater Med 2022;33:13.
[190] Lu Y, Zhou Y, Liang X, Zhang X, Zhang C, Zhu M, Tang K, Lin J. Early bone ingrowth of Cu-bearing CoCr scaffolds produced by selective laser melting: an in vitro and in vivo study. Mater Des 2023;228:111822.
[191] Bandyopadhyay A, Ciliveri S, Guariento S, Zuckschwerdt N, Hogg WW. Fatigue behavior of additively manufactured Ti3Al2V alloy. Mater Sci Addit Manuf 2023;2.
[192] Tamayo JA, Riascos M, Vargas CA, Baena LM. Additive manufacturing of Ti6Al4V alloy via electron beam melting for the development of implants for the biomedical industry. Heliyon 2021;7:e06892.
[193] Paluch E, Rewak-Soroczyńska J, Jędrusik I, Mazurkiewicz E, Jermakow K. Prevention of biofilm formation by quorum quenching. Appl Microbiol Biotechnol 2020;104:1871–81.
[194] Guzman-Soto I, McTiernan C, Gonzalez-Gomez M, Ross A, Gupta K, Suuronen EJ, Mah T-F, Griffith M, Alarcon EI. Mimicking biofilm formation and development: recent progress in in vitro and in vivo biofilm models. iScience 2021;24.
[195] Arnaouteli S, Bamford NC, Stanley-Wall NR, Kovács ÁT. Bacillus subtilis biofilm formation and social interactions. Nat Rev Microbiol 2021;19:600–14.

[196] Sauer K, Stoodley P, Goeres DM, Hall-Stoodley L, Burmølle M, Stewart PS, Bjarnsholt T. The biofilm life cycle: expanding the conceptual model of biofilm formation. Nat Rev Microbiol 2022;20:608–20.
[197] Ruhal R, Kataria R. Biofilm patterns in gram-positive and gram-negative bacteria. Microbiol Res 2021;251:126829.
[198] Little B, Blackwood D, Hinks J, Lauro F, Marsili E, Okamoto A, Rice S, Wade S, Flemming H-C. Microbially influenced corrosion—any progress? Corrosion Sci 2020;170:108641.
[199] Yin W, Wang Y, Liu L, He J. Biofilms: the microbial "protective clothing" in extreme environments. Int J Mol Sci 2019;20:3423.
[200] Ren L, Memarzadeh K, Zhang S, Sun Z, Yang C, Ren G, Allaker RP, Yang K. A novel coping metal material CoCrCu alloy fabricated by selective laser melting with antimicrobial and antibiofilm properties. Mater Sci Eng C Mater Biol Appl 2016;67:461–7.
[201] van Hengel IAJ, Riool M, Fratila-Apachitei LE, Witte-Bouma J, Farrell E, Zadpoor AA, Zaat SAJ, Apachitei I. Selective laser melting porous metallic implants with immobilized silver nanoparticles kill and prevent biofilm formation by methicillin-resistant Staphylococcus aureus. Biomaterials 2017;140:1–15.
[202] Macpherson A, Li X, McCormick P, Ren L, Yang K, Sercombe TB. Antibacterial titanium produced using selective laser melting. Jom 2017;69:2719–24.
[203] Guo S, Lu Y, Wu S, Liu L, He M, Zhao C, Gan Y, Lin J, Luo J, Xu X, Lin J. Preliminary study on the corrosion resistance, antibacterial activity and cytotoxicity of selective-laser-melted Ti6Al4V-xCu alloys. Mater Sci Eng C Mater Biol Appl 2017;72:631–40.
[204] Lu Y, Ren L, Wu S, Yang C, Lin W, Xiao S, Yang Y, Yang K, Lin J. CoCrWCu alloy with antibacterial activity fabricated by selective laser melting: densification, mechanical properties and microstructural analysis. Powder Technol 2018;325:289–300.
[205] Luo J, Guo S, Lu Y, Xu X, Zhao C, Wu S, Lin J. Cytocompatibility of Cu-bearing Ti6Al4V alloys manufactured by selective laser melting. Mater Char 2018;143:127–36.
[206] Wu F, Xu R, Yu X, Yang J, Liu Y, Ouyang J, Zhang C, Deng F. Enhanced biocompatibility and antibacterial activity of selective laser melting titanium with zinc-doped micro-nano topography. J Nanomater 2019;2019:5432040.
[207] Xu R, Zhao M-C, Zhao Y-C, Liu L, Liu C, Gao C, Shuai C, Atrens A. Improved biodegradation resistance by grain refinement of novel antibacterial ZK30-Cu alloys produced via selective laser melting. Mater Lett 2019;237:253–7.
[208] Rahmani R, Rosenberg M, Ivask A, Kollo L. Comparison of mechanical and antibacterial properties of TiO2/Ag ceramics and Ti6Al4V-TiO2/Ag composite materials using combined SLM-SPS techniques. Metals 2019;9.
[209] Qing Y, Li K, Li D, Qin Y. Antibacterial effects of silver incorporated zeolite coatings on 3D printed porous stainless steels. Mater Sci Eng C Mater Biol Appl 2020;108:110430.
[210] Guo Y, Zhao M-C, Xie B, Zhao Y-C, Yin D, Gao C, Shuai C, Atrens A. In vitro corrosion resistance and antibacterial performance of novel Fe– x Cu biomedical alloys prepared by selective laser melting. Adv Eng Mater 2021;23.
[211] Xie B, Zhao MC, Xu R, Zhao YC, Yin D, Gao C, Atrens A. Biodegradation, antibacterial performance, and cytocompatibility of a novel ZK30-Cu-Mn biomedical alloy produced by selective laser melting. Int J Bioprint 2021;7:300.
[212] Ji H, Zhao M-C, Xie B, Zhao Y-C, Yin D, Gao C, Shuai C, Atrens A. Corrosion and antibacterial performance of novel selective-laser-melted (SLMed) Ti-xCu biomedical alloys. J Alloys Compd 2021;864.
[213] Gao J, Jin Y, Fan Y, Xu D, Meng L, Wang C, Yu Y, Zhang D, Wang F. Fabricating antibacterial CoCrCuFeNi high-entropy alloy via selective laser melting and in-situ alloying. J Mater Sci Technol 2022;102:159–65.
[214] Rajendran A, Pattanayak DK. Bioactive and antimicrobial macro-/micro-nanoporous selective laser melted Ti–6Al–4V alloy for biomedical applications. Heliyon 2022;8:e09122.
[215] Sedaghat S, Krishnakumar A, Selvamani V, Barnard JP, Nejati S, Wang H, Detwiler DA, Seleem MN, Rahimi R. Laser-assisted surface alloying of titanium with silver to enhance antibacterial and bone-cell mineralization properties of orthopedic implants. J Mater Chem B 2024;12:4489–501.
[216] Cantor B, Chang I, Knight P, Vincent A. Microstructural development in equiatomic multicomponent alloys. Mater Sci Eng, A 2004;375:213–8.
[217] Yeh JW, Chen SK, Lin SJ, Gan JY, Chin TS, Shun TT, Tsau CH, Chang SY. Nanostructured high-entropy alloys with multiple principal elements: novel alloy design concepts and outcomes. Adv Eng Mater 2004;6:299–303.
[218] Zhou E, Qiao D, Yang Y, Xu D, Lu Y, Wang J, Smith JA, Li H, Zhao H, Liaw PK. A novel Cu-bearing high-entropy alloy with significant antibacterial behavior against corrosive marine biofilms. J Mater Sci Technol 2020;46:201–10.
[219] Wang Q, Ren L, Li X, Zhang S, Sercombe TB, Yang K. Antimicrobial Cu-bearing stainless steel scaffolds. Mater Sci Eng C Mater Biol Appl 2016;68:519–22.
[220] Chen P, Li S, Zhou Y, Yan M, Attallah MM. Fabricating CoCrFeMnNi high entropy alloy via selective laser melting in-situ alloying. J Mater Sci Technol 2020;43:40–3.
[221] Moore K, Gupta N, Gupta TT, Patel K, Brooks JR, Sullivan A, Litsky AS, Stoodley P. Mapping bacterial biofilm on features of orthopedic implants in vitro. Microorganisms 2022;10.
[222] Bandyopadhyay A, Mitra I, Ciliveri S, Avila JD, Dernell W, Goodman SB, Bose S. Additively manufactured Ti-Ta-Cu alloys for the next-generation load-bearing implants. Int J Extrem Manuf 2024;6:015503.
[223] Sedaghat S, Krishnakumar A, Selvamani V, Barnard JP, Nejati S, Wang H, Detwiler DA, Seleem MN, Rahimi R. Laser-assisted surface alloying of titanium with silver to enhance antibacterial and bone-cell mineralization properties of orthopedic implants. J Mater Chem B 2024;12:4489–501.
[224] Chen Dexin, Li Yaoxin, He Hongyuan, Li Wei, Zeng Rong, Wang Xiaojian. Covalent incorporation of Ag nanoparticles into TiO2 nanotubes on Ti6Al4V by molecular grafting for enhancing antibacterial effect. 2021.
[225] Xu JY, Li KL, Tang JC, Zhou YH, Luo JP, Tang W, Lai YX, Dargusch MS, Yan M. Additive manufacturing of anti-bacterial and low-cost Ti–Mo(–Ag) alloys using elemental powders through in situ laser alloying. J Mater Sci 2023;58:2268–93.
[226] Lowther M. Delivery of antimicrobial biomaterials through additive manufacturing. University of Birmingham; 2022.
[227] Liu X, Chen C, Zhang H, Tian A, You J, Wu L, Lei Z, Li X, Bai X, Chen S. Biocompatibility evaluation of antibacterial Ti-Ag alloys with nanotubular coatings. Int J Nanomed 2019;14:457–68.
[228] Jamuna-Thevi K, Bakar S, Ibrahim S, Shahab N, Toff M. Quantification of silver ion release, in vitro cytotoxicity and antibacterial properties of nanostuctured Ag doped TiO2 coatings on stainless steel deposited by RF magnetron sputtering. Vacuum 2011;86:235–41.
[229] Zheng Y, Zhang B, Wang B, Wang Y, Li L, Yang Q, Cui L. Introduction of antibacterial function into biomedical TiNi shape memory alloy by the addition of element Ag. Acta Biomater 2011;7:2758–67.
[230] Qi L, Guo B, Lu Q, Gong H, Wang M, He J, Jia B, Ren J, Zheng S, Lu Y. Preparation and photocatalytic and antibacterial activities of micro/nanostructured TiO2-based photocatalysts for application in orthopedic implants. Front Mater 2022;9:914905.
[231] Bedi TS, Kumar S, Kumar R. Corrosion performance of hydroxyapaite and hydroxyapaite/titania bond coating for biomedical applications. Mater Res Express 2019;7:015402.
[232] Alateyah AI, Alawad MO, Aljohani TA, El-Garaihy WH. Influence of ultrafine-grained microstructure and texture evolution of ECAPed ZK30 magnesium alloy on the corrosion behavior in different corrosive agents. Materials 2022;15:5515.
[233] Savaedi Z, Mirzadeh H, Aghdam RM, Mahmudi R. Thermal stability, grain growth kinetics, mechanical properties, and bio-corrosion resistance of pure Mg, ZK30, and ZEK300 alloys: a comparative study. Mater Today Commun 2022;33:104825.
[234] da Silva Rodrigues J, Antonini LM, da Cunha Bastos AA, Zhou J, de Fraga Malfatti C. Corrosion resistance and tribological behavior of ZK30 magnesium alloy coated by plasma electrolytic oxidation. Surf Coating Technol 2021;410:126983.
[235] Lv J, Xiu P, Tan J, Jia Z, Cai H, Liu Z. Enhanced angiogenesis and osteogenesis in critical bone defects by the controlled release of BMP-2 and VEGF: implantation of electron beam melting-fabricated porous Ti6Al4V scaffolds incorporating growth factor-doped fibrin glue. Biomed Mater 2015;10:035013.
[236] Liu H, Li W, Liu C, Tan J, Wang H, Hai B, Cai H, Leng HJ, Liu ZJ, Song CL. Incorporating simvastatin/poloxamer 407 hydrogel into 3D-printed porous Ti(6)Al(4)V scaffolds for the promotion of angiogenesis, osseointegration and bone ingrowth. Biofabrication 2016;8:045012.
[237] Xu J-y, Chen X-s, Zhang C-y, Liu Y, Wang J, Deng F-l. Improved bioactivity of selective laser melting titanium: surface modification with micro-/nano-textured hierarchical topography and bone regeneration performance evaluation. Mater Sci Eng C 2016;68:229–40.
[238] Luo J, Jia X, Gu R, Zhou P, Huang Y, Sun J, Yan M. 316L stainless steel manufactured by selective laser melting and its biocompatibility with or without hydroxyapatite coating. Metals 2018;8.
[239] Feng J, Wang J, Yang K, Rong J. Microstructure and performance of YTaO4 coating deposited by atmospheric plasma spraying on TC4 titanium alloy surface. Surf Coating Technol 2022;431:128004.
[240] Mändl S, Manova D. Modification of metals by plasma immersion ion implantation. Surf Coating Technol 2019;365:83–93.
[241] Khamseh S, Ganjaee Sari M, Alibakhshi E, Nemati M. Hydrogen-free Cu: amorphous-C: N coating on TC4 titanium alloy: the role of gas ratio on mechanical and antibacterial potency. Progress in Color, Colorants and Coatings 2021;14:281–91.
[242] Li HQ, Guo H, Shen FL, Lou DJ, Xia WL, Fang XY. Tribological and corrosion performance of the plasma-sprayed conformal ceramic coating on selective laser melted CoCrMo alloy. J Mech Behav Biomed Mater 2021;119:104520.
[243] Liang C, Hu Y, Liu N, Zou X, Wang H, Zhang X, Fu Y, Hu J. Laser polishing of Ti6Al4V fabricated by selective laser melting. Metals 2020;10:191.
[244] Zhao C, Qu N, Tang X. Electrochemical mechanical polishing of internal holes created by selective laser melting. J Manuf Process 2021;64:1544–62.
[245] Schupbach P, Glauser R, Bauer S. Al 2 O 3 particles on titanium dental implant systems following sandblasting and acid-etching process. Int J Biomater 2019;2019.
[246] Obeidi MA, McCarthy E, O'Connell B, Ul Ahad I, Brabazon D. Laser polishing of additive manufactured 316L stainless steel synthesized by selective laser melting. Materials 2019;12.
[247] Bai Y, Zhao C, Yang J, Fuh JYH, Lu WF, Weng C, Wang H. Dry mechanical-electrochemical polishing of selective laser melted 316L stainless steel. Mater Des 2020;193.
[248] Li Y, Zhang Z, Guan Y. Thermodynamics analysis and rapid solidification of laser polished Inconel 718 by selective laser melting. Appl Surf Sci 2020;511.
[249] Yang J, Yu X, Zhang Z, Xu R, Wu F, Wang T, Liu Y, Ouyang J, Deng F. Surface modification of titanium manufactured through selective laser melting inhibited osteoclast differentiation through mitogen-activated protein kinase signaling pathway. J Biomater Appl 2020;35:169–81.
[250] Lv S, Tao H, Hong Y, Zheng Y, Zhou C, Zheng J, Zhang L. Surface treatment and corrosion behavior of 316L stainless steel fabricated by selective laser melting. Mater Res Express 2019;6:106518.
[251] Baciu A, Bejinariu C, Corăbieru A, Mihalache E, Lupu–Poliac M, Baciu C, Baciu E. Influence of process parameters for Selective Laser Melting on the roughness of

3D printed surfaces in Co-Cr dental alloy powder. In: IOP conference series: materials science and engineering. IOP Publishing; 2019, 012054.
[252] Kadam NR, Karthikeyan G, Jagtap PM, Kulkarni DM. An atmospheric plasma spray and electron beam-physical vapour deposition for thermal barrier coatings: a review. Aust J Mech Eng 2023;21:1729–54.
[253] Lassègue P, Salvan C, De Vito E, Soulas R, Herbin M, Hemberg A, Godfroid T, Baffie T, Roux G. Laser powder bed fusion (L-PBF) of Cu and CuCrZr parts: influence of an absorptive physical vapor deposition (PVD) coating on the printing process. Addit Manuf 2021;39:101888.
[254] Wozniak A, Adamiak M, Chladek G, Bonek M, Walke W, Bialas O. The influence of hybrid surface modification on the selected properties of CP titanium grade II manufactured by selective laser melting. Materials 2020;13.
[255] Konovalov S, Osintsev K, Golubeva A, Smelov V, Ivanov Y, Chen X, Komissarova I. Surface modification of Ti-based alloy by selective laser melting of Ni-based superalloy powder. J Mater Res Technol 2020;9:8796–807.
[256] Sitek R, Molak R, Zdunek J, Bazarnik P, Wiśniewski P, Kubiak K, Mizera J. Influence of an aluminizing process on the microstructure and tensile strength of the nickel superalloy IN 718 produced by the Selective Laser Melting. Vacuum 2021;186:110041.
[257] Macera L, Pullini D, Boschetto A, Bottini L, Mingazzini C, Falleti GL. Sol–gel silica coatings for corrosion protection of aluminum parts manufactured by selective laser melting (SLM) technology. Coatings 2023;13:1081.
[258] Koo B, Jang M-S, Nam YG, Yang S, Yu J, Park YH, Jeong JW. Structurally-layered soft magnetic Fe-Si components with surface insulation prepared by shell-shaping selective laser melting. Appl Surf Sci 2021;553:149510.
[259] Gu Y, Wei L, Zhang Z, Van Dessel J, Driesen RB, Lambrichts I, Jacobs R, Tian L, Sun Y, Liu Y, Politis C. BMP-2 incorporated biomimetic CaP coating functionalized 3D printed Ti6Al4V scaffold induces ectopic bone formation in a dog model. Mater Des 2022;215.
[260] Sun X, Lin H, Zhang C, Liu Y, Jin J, Di S. A biomimetic hierarchical structure on selective laser melting titanium with enhanced hydrophilic/hydrophobic surface. J Alloys Compd 2022;895:162585.
[261] Vaithilingam J, Kilsby S, Goodridge RD, Christie SD, Edmondson S, Hague RJ. Functionalisation of Ti6Al4V components fabricated using selective laser melting with a bioactive compound. Mater Sci Eng C Mater Biol Appl 2015;46:52–61.
[262] Liu H, Li W, Liu C, Tan J, Wang H, Hai B, Cai H, Leng HJ, Liu ZJ, Song CL. Incorporating simvastatin/poloxamer 407 hydrogel into 3D-printed porous Ti6Al4V scaffolds for the promotion of angiogenesis, osseointegration and bone ingrowth. Biofabrication 2016;8:045012.
[263] Bezuidenhout MB, Booysen E, van Staden AD, Uheida EH, Hugo PA, Oosthuizen GA, Dimitrov DM, Dicks LMT. Selective laser melting of integrated Ti6Al4V ELI permeable walls for controlled drug delivery of vancomycin. ACS Biomater Sci Eng 2018;4:4412–24.
[264] Zhang T, Wei Q, Zhou H, Zhou W, Fan D, Lin X, Jing Z, Cai H, Cheng Y, Liu X, Li W, Song C, Tian Y, Xu N, Zheng Y, Liu Z. Sustainable release of vancomycin from micro-arc oxidised 3D-printed porous Ti6Al4V for treating methicillin-resistant Staphylococcus aureus bone infection and enhancing osteogenesis in a rabbit tibia osteomyelitis model. Biomater Sci 2020;8:3106–15.
[265] Li J, Mutreja I, Hooper GJ, Clinch K, Lim K, Evans G, Woodfield TF. Combined infection control and enhanced osteogenic differentiation capacity on additive manufactured Ti-6Al-4V are mediated via titania nanotube delivery of novel biofilm inhibitors. Adv Mater Interfac 2020;7.
[266] Micheletti C, Suriano R, Grandfield K, Turri S. Drug release from polymer-coated TiO2 nanotubes on additively manufactured Ti-6Al-4V bone implants: a feasibility study. Nano Express 2021;2.
[267] Chudinova E, Koptyug A, Mukhortova Y, Pryadko A, Volkova A, Ivanov A, Plotnikov E, Khan Y, Epple M, Sokolova V, Prymak O, Douglas T, Surmenev R, Surmeneva M. Functionalization of additive-manufactured Ti6Al4V scaffolds with poly(allylamine hydrochloride)/poly(styrene sulfonate) bilayer microcapsule system containing dexamethasone. Mater Chem Phys 2021;273.
[268] Zhang X, Huang Y, Wang B, Chang X, Yang H, Lan J, Wang S, Qiao H, Lin H, Han S, Guo Y, Zhang X. A functionalized Sm/Sr doped TiO2 nanotube array on titanium implant enables exceptional bone-implant integration and also self-antibacterial activity. Ceram Int 2020;46:14796–807.
[269] Fina F, Goyanes A, Madla CM, Awad A, Trenfield SJ, Kuek JM, Patel P, Gaisford S, Basit AW. 3D printing of drug-loaded gyroid lattices using selective laser sintering. Int J Pharm 2018;547:44–52.
[270] Miljanovic D, Seyedmahmoudian M, Stojcevski A, Horan B. Design and fabrication of implants for mandibular and craniofacial defects using different medical-additive manufacturing technologies: a review. Ann Biomed Eng 2020;48:2285–300.
[271] Abdulhameed O, Al-Ahmari A, Ameen W, Mian SH. Additive manufacturing: challenges, trends, and applications. Adv Mech Eng 2019;11:1687814018822880.
[272] Peel S, Eggbeer D, Sugar A, Evans PL. Post-traumatic zygomatic osteotomy and orbital floor reconstruction. Rapid Prototyp J 2016;22:878–86.
[273] Sharma N, Ostas D, Rotar H, Brantner P, Thieringer FM. Design and additive manufacturing of a biomimetic customized cranial implant based on voronoi diagram. Front Physiol 2021;12:647923.
[274] Colen S, HarakE R, De Haan J, MuliER M. A modified custom-made triflanged acetabular reconstruction ring (MCTARR) for revision hip arthroplasty with severe acetabular defects. Acta Orthop Belg 2013;79:71–5.
[275] Baauw M, van Hellemondt GG, Van Hooff M, Spruit M. The accuracy of positioning of a custom-made implant within a large acetabular defect at revision arthroplasty of the hip. The Bone Joint J 2015;97:780–5.
[276] Wang S, Wang L, Liu Y, Ren Y, Jiang L, Li Y, Zhou H, Chen J, Jia W, Li H. 3D printing technology used in severe hip deformity. Exp Ther Med 2017;14:2595–9.
[277] Merema BJ, Kraeima J, Ten Duis K, Wendt KW, Warta R, Vos E, Schepers RH, Witjes MJH, Ffa IJ. The design, production and clinical application of 3D patient-specific implants with drilling guides for acetabular surgery. Injury 2017;48:2540–7.
[278] Weißmann V, Boss C, Schulze C, Hansmann H, Bader R. Experimental characterization of the primary stability of acetabular press-fit cups with open-porous load-bearing structures on the surface layer. Metals 2018;8:839.
[279] Song C, Yang Y, Wang Y, Yu J-k, Wang D. Personalized femoral component design and its direct manufacturing by selective laser melting. Rapid Prototyp J 2016;22:330–7.
[280] Zhang Y, Gulati K, Li Z, Di P, Liu Y. Dental implant nano-engineering: advances, limitations and future directions. Nanomaterials 2021;11:2489.
[281] Sailer I, Karasan D, Todorovic A, Ligoutsikou M, Pjetursson BE. Prosthetic failures in dental implant therapy. Periodontology 2000 2022;88:130–44.
[282] Huang Y-C, Huang Y-C, Ding S-J. Primary stability of implant placement and loading related to dental implant materials and designs: a literature review. J Dent Sci 2023;18:1467–76.
[283] Elsayed H, Brunello G, Gardin C, Ferroni L, Badocco D, Pastore P, Sivolella S, Zavan B, Biasetto L. Bioactive sphene-based ceramic coatings on cpTi substrates for dental implants: an in vitro study. Materials 2018;11:2234.
[284] Chen X, Shah K, Dong S, Peterson L, La Plante EC, Sant G. Elucidating the corrosion-related degradation mechanisms of a Ti-6Al-4V dental implant. Dent Mater 2020;36:431–41.
[285] Wang Y, Zhang Y, Sculean A, Bosshardt DD, Miron RJ. Macrophage behavior and interplay with gingival fibroblasts cultured on six commercially available titanium, zirconium, and titanium-zirconium dental implants. Clin Oral Invest 2019;23:3219–27.
[286] Kniha K, Bock A, Peters F, Magnuska ZA, Gremse F, Moehlhenrich SC, Hoelzle F, Modabber A. Microstructural volumetric analysis of the jaw following dental implantation under systemic bisphosphonate delivery: an in vivo and ex vivo rat study. J Periodontol 2021;92:e66–75.
[287] Zhang H, Man C, Dong C, Wang L, Li W, Kong D, Wang L, Wang X. The corrosion behavior of Ti6Al4V fabricated by selective laser melting in the artificial saliva with different fluoride concentrations and pH values. Corrosion Sci 2021;179:109097.
[288] Kim HR, Jang S-H, Kim YK, Son JS, Min BK, Kim K-H, Kwon T-Y. Microstructures and mechanical properties of Co-Cr dental alloys fabricated by three CAD/CAM-based processing techniques. Materials 2016;9:596.
[289] Robinson DK, Lagnau A, Boon WP. Innovation pathways in additive manufacturing: methods for tracing emerging and branching paths from rapid prototyping to alternative applications. Technol Forecast Soc Change 2019;146:733–50.
[290] Elambasseril J, Brandt M. Artificial intelligence: way forward to empower metal additive manufacturing product development–an overview. Mater Today Proc 2022;58:461–5.
[291] Tamayo JA, Riascos M, Vargas CA, Baena LM. Additive manufacturing of Ti6Al4V alloy via electron beam melting for the development of implants for the biomedical industry. Heliyon 2021;7:e06892.
[292] Saha S, Roy S. Metallic dental implants wear mechanisms, materials, and manufacturing processes: a literature review. Materials 2022;16:161.
[293] Sola A, Nouri A. Microstructural porosity in additive manufacturing: the formation and detection of pores in metal parts fabricated by powder bed fusion. J Adv Manuf Process 2019;1:e10021.
[294] Laleh M, Hughes AE, Yang S, Wang J, Li J, Glenn AM, Xu W, Tan MY. A critical insight into lack-of-fusion pore structures in additively manufactured stainless steel. Addit Manuf 2021;38:101762.
[295] Meng L, Yang H, Ben D, Ji H, Lian D, Ren D, Li Y, Bai T, Cai Y, Chen J. Effects of defects and microstructures on tensile properties of selective laser melted Ti6Al4V alloys fabricated in the optimal process zone. Mater Sci Eng, A 2022;830:142294.
[296] Meng L, Ben D, Yang H, Ji H, Lian D, Zhu Y, Chen J, Yi J, Wang L, Yang J. Effects of embedded spherical pore on the tensile properties of a selective laser melted Ti6Al4V alloy. Mater Sci Eng, A 2021;815:141254.
[297] Liu J, Song Y, Chen C, Wang X, Li H, Wang J, Guo K, Sun J. Effect of scanning speed on the microstructure and mechanical behavior of 316L stainless steel fabricated by selective laser melting. Mater Des 2020;186:108355.
[298] Baghi AD, Nafisi S, Hashemi R, Ebendorff-Heidepriem H, Ghomashchi R. Effective post processing of SLM fabricated Ti-6Al-4 V alloy: machining vs thermal treatment. J Manuf Process 2021;68:1031–46.
[299] Gao Y, Zhu Q, Huang Z, Zhang S, Wang Y, Li H, Zhang X, Hou Z, Zhang H. A nanoporous Cu-based metamaterial for fenton-like catalysis. Chem Eng J 2023:146902.
[300] Liang S-X, Wang X, Zhang W, Liu Y-J, Wang W, Zhang L-C. Selective laser melting manufactured porous Fe-based metallic glass matrix composite with remarkable catalytic activity and reusability. Appl Mater Today 2020;19:100543.
[301] Tang D, Hu Y, Yang L. New insights into the mechanical properties, functional fatigue, and structural fatigue of Ni-Ti alloy porous structures. Metals 2023;13:931.
[302] Dresler N, Inberg A, Ashkenazi D, Shacham-Diamand Y, Stern A. Silver electroless finishing of selective laser melting 3D-printed AlSi10Mg artifacts. Metallography, Microstruct Anal 2019;8:678–92.
[303] Varol T, Hacısalihoğlu İ, Kaya G, Güler O, Yıldız F, Aksa HC, Akçay SB. The effect of selective laser melting process on the microstructure, density, and electrical

conductivity of silver-coated copper cores. J Mater Eng Perform 2021;30:5216–26.
[304] Chen C, Enrico A, Pettersson T, Ek M, Herland A, Niklaus F, Stemme G, Wågberg L. Bactericidal surfaces prepared by femtosecond laser patterning and layer-by-layer polyelectrolyte coating. J Colloid Interface Sci 2020;575:286–97.
[305] Meng M, Wang J, Huang H, Liu X, Zhang J, Li Z. 3D printing metal implants in orthopedic surgery: methods, applications and future prospects. J Orthopaedic Transl 2023;42:94–112.